

NAVAL POSTGRADUATE SCHOOL

Monterey, California



THESIS

**COMPUTATIONAL FLUID DYNAMICS ANALYSIS OF A
DUAL MODE THRUSTER**

by

Adam N. Williams

September 1999

Thesis Advisor:

Garth V. Hobson

Approved for public release; distribution is unlimited.

19991126 067

REPORT DOCUMENTATION PAGE			Form Approved OMB No. 0704-0188	
Public reporting burden for this collection of information is estimated to average 1 hour per response, including the time for reviewing instruction, searching existing data sources, gathering and maintaining the data needed, and completing and reviewing the collection of information. Send comments regarding this burden estimate or any other aspect of this collection of information, including suggestions for reducing this burden, to Washington headquarters Services, Directorate for Information Operations and Reports, 1215 Jefferson Davis Highway, Suite 1204, Arlington, VA 22202-4302, and to the Office of Management and Budget, Paperwork Reduction Project (0704-0188) Washington DC 20503.				
1. AGENCY USE ONLY (Leave blank)		2. REPORT DATE September 1999		3. REPORT TYPE AND DATES COVERED Master's Thesis
4. TITLE AND SUBTITLE Computational Fluid Dynamics Analysis of a Dual Mode Thruster				5. FUNDING NUMBERS
6. AUTHOR(S) Williams, Adam N.				
7. PERFORMING ORGANIZATION NAME(S) AND ADDRESS(ES) Naval Postgraduate School Monterey, CA 93943-5000				8. PERFORMING ORGANIZATION REPORT NUMBER
9. SPONSORING / MONITORING AGENCY NAME(S) AND ADDRESS(ES) NASA Johnson Space Center, Code EP, Houston, TX				10. SPONSORING/MONITORING AGENCY REPORT NUMBER
11. SUPPLEMENTARY NOTES The views expressed in this thesis are those of the author and do not reflect the official policy or position of the Department of Defense or the U.S. Government.				
12a. DISTRIBUTION / AVAILABILITY STATEMENT Approved for public release; distribution unlimited.				12b. DISTRIBUTION CODE
13. ABSTRACT (Maximum 200 words) Current objectives at NASA Johnson Space Center are directed at future upgrade and replacement of the U. S. Space Shuttle's, currently toxic, Reaction Control System thrusters with dual mode thrusters that use nontoxic propellants. Experimentation to determine any performance advantages obtained using a dual mode thruster has not been performed by NASA. A computational fluid dynamics analysis is performed to evaluate the internal flow characteristics of this thruster under low thrust mode, torch igniter only, conditions. Several computational models, both two- and three-dimensional, are constructed to simulate the internal, steady-state flow characteristics. Comparison is made with current data on a similar type of flow (highly underexpanded free-jet flow) to show the appearance of barrel shocks and Mach disks. Regions of stagnate flow where heat transfer to chamber surfaces will be high and engine thrust performance are predicted based on computational data. Two different flow solvers, one using a finite volume method and the other using a finite difference method, are used to predict the engine's performance. A comparison of the two flow solvers is given based on their relative performance to compute solutions to this problem.				
14. SUBJECT TERMS Computational Fluid Dynamics, Dual Mode Thruster, Underexpanded Flow, Barrel Shock, Mach Disk, Finite Difference Method, Finite Volume Method				15. NUMBER OF PAGES 153
				16. PRICE CODE
17. SECURITY CLASSIFICATION OF REPORT Unclassified	18. SECURITY CLASSIFICATION OF THIS PAGE Unclassified	19. SECURITY CLASSIFICATION OF ABSTRACT Unclassified	20. LIMITATION OF ABSTRACT UL	

NSN 7540-01-280-5500

Standard Form 298 (Rev. 2-89)
Prescribed by ANSI Std Z39-18

Approved for public release; distribution is unlimited.

**COMPUTATIONAL FLUID DYNAMICS ANALYSIS OF A DUAL MODE
THRUSTER**

Adam N. Williams
Captain, United States Marine Corps
B.S., Texas A&M University, 1994


Submitted in partial fulfillment of the
requirements for the degree of

MASTER OF SCIENCE IN ASTRONAUTICAL ENGINEERING

from the

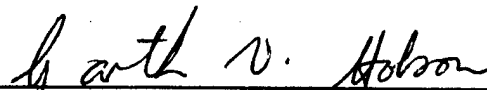
**NAVAL POSTGRADUATE SCHOOL
September 1999**

Author:

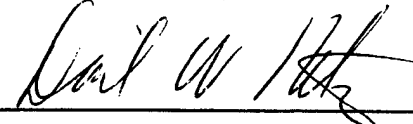


Adam N. Williams

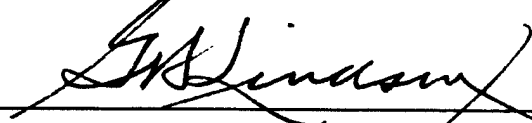
Approved by:



Garth V. Hobson, Thesis Advisor



David W. Netzer, Second Reader



Gerald H. Lindsey, Chairman
Department of Aeronautics and Astronautics

ABSTRACT

Current objectives at NASA Johnson Space Center are directed at future upgrade and replacement of the U. S. Space Shuttle's, currently toxic, Reaction Control System thrusters with dual mode thrusters that use nontoxic propellants. Experimentation to determine any performance advantages obtained using a dual mode thruster has not been performed by NASA. A computational fluid dynamics analysis is performed to evaluate the internal flow characteristics of this thruster under low thrust mode, torch igniter only, conditions. Several computational models, both two- and three-dimensional, are constructed to simulate the internal, steady-state flow characteristics. Comparison is made with current data on a similar type of flow (highly underexpanded free-jet flow) to show the appearance of barrel shocks and Mach disks. Regions of stagnate flow where heat transfer to chamber surfaces will be high and engine thrust performance are predicted based on computational data. Two different flow solvers, one using a finite volume method and the other using a finite difference method, are used to predict the engine's performance. A comparison of the two flow solvers is given based on their relative performance to compute solutions to this problem.

TABLE OF CONTENTS

I.	INTRODUCTION.....	1
A.	PURPOSE	1
B.	BACKGROUND.....	1
C.	OVERVIEW	4
II.	DISCUSSION OF GEOMETRY/GRID GENERATION SOFTWARE AND FLOW SOLVERS	7
A.	PHYSICAL DESCRIPTION OF GEOMETRY	7
	1. Main Combustion Chamber	7
	2. Torch Igniter Chamber	9
B.	FLUENT 5.1 GRID GENERATION (GAMBIT).....	10
	1. Two-Dimensional Models.....	10
	a. Geometry	10
	b. Structured Grid	11
	2. Three-Dimensional Models.....	12
C.	OVERFLOW GEOMETRY AND GRID GENERATION (GRIDGEN, GRIDED, PEGSUS 4.01, RMG2PEG, AND MERGE).....	13
	1. Grid Creation/Modification Software Tools	13
	a. GRIDED	13
	b. PEGSUS 4.1 and RMG2PEG.....	14
	c. MERGE41	15
	2. Two-Dimensional Single-Block Grids.....	15

3.	Three-Dimensional Single/Multi-Block Grids.....	15
D.	FLUENT SOLVER.....	18
1.	Inviscid Model.....	19
2.	Turbulence Models.....	19
a.	Spalart-Allmaras One-Equation Model.....	19
b.	k- ϵ Two-Equation Model.....	19
E.	OVERFLOW SOLVER.....	20
1.	Turbulence Models.....	20
a.	Spalart-Allmaras One-Equation Model.....	20
b.	k- ω Two-Equation Model.....	20
III.	NUMERICAL ANALYSIS RESULTS AND DISCUSSION.....	21
A.	FLUENT TWO-DIMENSIONAL MODEL RESULTS.....	21
1.	Boundary and Initial Conditions.....	21
a.	Boundary Conditions.....	21
b.	Initial Conditions.....	23
2.	Inviscid Model Results.....	23
a.	Convergence History.....	23
b.	Mach Number Contours and Centerline Profile.....	24
c.	Static Temperature Contours.....	26
3.	Spalart-Allmaras Turbulence Model Results.....	27
a.	Convergence History.....	27
b.	Mach Number Contours and Centerline Profile.....	28

c. Static Temperature Contours	30
4. k- ϵ Turbulence Model Results	31
a. Convergence History	31
b. Mach Number Contours and Centerline Profile	32
c. Static Temperature Contours	34
B. OVERFLOW TWO-DIMENSIONAL MODEL RESULTS	35
1. Boundary Conditions	35
2. Inviscid Model Results	36
a. Convergence History	36
b. Mach Number Contours and Centerline Profiles	37
c. Static Temperature Contours	40
3. Spalart-Allmaras Turbulence Model Results	41
a. Convergence History	41
b. Mach Number Contours and Centerline Profiles	42
c. Static Temperature Contours	45
4. k- ω Turbulence Model Results	46
a. Convergence History	46
b. Mach Number Contours and Centerline Profiles	47
c. Static Temperature Contours	50
C. COMPARISON OF FLOW SOLVER RESULTS FOR TWO-DIMENSIONAL MODELS	51
D. OVERFLOW THREE-DIMENSIONAL SINGLE-BLOCK MODEL RESULTS	54

1. Boundary Conditions.....	54
2. Inviscid Model Results.....	55
a. Convergence History	55
b. Mach Number Contours and Centerline Profiles	55
3. Spalart-Allmaras Turbulence Model Results	58
a. Convergence History	58
b. Mach Number Contours and Centerline Profiles	59
4. k- ω Turbulence Model Results	62
a. Convergence History	62
b. Mach Number Contours and Centerline Profiles	63
E. OVERFLOW THREE-DIMENSIONAL MULTI-BLOCK MODEL RESULTS	67
1. Boundary Conditions.....	67
2. k- ω Turbulence Model Results	68
a. Convergence History	68
b. Mach Number Contours and Profiles	68
F. MAIN CHAMBER THRUST PROFILES	73
IV. CONCLUSIONS AND RECOMMENDATIONS.....	77
APPENDIX A. FLUENT 3D GRID AND RESULTS	79
APPENDIX B. OVERFLOW SINGLE-BLOCK IGNITER RESULTS.....	91
APPENDIX C. 2D INVISCID MACH NUMBER CONTOUR CHRONOLOGY.....	95
APPENDIX D. 2D MODEL OVERFLOW INPUT FILES.....	99

APPENDIX E. 3D MODEL OVERFLOW INPUT FILES	103
APPENDIX F. 3D MULTI-BLOCK MODEL OVERFLOW INPUT FILES.....	107
APPENDIX G. PEGSUS INPUT FILES	111
APPENDIX H. MULTI-BLOCK MODEL RESULTS	115
APPENDIX I. THRUST PROFILES	119
APPENDIX J. 2D MAIN CHAMBER MODEL VELOCITY COEFFICIENTS WITH SAMPLE THRUST CALCULATION.....	123
APPENDIX K. TEP OUTPUT FILE	129
LIST OF REFERENCES	135
INITIAL DISTRIBUTION LIST	137

ACKNOWLEDGEMENT

The author would like to acknowledge the support of the personnel of the Propulsion and Fluid Systems Branch, Energy Systems Division of the National Aeronautics and Space Administration's (NASA) Johnson Space Center.

I. INTRODUCTION

A. PURPOSE

The motivation for this thesis stems primarily from current objectives of the National Aeronautics and Space Administration's (NASA) proposed non-toxic upgrades to the U. S. Space Shuttle. A liquid rocket engine, that currently has only one thrust setting, is being evaluated and modified to perform as a dual thruster. Testing of the engine in dual thrust mode has yet to be performed. The prediction of the performance characteristics of this engine forms the objectives of this thesis.

The first of these objectives was to qualitatively and quantitatively determine the internal flow characteristics of the liquid propellant rocket engine with a particular injector configuration. The engine being evaluated and tested by NASA, Johnson Space Center (JSC) serves as a test-bed engine and possible upgrade for the Space Shuttle's Reaction Control System (RCS) engines. From the first objective stems the second; predict the location of the hot spots and regions of stagnate flow within the main combustion chamber, which would require significant cooling, and, knowing this, possibly provide a suitable model to analyze the effects of different cooling configurations.

Computational Fluid Dynamics (CFD) was selected as the means to achieve the above objectives. From a CFD standpoint, this problem provided a test case for the evaluation of two different flow solvers to the same problem, each using a different numerical technique.

B. BACKGROUND

NASA, JSC is currently evaluating the use of a liquid bipropellant rocket engine, using gaseous oxygen (GOX) and ethanol, as a possible replacement for the Space Shuttle's RCS engines. [1] These engines currently use monomethylhydrazine and nitrogen tetroxide propellants, which are toxic and expensive to maintain. They are also not dual mode engines. The idea of using a dual mode thruster for the RCS thrusters is to

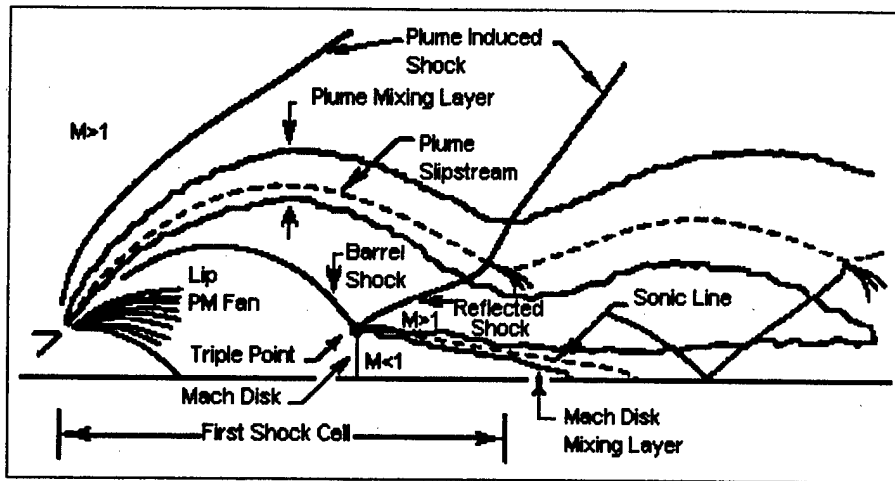
eliminate the current thruster configuration which uses two separate types of engines; one type numbering six to perform vernier orbit adjustments and another type numbering 38 to perform larger orbit adjustments.

A prototype engine built by Aerojet in the 1980's is being evaluated by NASA at the White Sands Test Facility as a replacement; however, limited analysis on engine performance and heat transfer has been performed. The engine, which currently has one thrust setting of 620 lbf, is being modified to operate as a dual thruster with two settings, a high (full) setting, which produces 620 lbf of thrust, and a low (vernier) setting, which produces 10 lbf. Analysis of the steady-state heat transfer to the main chamber walls and injector face-plate under low thrust conditions as well as analysis of the internal aerodynamics and throat choking conditions are critical to determining the suitability of using this engine as a dual thruster.

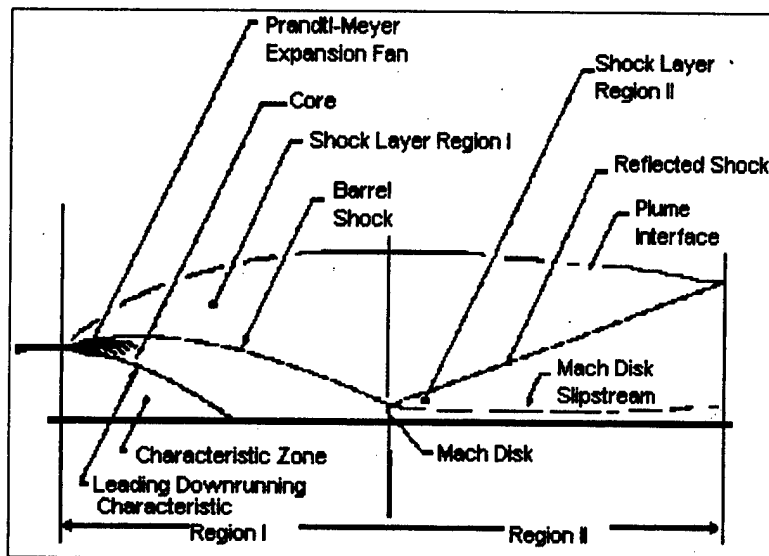
In full thrust mode the main chamber nozzle completely chokes the main chamber's flow through the nozzle throat, resulting in supersonic expansion of the combustion gases occurring after passage through the throat. This can be confirmed based upon tests already conducted for the full thrust mode firing. [2] The exact influence of the main chamber's converging-diverging nozzle section during low thrust firing, however, is not known since there is, to date, no experimental data on the engine in this firing mode.

Physically, firing the torch igniter into the main chamber section (not including converging-diverging nozzle section) represents exhausting a small diameter, under-expanded free-jet into much larger, lower pressure surroundings. This can be likened in some respects to that of an under-expanded solid rocket plume. In Reference 3, computation of an under-expanded solid rocket was simulated using a Total Variation Diminishing discretization scheme within the Unified Solutions Algorithm. The characteristics of the first shock cell (near field structure) were predicted in these computations and compare well with physical data. The physical characteristics of this near field structure are also well illustrated in Reference 4; a brief description here is

applicable to the understanding of the results of this work. Figure 1 shows the basic characteristics as given in References 3 and 4.



(a) Plume Flowfield, Nearfield Structure. From Ref. [3]



(b) Flow Structure of an Inviscid Shock Cell. From Ref. [4]

Figure 1. (a) Plume Flowfield, Nearfield Structure. (b) Flow Structure of an Inviscid Shock Cell.

This figure shows the nearfield structure of an under-expanded exhaust plume and a corresponding nomenclature diagram for the first inviscid shock cell at the exit plane. The important and distinguishing features of this flow are the formation of the barrel shock, which separates the exhaust gases into the regions of the core and the barrel shock layer; the rapidly expanding (Prandtl-Meyer) flow immediately following the nozzle exit plane; the formation of the Mach disk, representing the coalescence of the barrel shock waves into a much stronger normal shock centered along the flow axis; and finally, the Mach disk mixing layer that separates the higher temperature, subsonic gases downstream of the Mach disk with those in the cooler supersonic shock layer regions. [4] Without the presence of any external surfaces beyond the nozzle exit plane, these typical phenomenon are observed. For this work, the effects of the introduction of the surfaces of the main chamber and converging/diverging nozzle on the overall flow structure were not known a priori. Thus arose the important questions of whether or not the main chamber's throat caused the flow to be sonic, choking the flow, and if it did choke it, to what degree?

C. OVERVIEW

Two- and three-dimensional computational models were constructed using two different grid generation software packages, GRIDGEN and GAMBIT. The GRIDGEN models were then used by the OVERFLOW version 1.8b Navier-Stokes code to determine various flow properties and internal flow characteristics. The GAMBIT models were used by the flow solver FLUENT 5.1 to compute the flowfield properties and characteristics.

OVERFLOW version 1.8b is a complete rewrite of the F3D/Chimera code developed by Joseph Steger at NASA, Ames Research Center. [5] This code requires a structured grid and uses finite difference methods to arrive at the numerical solution. It also uses the Chimera overlapping grid scheme, enabling its application to problems with complex geometries or geometries that must be modeled as a set of smaller, simpler grids. By using this scheme several single-block grids can be merged together to form a multi-block grid.

Several computational models were generated using GRIDGEN and then, depending on whether the models were to be solved using single or multiple blocks, formatted for use in OVERFLOW by other software packages or FORTRAN programs (GRIDED, PEGSUS 4.01, MERGE, RMG2PEG).

FLUENT 5.1 is a fluid dynamics software package developed by Fluent Incorporated to model fluid flow and heat transfer in complex geometries. This code offers a wide range of capabilities, solving flow problems with both structured and unstructured grids using finite volume methods (FVM). [6,7]

Models generated in GAMBIT were used directly by FLUENT 5.1 without the requirement for grid formatting. FLUENT 5.1 solves both inviscid and viscous problems and offers a range of turbulence models.

Solutions were computed within OVERFLOW using an inviscid model, a one-equation turbulence model (Spalart-Allmaras), and a two-equation turbulence model ($k-\omega$). Solutions were computed within FLUENT 5.1 using an inviscid model, a one-equation model (Spalart-Allmaras), and a two-equation model ($k-\epsilon$).

II. DISCUSSION OF GEOMETRY/GRID GENERATION AND FLOW SOLVERS

A. PHYSICAL DESCRIPTION OF GEOMETRY

Before describing the grids that were used to create the computational models a brief introduction to the overall geometry of a dual mode thruster is given. Figure 2 shows the basic configuration of the dual mode thruster considered for this study.

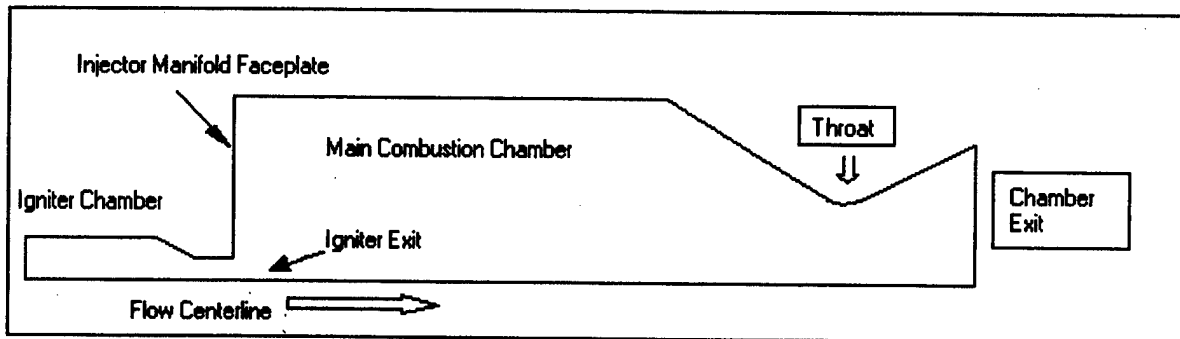


Figure 2. Schematic of a Dual Mode Thruster.

The igniter chamber serves as a torch that ignites the propellants injected into the main combustion chamber during full thrust mode, and also as a combustion chamber with converging nozzle capable of producing thrust without further addition of propellants within the main chamber. In other words, in the full thrust mode, oxidizer and fuel are mixed and combusted in both the torch igniter and main chamber. In the vernier thrust mode, oxidizer and fuel are mixed and combusted in the igniter chamber.

1. Main Combustion Chamber

The geometry of the main combustion chamber was created based upon dimensions taken from several CAD diagrams of the main combustion chamber with converging/diverging nozzle. [8] Figure 3 shows the CAD diagram of the main chamber and nozzle section of the engine. The chamber diameter taken from the diagram was 3.4 inches while the length from injector faceplate to nozzle throat was set at 4.818 inches for the basic model. Figure 3 shows a length of 5.0 inches from chamber end to nozzle

throat; however, the injector faceplate is mounted 0.182 inches inside the chamber so the distance from igniter exit plane to nozzle throat is the previously mention 4.818 inches. The nozzle exit to throat area ratio was 1.898 and was not modified. The main chamber was modeled for both FLUENT 5.1and OVERFLOW.

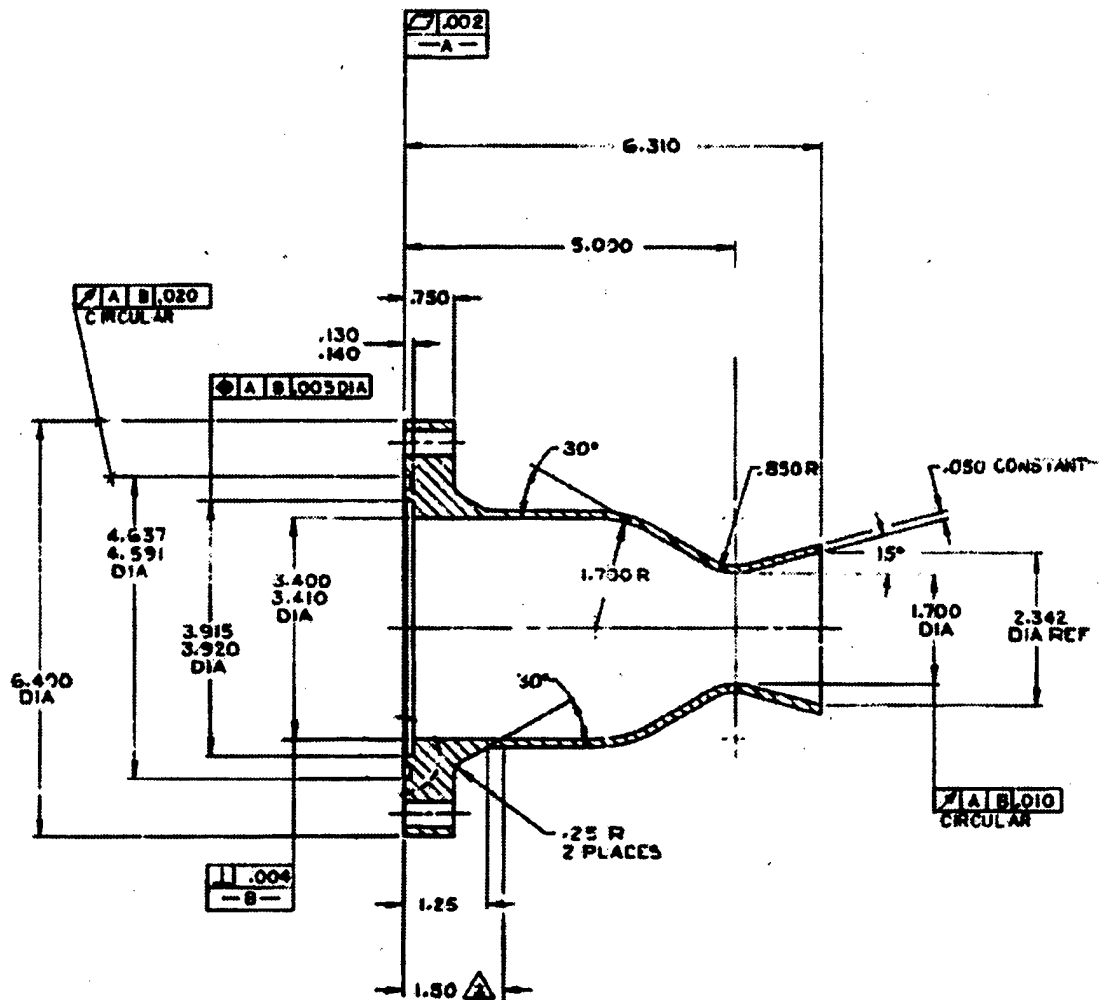


Figure 3. CAD Schematic Showing Main Chamber and Nozzle Sections. From Ref. [8]

Figure 4 shows the actual physical model of the manifold faceplate. The igniter port is the inlet into the main chamber. The like-on-like oxidizer and fuel orifices were not modeled for this thesis.

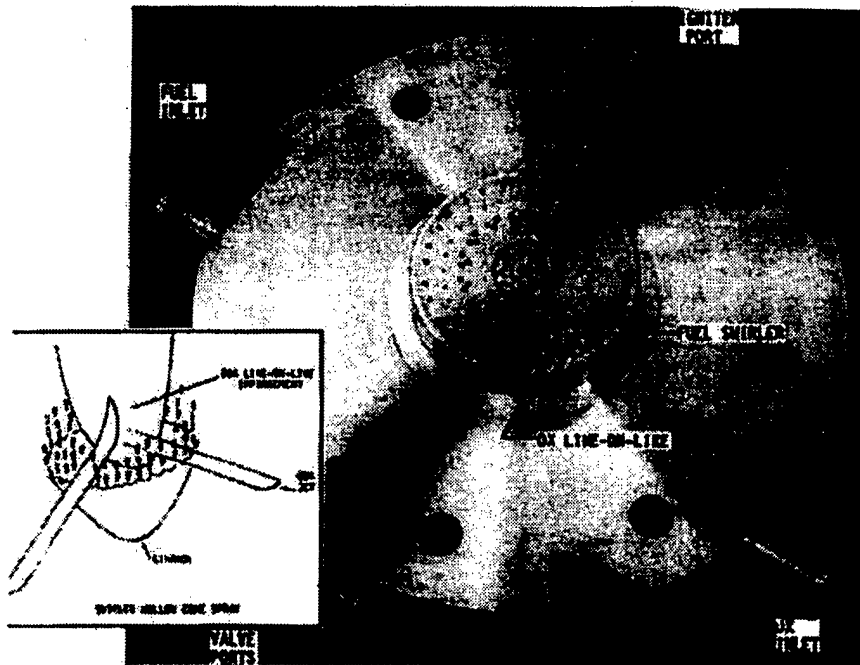


Figure 19. GOX/Ethanol Pulse Thruster Injector

Figure 4. Main Chamber Injector Manifold Faceplate. From Ref. [9]

2. Torch Igniter Chamber

Figure 5 shows a schematic of the torch igniter combustion chamber. The diameter of the igniter port which exhausts into the main chamber was 0.2 inches. The entire length of the igniter's combustion chamber, which in the drawing was 2.1 inches, was not modeled. The torch igniter chamber was only modeled for use by OVERFLOW. It was not modeled for use in FLUENT 5.1.

commands in GAMBIT. The curved parts of the nozzle were created by connecting vertex points with a series of curve fitted edges. Due to the different methods used to create the curved nozzle geometry in GAMBIT and GRIDGEN, slight curvature differences exist between the two models.

b. Structured Grid

A structured grid similar to that which was created in GRIDGEN was modeled in GAMBIT to serve as a benchmark for comparing two dimensional solutions from OVERFLOW with those of FLUENT 5.1. The dimensions of this grid were 80 x 150 (width by length) and consisted of approximately 12,000 quadrilaterals. Figure 6 shows the two-dimensional grid of the nozzle. Points were clustered along the edges closest to the torch igniter exit along both the nozzle centerline axis and the injector face. Points were also clustered along the upper portion of the injector face so that boundary layers along the chamber walls could be resolved.



Figure 6. Side View of GAMBIT Two-Dimensional Model of Main Chamber.

2. Three-Dimensional Models

A three-dimensional geometry was created in an effort to provide a working model that could later be used to model the three-dimensional swirling flow effects, created by the like-on-like orifices on the injector faceplate. Flow swirl was not taken into account for this thesis. A three-dimensional GAMBIT model was created by simply revolving the single face of the two-dimensional model geometry through 12 degrees, thus, preserving nozzle curvature and grid point spacing. Both the grid and results of computations performed on this grid are shown in Appendix A.

C. OVERFLOW GEOMETRY AND GRID GENERATION (GRIDGEN, GRIDED, PEGSUS 4.01, RMG2PEG, AND MERGE)

As with the GAMBIT model, the GRIDGEN model was also built by plotting several vertices, linking the vertices to form a two-dimensional, axisymmetric representation of the geometry, which was then meshed. Due to formatting and structural limitations required by using OVERFLOW, several other grid preparation and modification tools were used to modify the grids created in GRIDGEN. For more information on GRIDGEN, see Reference 11. These grid modification tools are discussed below.

1. Grid Creation/Modification Software Tools

a. GRIDED

GRIDED is a grid manipulation and modification software tool that can be used to make a variety of modifications to an existing grid. For the two-dimensional models of the igniter and main chamber, it was used to add additional planes by reflection of the existing single plane around the flow direction axis (x-axis). Figure 7 shows a perspective view of the middle plane looking down the flow axis of the two-dimensional GRIDGEN model. The reflected symmetry planes are rotated automatically by GRIDED about the x-axis by ± 1.0 degrees. This modification was necessary in order to use the two-dimensional axisymmetric boundary condition offered in OVERFLOW. The grid dimensions were 81 x 3 x 129: 81 radially outward from centerline, 3 planes rotated about the centerline, and 129 from igniter exit plane to main chamber exit plane.

For the three-dimensional GRIDGEN models, which were a 90 degree wedge-like grid for both the main chamber and the igniter, GRIDED was used to add additional planes by reflected symmetry of the single outermost planes, the planes at 0 and 90 degrees. The addition of these two planes was required by OVERFLOW, as well.

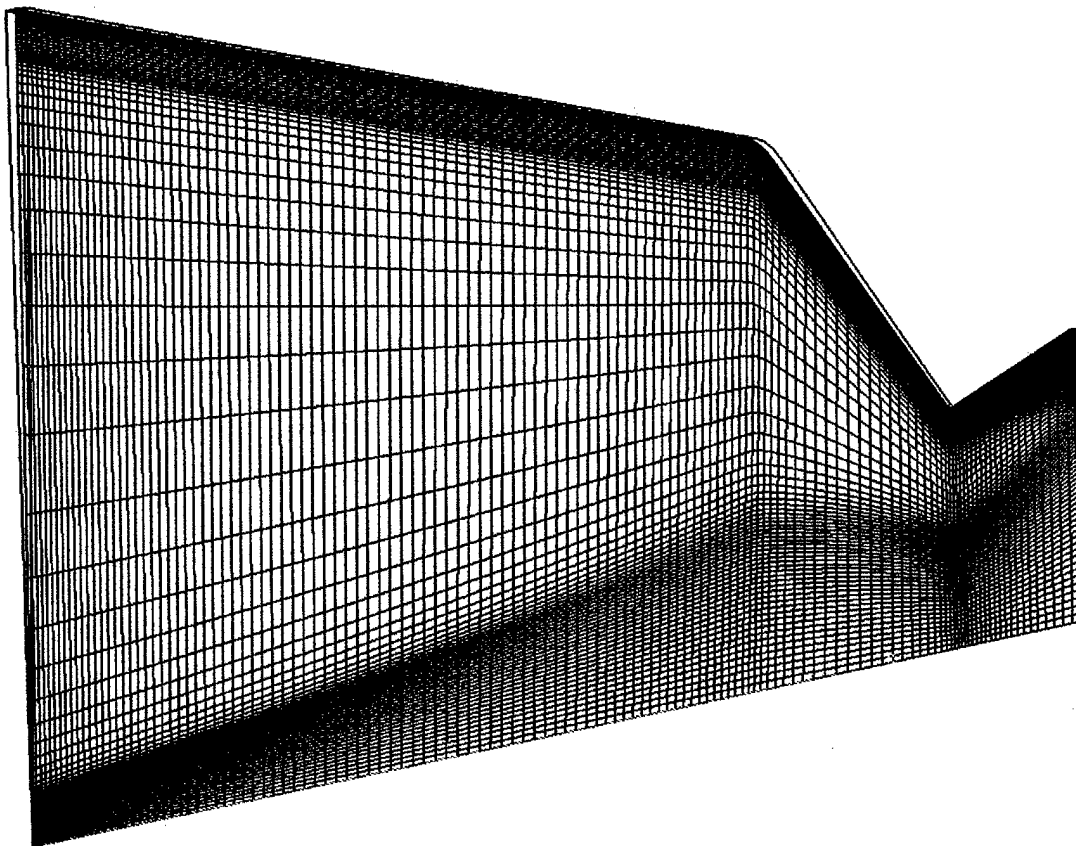


Figure 7. Perspective View of Single (Middle) Plane of Two-Dimensional Axisymmetric Grid Looking Down Flow Axis.

b. PEGSUS 4.1 and RMG2PEG

PEGSUS 4.1 was a software tool used to create a boundary point interpolation file (INTOUT), a grid point blanking file (IBPLOT), and a composite mesh file (COMPOUT) from an existing multi-block grid input file (INGRID). The multiple overlapping block or Chimera domain decomposition scheme available in OVERFLOW required the interpolation file and the concatenation of the files COMPOUT and IBPLOT into a grid file. The Chimera scheme is a process whereby a system of relatively simple, structured grids are used to model a physically complex structure that cannot, otherwise, be modeled with a single-block structured grid. For more information on the Chimera scheme, see Reference 5.

The mesh interpolation file (INTOUT), which was created by PEGSUS, contained the interpolation stencil relating flow variables calculated at points of overlap of the predefined multiple block grids. In other words, the boundary points of overlap for each grid are given a means to properly communicate between the respective grids with the interpolation stencil. See Reference 12 for more information on PEGSUS. This required the concatenation of two existing meshes into a composite mesh with complementary mesh interpolation file, which was performed in RMG2PEG.

c. MERGE41

MERGE41 is a FORTRAN program that concatenates two of the output files produced by PEGSUS into a single grid file upon which OVERFLOW can compute a solution. These two output files are COMPOUT and IBPLOT. COMPOUT is the composite mesh output file produced in PEGSUS. IBPLOT is a table of blanking information on the composite grid file. For more information on blanking points, see Reference #.

2. Two-Dimensional Single-Block Grids

For single-block grids, the domain was generated in GRIDGEN, modified in GRIDDED to add additional planes for use with OVERFLOW's two-dimensional axisymmetric boundary conditions. Single-block grids were created to model both the main chamber and the torch igniter separately. This facilitated separate testing of each grid to determine whether or not there was adequate grid resolution and served as a basis for understanding the complex internal flow of each chamber, the torch igniter and main chamber.

3. Three-Dimensional Single/Multi-Block Grids

As a precursor to modeling the internal flow with a three-dimensional, multi-block structured grid, separate three-dimensional, single-block grids modeling the igniter chamber and main chamber were independently generated. Results for the main chamber are discussed in the results section while the igniter results are given in Appendix B.

Each three-dimensional grid was created by revolving the previously tested two-dimensional axisymmetric grids through 90 degrees. While the number of flow axis grid points remained the same as the two-dimensional model, the spacing was readjusted to cluster more points towards the injector faceplate. Figures 8, 9 and 10 show the independent single-block chamber and igniter grid structures and the multi-block grid structure, respectively.

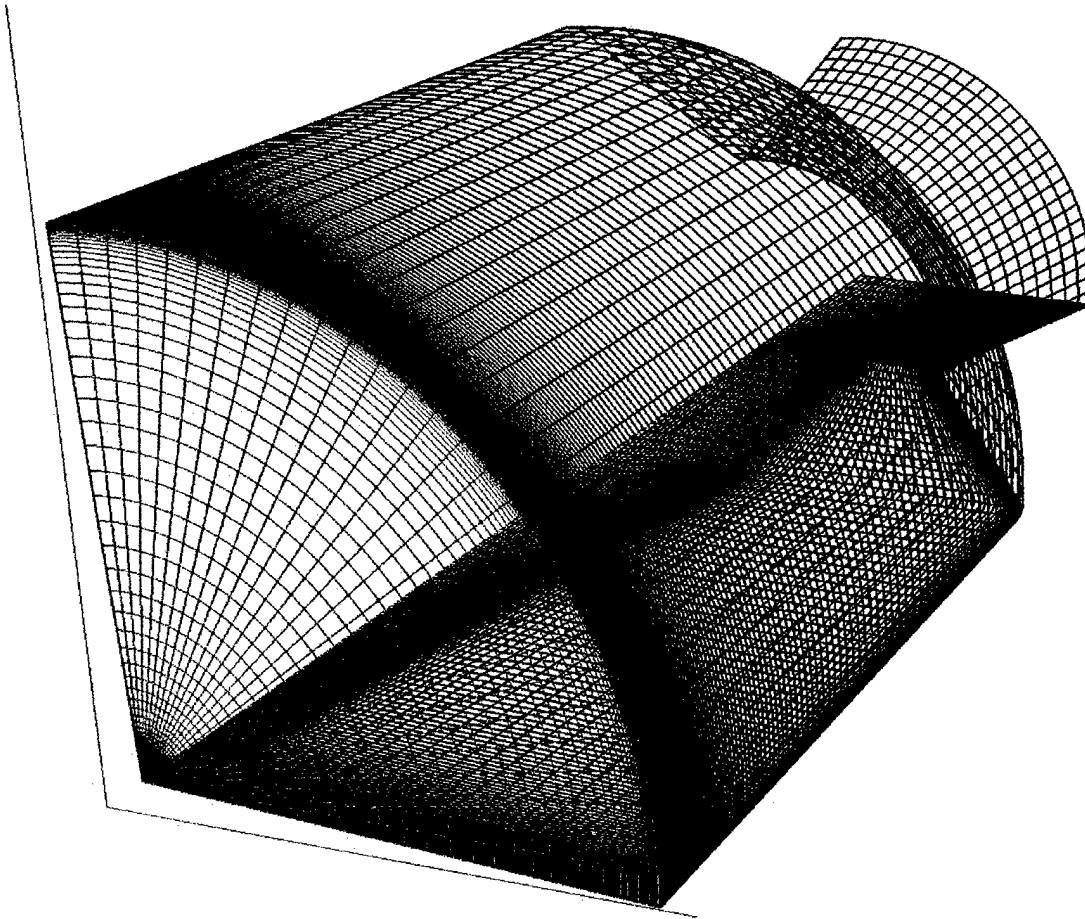


Figure 8. Single-Block Main Chamber Grid, (81 x 29 x 129).

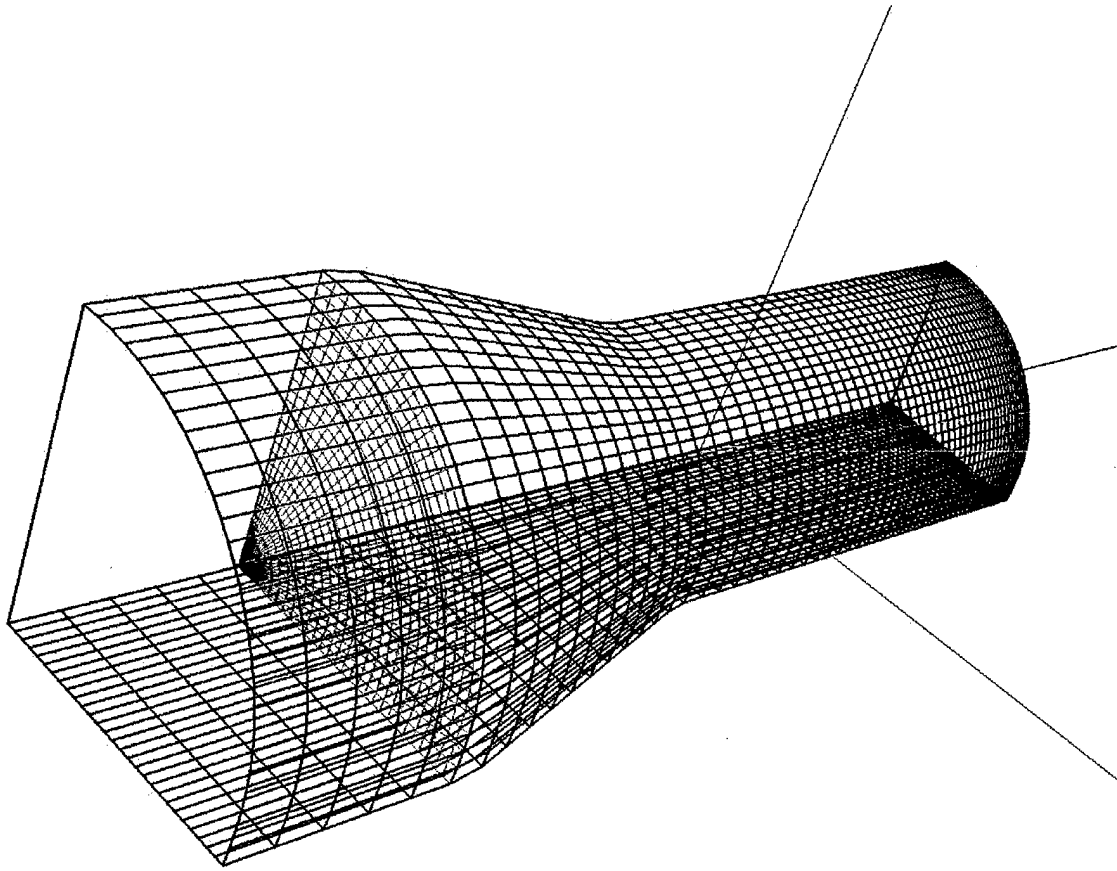


Figure 9. Single-Block Igniter Grid, (30 x 29 x 60).

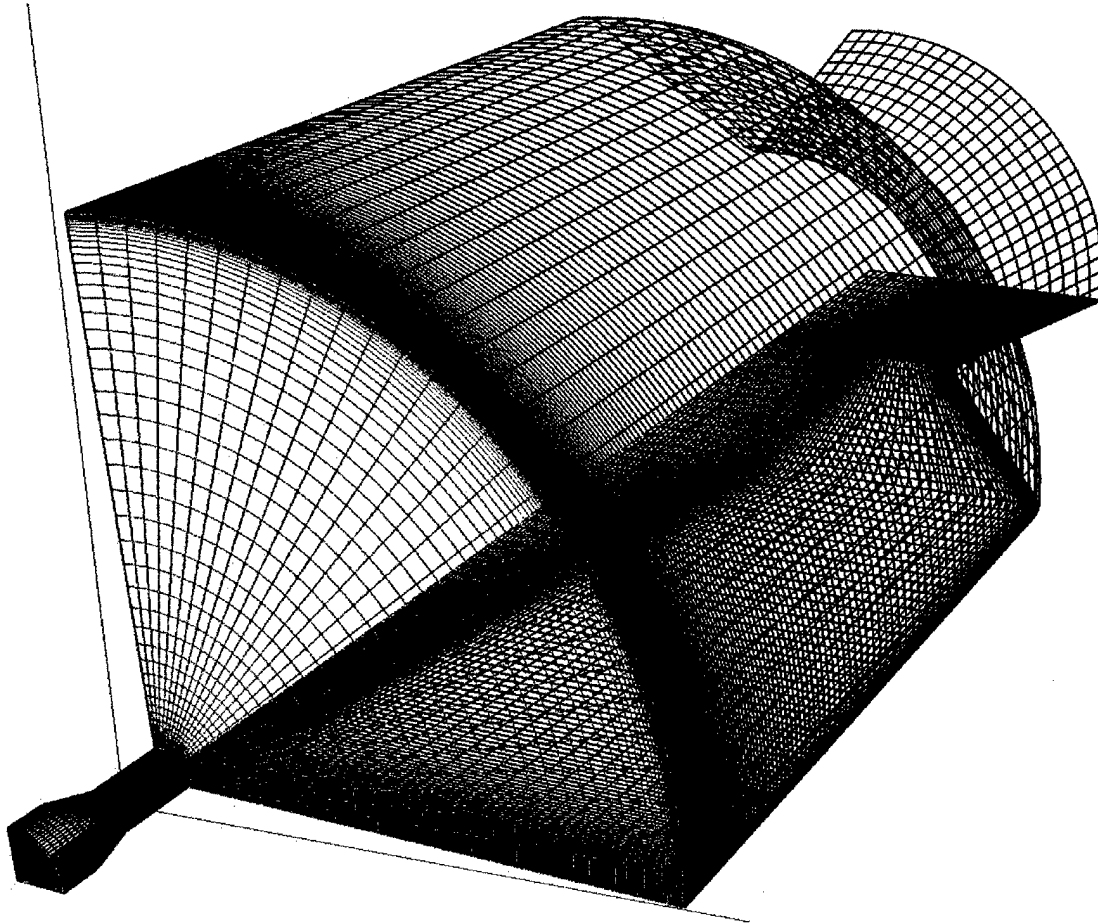


Figure 10. Multi-Block Chamber with Torch Igniter Grids.

D. FLUENT SOLVER

The FLUENT 5.1 flow solver is an unstructured finite volume method offering a range of solver algorithms to meet a variety of industrial type flow problems. FLUENT 5.1 is suited for compressible as well as incompressible flows. For this study, it was run on a Sun Sparc10 workstation at NASA Johnson Space Center.

Solver options in this version include segregated-implicit and coupled-explicit/implicit. For this study the coupled-implicit method was used because of its robustness relative to the explicit scheme. All computed solutions were first-order accurate and used an upwind-differencing scheme, which was the default scheme for compressible flow solutions. An axisymmetric option was also included that

automatically set the solution domain boundary conditions to that of an axisymmetric flow.

Both viscous and inviscid solutions were calculated in FLUENT 5.1. Several turbulence models were also available. These included the following: Spalart-Allmaras, standard $k-\epsilon$, Renormalization-Group (RNG) $k-\epsilon$, Realizable $k-\epsilon$, a Reynolds stress model (RSM), and a large eddy simulation model (LES). For more information about the turbulence models given in FLUENT 5.1 see References 6 or 7.

1. Inviscid Model

The inviscid solver within FLUENT solved the Euler equations. Inviscid solutions were calculated on the main chamber model in order to gain a qualitative understanding of the complicated flow physics occurring while minimizing computational effort.

2. Turbulence Models

a. Spalart-Allmaras One-Equation Model

The first and primary turbulence model selected within FLUENT 5.1 was the Spalart-Allmaras one-equation turbulence model. This model was selected based upon its implementation in both OVERFLOW and FLUENT 5.1, thus, serving as a means of comparing viscous solutions between the two solvers.

b. $k-\epsilon$ Two-Equation Model

FLUENT 5.1 also implemented a standard $k-\epsilon$ turbulence model in which two additional equations are solved for the turbulent kinetic energy and dissipation rate. This model used standard wall functions and was selected based on its wide acceptance within the engineering field and to serve as a third and final means of comparison of solutions computed solely within FLUENT5.1.

E. OVERFLOW SOLVER

This code was used extensively to model the aerodynamics of the U. S. Space Shuttle and has proven accurate for a variety of compressible flow problems. The OVERFLOW solver was a finite difference method developed mainly for use with overset (multi-block) structured grids. For this study the code was run on a Cray Y-MP J94 at the Naval Postgraduate School, Monterey, California. Due to time and software code availability, a more in-depth analysis was performed using OVERFLOW

A variety of differencing schemes can also be implemented within OVERFLOW. For all computed solutions, central differencing was selected because of its robustness given the combination of both subsonic and supersonic flow encountered within this problem. For this study, both inviscid and viscous wall boundary type solutions were computed as well using the following turbulence models.

1. Turbulence Models

a. Spalart-Allmaras One-Equation Model

This turbulence model was selected based upon its implementation in both OVERFLOW and FLUENT 5.1, thus, serving as a means of comparing similar viscous solutions between the two solvers. Two variations of this model are implemented in this version of OVERFLOW, but only the fully turbulent variation was used.

b. $k-\omega$ Two-Equation Model

Analysis was also performed using the $k-\omega$ turbulence model offered in OVERFLOW. This turbulence model was selected to serve as a means of comparison between computed solutions within OVERFLOW.

III. NUMERICAL ANALYSIS RESULTS AND DISCUSSION

In the absence of experimental data with which to compare the computed solutions, an effort was made to compute and compare solutions within each respective flow solver, and to then compare applicable solutions between the two flow solvers. Some of the solutions generated within the FLUENT solver were considered less than ideal as far as convergence was concerned. Unfortunately due to time constraints and computational limitations imposed by running FLUENT on a Sun workstation, the FLUENT solutions were not run for as many iterations as would be ideal in this case. They are presented here in an effort to distinguish the applicability of each flow solver to this particular problem and to illustrate some of the basic phenomenon.

Convergence history profiles are given for each computed solution for both the FLEUNT 5.1 two-dimensional model and the two and three-dimensional OVERFLOW models. For the FLUENT 5.1 model, the measure of solution convergence was based upon the magnitude of residual decrease of the continuity equation. For the OVERFLOW models, the measure of convergence was based upon the magnitude of residual decrease for the L-2 density normal.

As mentioned in the overview, solutions were run with each solver using an inviscid model and two different turbulence models. The turbulence models used in FLUENT 5.1 were the Spalart-Allmaras one-equation model and the k- ϵ two-equation model. The turbulence models used within OVERFLOW were the Spalart-Allmaras one-equation model and the k- ω two-equation model.

A. FLUENT TWO-DIMENSIONAL MODEL RESULTS

1. Boundary and Initial Conditions

a. Boundary Conditions

For the FLUENT models, all wall boundaries were defined in GAMBIT. These wall definitions were then exported as part of the mesh file to FLUENT 5.1 where

further specifications were made for the wall conditions. For example, the method used to define wall boundary conditions within FLUENT 5.1 as being either inviscid or viscous was set by selection of an inviscid computation or computation using a turbulence model for viscous flow. The other boundary conditions for the two-dimensional model were as follows.

The edges representing the injector-manifold faceplate and the walls of the main combustion chamber and convergent-divergent nozzle were defined as adiabatic wall boundaries. Since the design igniter chamber stagnation pressure for the real engine is 150 psi and the igniter chamber exit that exhausts into the main chamber is sonic, the edge representing the igniter chamber exit into the main chamber was set as a pressure-inlet boundary with a total pressure of 150 psi and a static pressure of 79.23 psi. This static pressure to total pressure ratio gave the required Mach 1 flow at this inlet while meeting the stagnation pressure conditions. The total temperature for this boundary was set to 5598 °R, which was the exit thermodynamic equilibrium combustion temperature of the igniter chamber determined using the TEP code. [12] A brief discussion on the use of TEP for this analysis is given in the following paragraph. The edge representing the exit of the main chamber nozzle section was set as a pressure-outlet boundary condition of 0.01 psi, which corresponded to an inlet total pressure to an exit static pressure ratio of 15,000. This was a very extreme pressure ratio, which was representative of that which will be experienced by the engine when it is tested in a vacuum. Finally, the edge representing the chamber centerline was defined as an axis boundary.

The fluid was modeled with a molecular weight and ratio of specific heats of standard air ($MW=28.79$, $\gamma=1.4$). The fluid stagnation temperature was set to 5598 °R. This temperature was arrived at by using TEP to calculate the thermodynamic equilibrium combustion temperature for gaseous oxygen and liquid ethanol at a mixture ratio of 1.8 and a chamber pressure of 150 psi. Chemical equilibrium combustion was assumed within the igniter combustion chamber. The flow was then assumed to exhaust with fixed composition through the convergent and constant area sections of the igniter

nozzle into the main combustion chamber. Although TEP determined the post combustion (O_2 and ethanol) molecular weight of the products of the combustion gases to be 23.525 with a ratio of specific heats of 1.2, this was not used for this study.

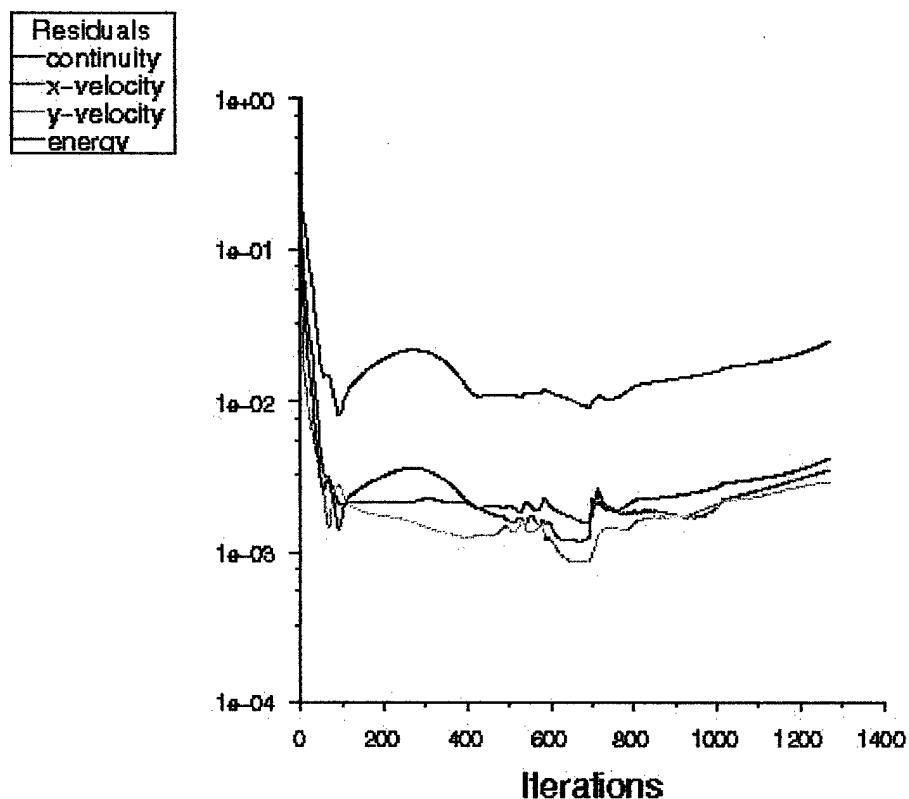
b. Initial Conditions

FLUENT 5.1 allowed for initialization of the solution based upon a user selected initialization zone. An edge or the entire solution domain can be initialized to a particular set of parameters, all of which affect convergence. For the two-dimensional models several different initializations were tried before a suitable one was found. The best initialization occurred by setting the main chamber nozzle exit (pressure outlet boundary) to an exit pressure of above one psi. Setting the pressure lower than this caused the solution to diverge almost immediately. Solution initialization using this setting remained consistent for both inviscid and viscous wall boundary solutions.

2. Inviscid Model Results

a. Convergence History

Figure 11 shows the convergence history of the two-dimensional axisymmetric computation. The residuals dropped initially, but then began to slowly diverge. This was a consistent problem with the FLUENT inviscid model. The convergence of the continuity equation was considered to be the measure of solution convergence, but as can be seen, none of the four conservation equations converged.



Scaled Residuals

Jul 03, 1999
FLUENT 5.1 (axi, coupled imp)

Figure 11. Inviscid Convergence History.

b. Mach Number Contours and Centerline Profile

The measure used to determine internal flow characteristics and throat choking conditions was the Mach number. Figure 12 shows the Mach number contours of the main chamber corresponding to the convergence history plot above. Although this solution was by no means converged, it was illustrative of the formation of the barrel shock and Mach disk structures associated with the expansion of the underexpanded Mach 1.0 flow exhausting from the igniter into the main chamber. Zones of recirculation in the regions outside the barrel shock and slipstream boundaries were also observed.

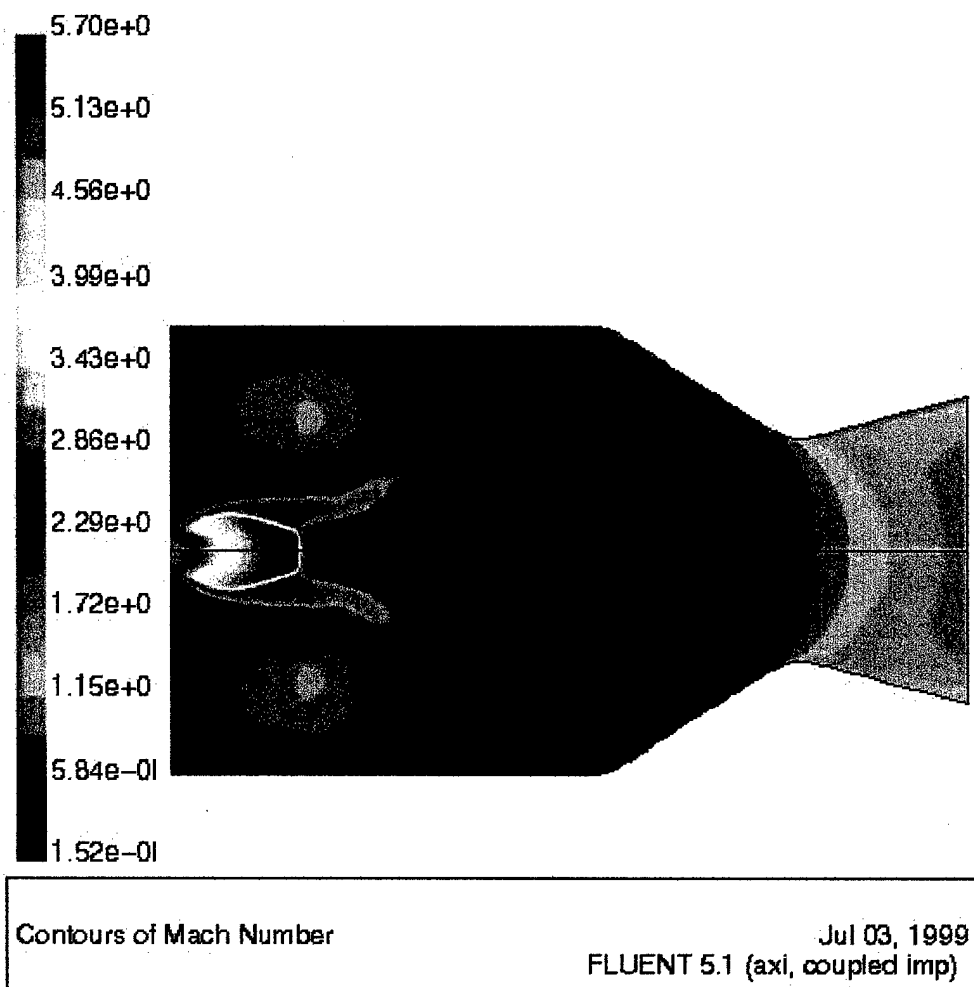
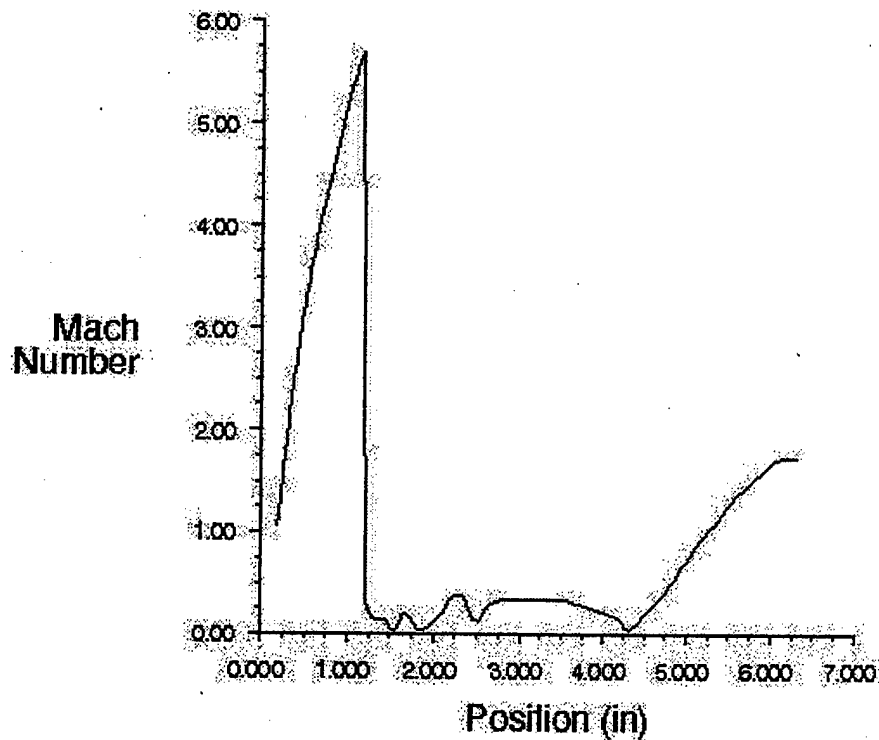


Figure 12. Inviscid Mach Number Contours.

The corresponding chamber/nozzle centerline Mach number profile is given below in Figure 13. The beginning of the main chamber is positioned 0.182 inches from the axis origin. Consequently, the plots of Mach number along the chamber and nozzle centerline, begin at station x equals 0.182 inches instead of at x equals 0.0. The nozzle throat plane is at station x equals 5.00 inches and the beginning of the convergent portion of the nozzle is at station x equals 3.5 inches.

axis 39



Mach Number

Jul 04, 1999
FLUENT 5.1 (axi, coupled imp)

Figure 13. Inviscid Centerline Mach Number Profile.

c. Static Temperature Contours

In order to determine the hottest parts of the flow, static temperature profiles were plotted for the inviscid solution. Figure 14 shows these contours. The hottest locations were the injector faceplate and the converging section of the nozzle. Static temperatures on these surfaces looked to be approximately 5,000 °R, which would be almost 90 percent of the inlet stagnation temperature.

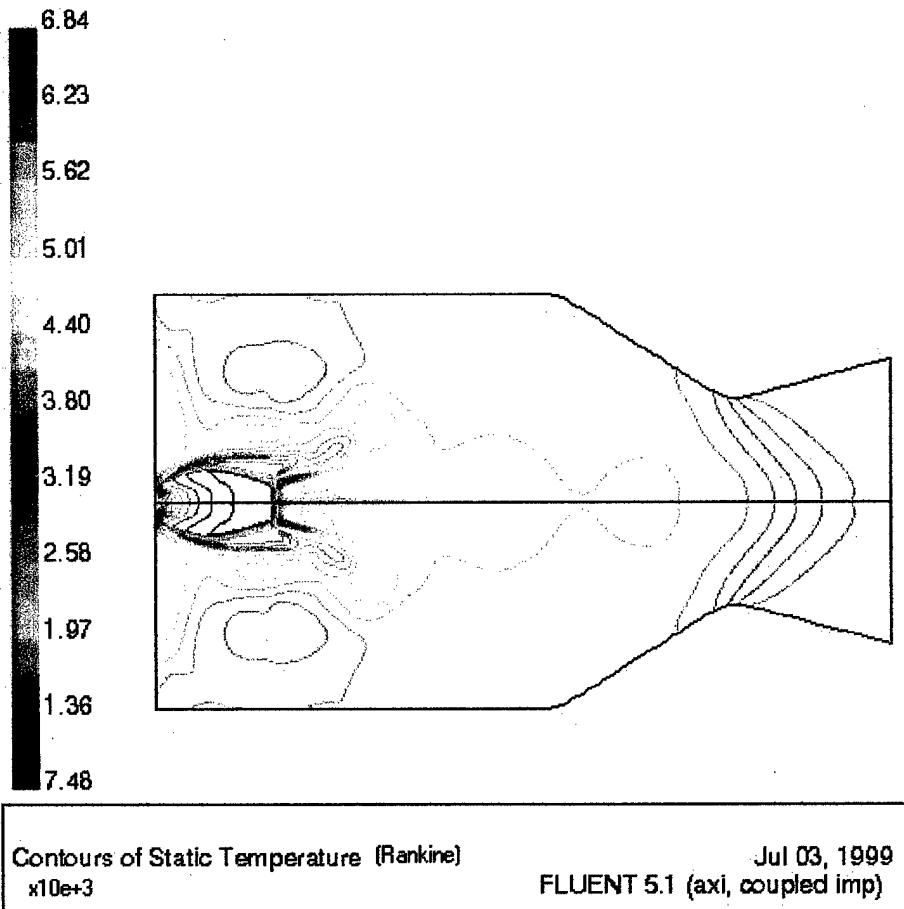
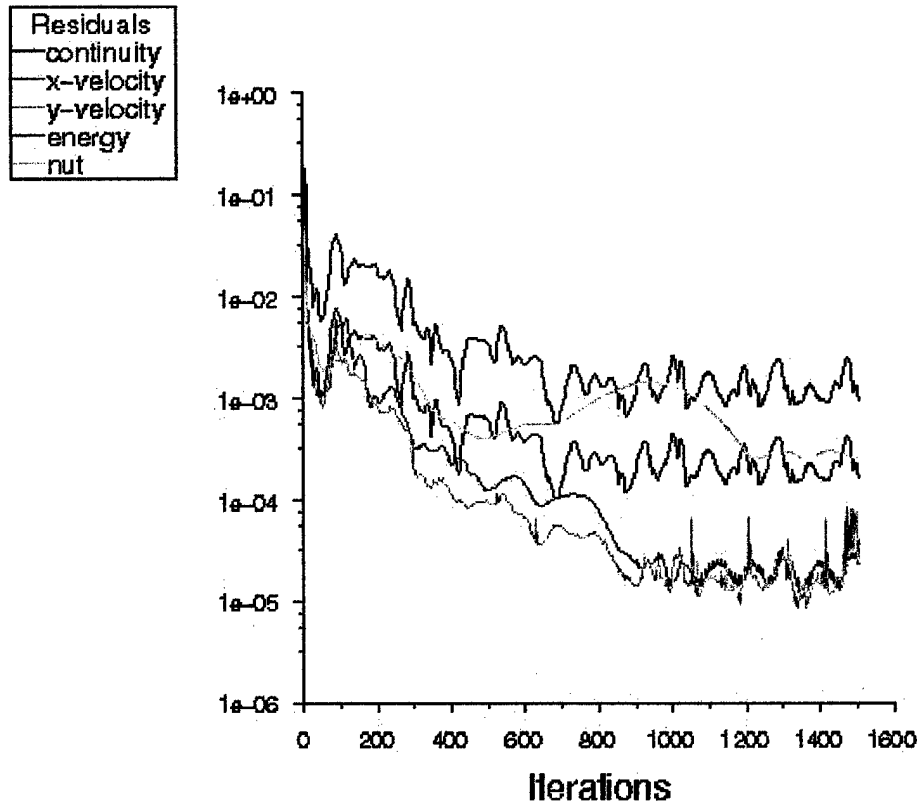


Figure 14. Inviscid Static Temperature Contours.

3. Spalart-Allmaras Turbulence Model Results

a. *Convergence History*

The convergence history computed using the Spalart-Allmaras turbulence model was slightly better than the inviscid solution's convergence history. Figure 15 shows the convergence history for the Spalart-Allmaras turbulence model. Convergence of the continuity equation is represented by the top line and dropped almost two orders of magnitude, however, it had leveled off after 1,000 iterations and continued to oscillate.



Scaled Residuals

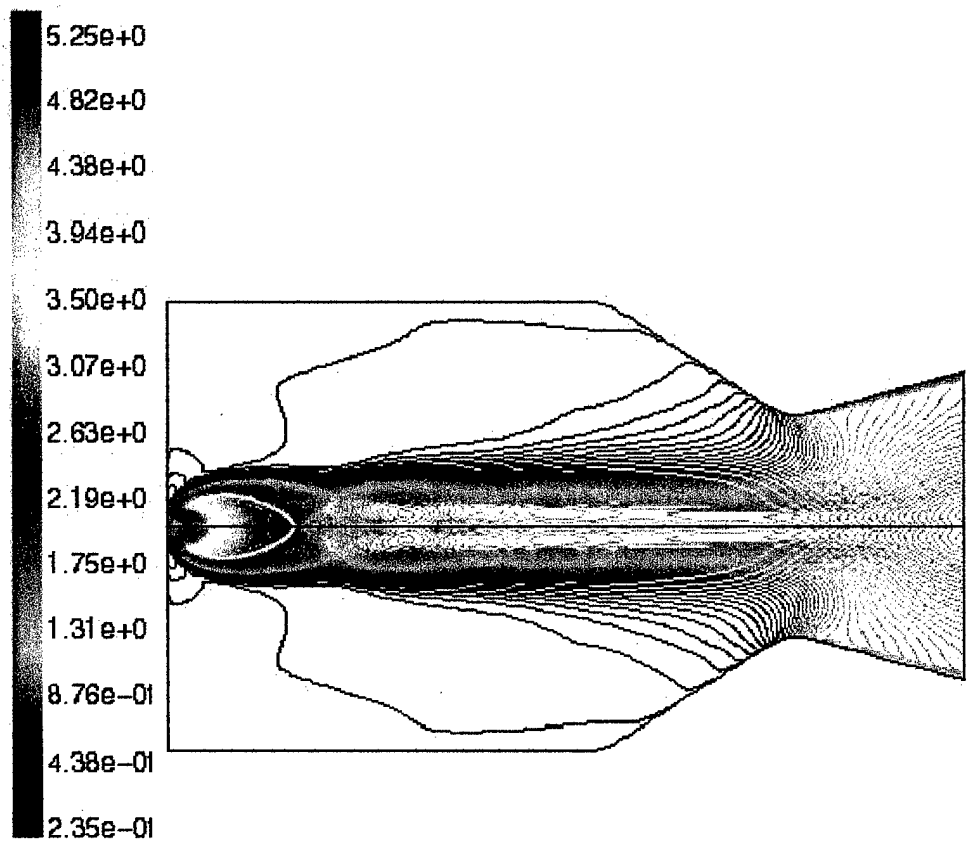
Jul 03, 1999

FLUENT 5.1 (axi, coupled imp, S-A)

Figure 15. Spalart-Allmaras Convergence History.

b. Mach Number Contours and Centerline Profile

Figure 16 shows the corresponding Mach number contours computed using the Spalart-Allmaras model. The maximum Mach number was 5.25. This occurred just upstream of what appeared to be an initial formation of a small Mach disk along the centerline.



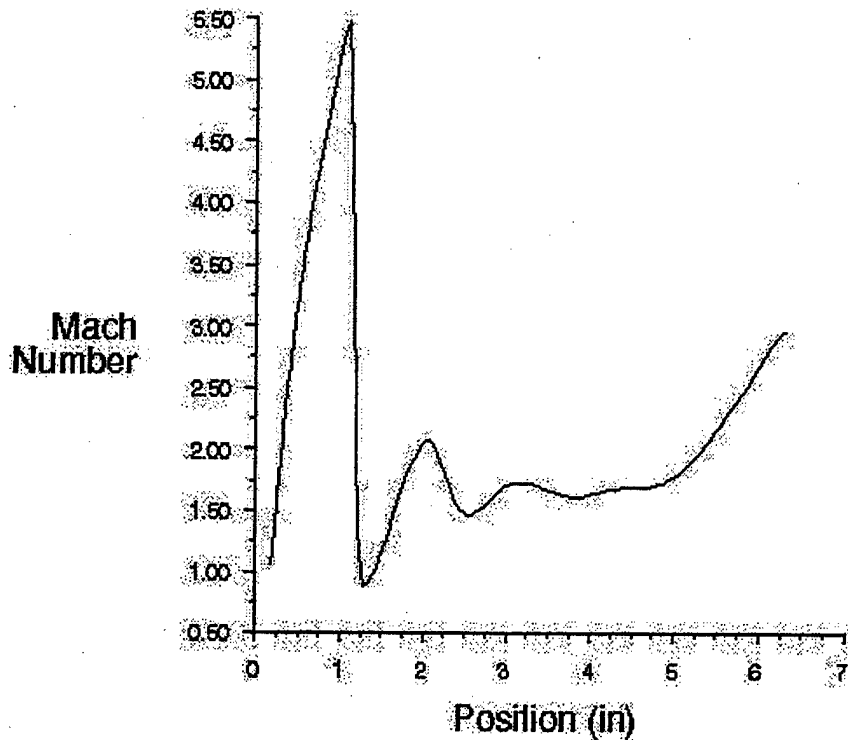
Contours of Mach Number

Jul 03, 1999
FLUENT 5.1 (axi, coupled imp, S-A)

Figure 16. Spalart-Allmaras Mach Number Contours.

The corresponding centerline Mach number profile for this solution is given in Figure 17. Along the centerline the flow shocked to subsonic conditions just downstream of the Mach disk, rapidly expanded to supersonic conditions and then went through a series of oblique shocks, remaining supersonic through the nozzle throat. It never shocked back to subsonic conditions after expanding downstream of the Mach disk.

axis 39



Mach Number

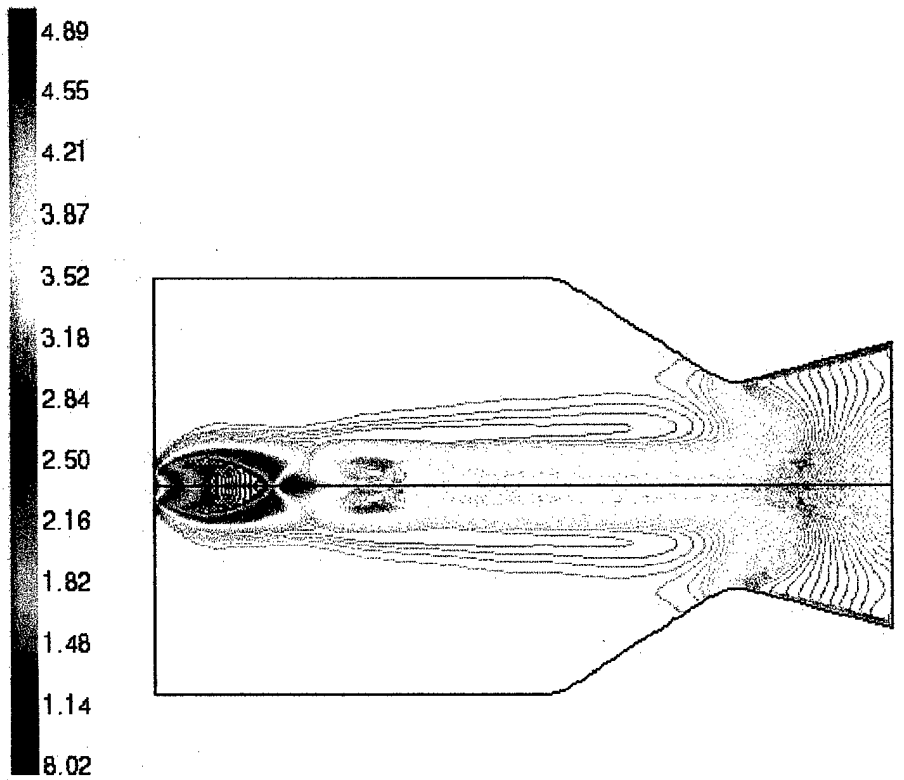
FLUENT 5.1 (axi, coupled imp, S-A)

Jul 04, 1999

Figure 17. Spalart-Allmaras Centerline Mach Number Profile.

c. Static Temperature Contours

Figure 18 shows the static temperature contours for the Spalart-Allmaras model. There was no appearance of recirculation regions outside the shock layers, so the flow in these regions was considered stagnate. From the figure the static temperature on the walls was approximately 4100 °R. This equates to 75 percent of the inlet stagnation temperature for almost the entire surface inside the main chamber.



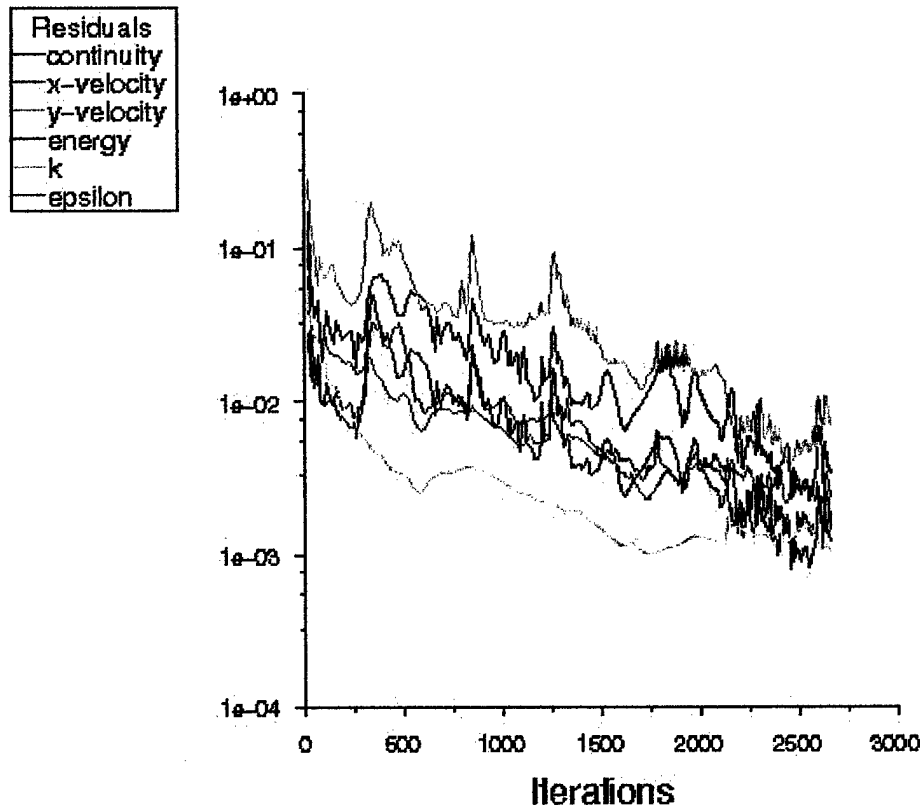
Contours of Static Temperature (Rankine) Jul 03, 1999
 x 10e +3 FLUENT 5.1 (axi, coupled imp, S-A)

Figure 18. Spalart-Allmaras Static Temperature Contours.

4. k - ϵ Turbulence Model Results

a. *Convergence History*

The computed solution using the k - ϵ turbulence model represented the best of the FLUENT 5.1 results in terms of solution convergence. As can be seen from Figure 19, the continuity equation residual has dropped approximately two and a half orders of magnitude after 2,500 iterations, and was still dropping.



Scaled Residuals

Jul 03, 1999
FLUENT 5.1 (axi, coupled imp, ke)

Figure 19. k-ε Convergence History.

b. Mach Number Contours and Centerline Profile

Mach number contours for this solution, shown in Figure 20, were more representative of what has been physically observed in similar types of flows. The highest Mach number achieved was 5.61 and occurred just upstream of a strong Mach disk. A region of subsonic flow following the Mach disk extended downstream of the disk station, terminating just short of the nozzle throat. There was a mixture of subsonic and supersonic flow at the nozzle throat. The subsonic flow started near the throat walls and extended almost one half a throat radii outward, but was supersonic at the centerline.

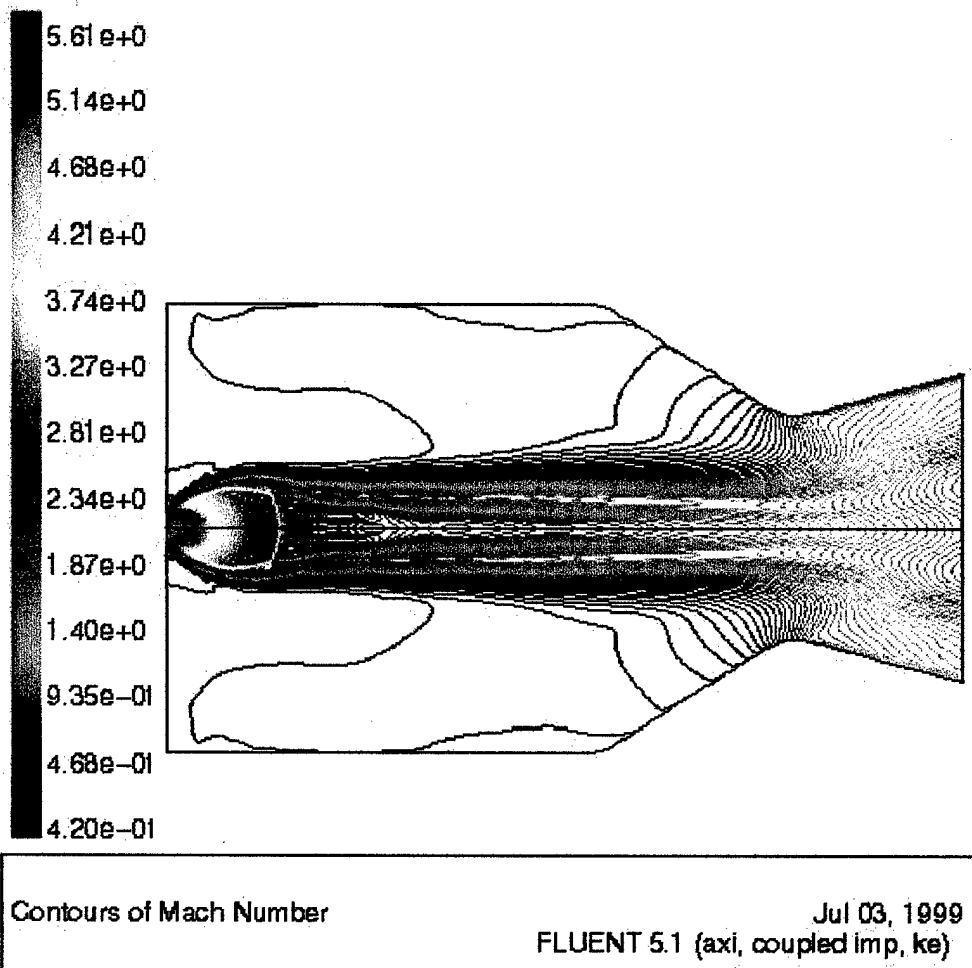
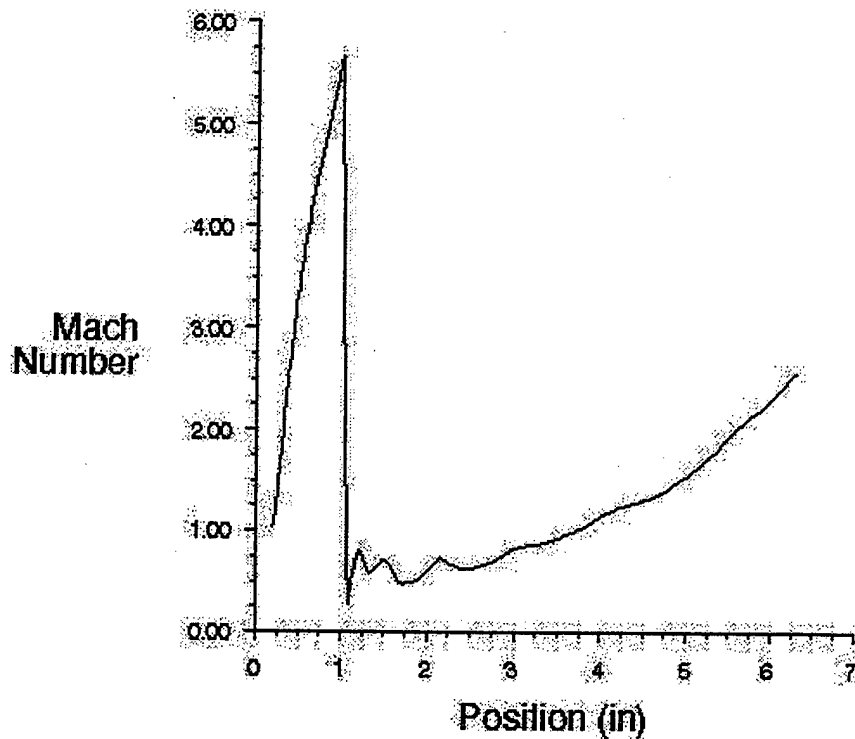


Figure 20. k- ϵ Mach Number Contours.

The profile of centerline Mach number given in Figure 21 shows that the flow was indeed not subsonic at the throat, but was approximately Mach 1.5. The subsonic region downstream of the Mach disk was also visible. Like the inviscid solution the Mach number along the centerline did not immediately expand to supersonic conditions. It did, however, reach sonic conditions upstream of the throat station. From Figure 21 it can be seen that at x equals 4.0 inches the flow was again sonic. This location was approximately one third of the way into the converging nozzle section, so the effective throat station for the centerline of the flow was inside the convergent section of the nozzle and not at the physical throat.

axis.39



Mach Number

Jul 04, 1999
FLUENT 5.1 (axi, coupled imp, ke)

Figure 21. k-ε Centerline Mach Number Profile.

c. Static Temperature Contours

Figure 22 shows the static temperature contours for the k-ε turbulence model. The hottest region were at the same locations as the Spalart-Allmaras turbulence model, but the static temperature of the flow at these locations was slightly lower. From the figure the static temperature in these areas was approximately 3900 °R, which would be almost 70 percent of the inlet stagnation temperature.

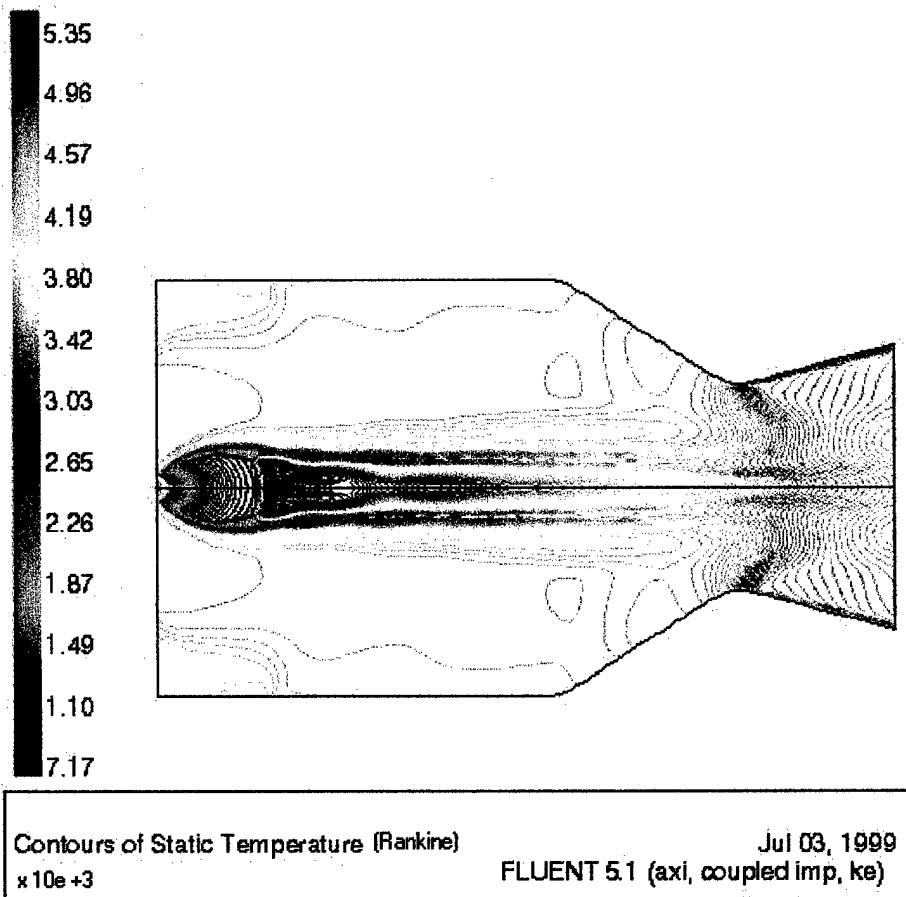


Figure 22. k-ε Static Temperature Contours.

B. OVERFLOW TWO-DIMENSIONAL MODEL RESULTS

1. Boundary Conditions

OVERFLOW does not require the input of an initial condition, so only boundary conditions need be specified. The type of boundary conditions used were similar to that of FLUENT; however, the implementation used in OVERFLOW was slightly different from FLUENT.

The main difference in implementation was that the pressure outlet boundary of the main chamber was specified by a pressure ratio instead of with a pressure value. The value used for this represented the ratio of the outlet static pressure to inlet total pressure and was set to 0.0001 or 10,000 for the inlet total to outlet static pressure ratio. This was

slightly lower than that which was used in FLUENT, but it was of the same order of magnitude so it was not assumed to affect differences for the respective solutions from OVERFLOW. For the single-block two- and three-dimensional models the pressure inlet boundary was defined as a freestream boundary with Mach number of 1.0. This was based upon the assumption that the flow from the igniter was choked at the inlet to the main chamber. This was the same assumption used for the FLUENT model. The inlet stagnation temperature was also defined as 5598 °R. All wall boundaries were specified with either inviscid wall conditions or viscous wall conditions, depending on whether the solution was computed using an inviscid flow or a turbulence model. The assumptions of the properties of the fluid were the same as those used for the FLUENT model. All input files used within OVERFLOW are given in Appendices D, E and F.

2. Inviscid Model Results

As with the FLUENT model, an inviscid model proved instrumental to qualitatively understanding the internal flow of the main chamber. The results for this model are given below.

a. Convergence History

Figure 23 shows the convergence history of the inviscid solution computed within OVERFLOW. The density residual dropped approximately four orders of magnitude, using the full multi-grid capability within OVERFLOW. The residual did not level until approximately 20,000 iterations were computed. A solution was also computed without using the full multi-grid capability to ensure that it was not affecting the solution. Both computations reached the same convergence.

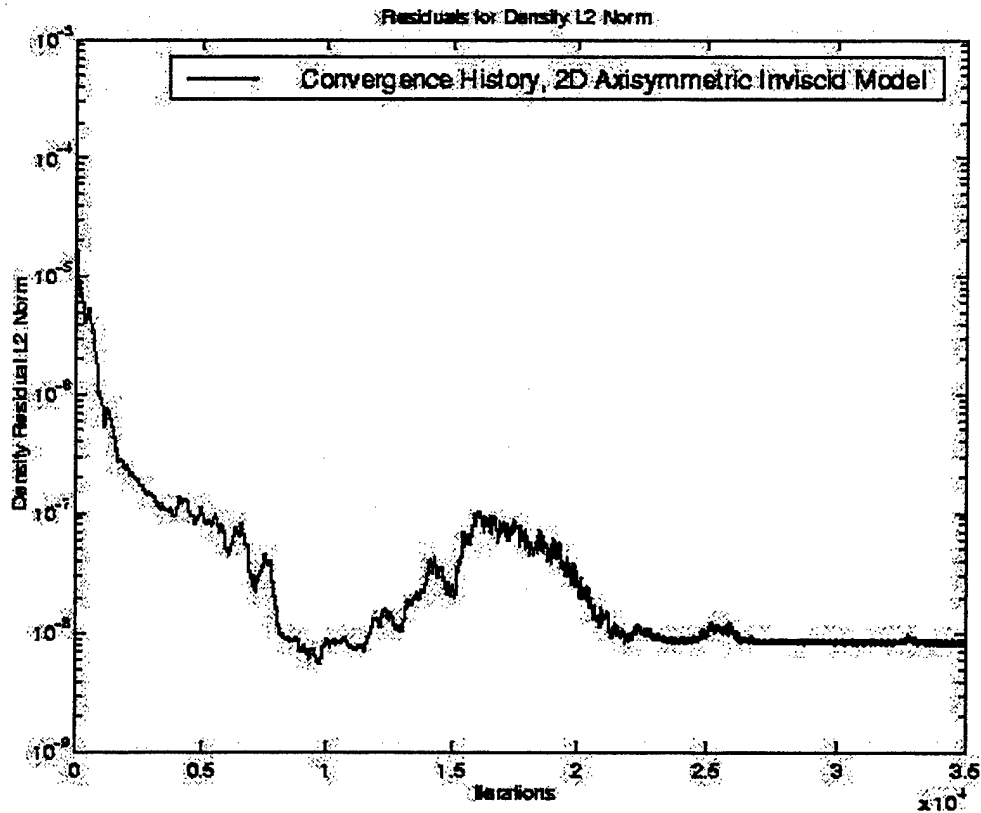


Figure 23. Inviscid Convergence History.

b. Mach Number Contours and Centerline Profiles

Mach number contours for this solution are shown in Figure 24. The jet exhausted through the igniter exit and expanded radially without forming the overall barrel shock structure. The Mach disk was almost a complete normal shock with oblique shocks extending from the triple point to the chamber walls. See Figure 1(a) for the triple point location. The maximum Mach number achieved during expansion was 6.43. A Mach number contour chronology is given in Appendix C, showing the development of Mach number contours from 5,000 to 30,000 iterations.

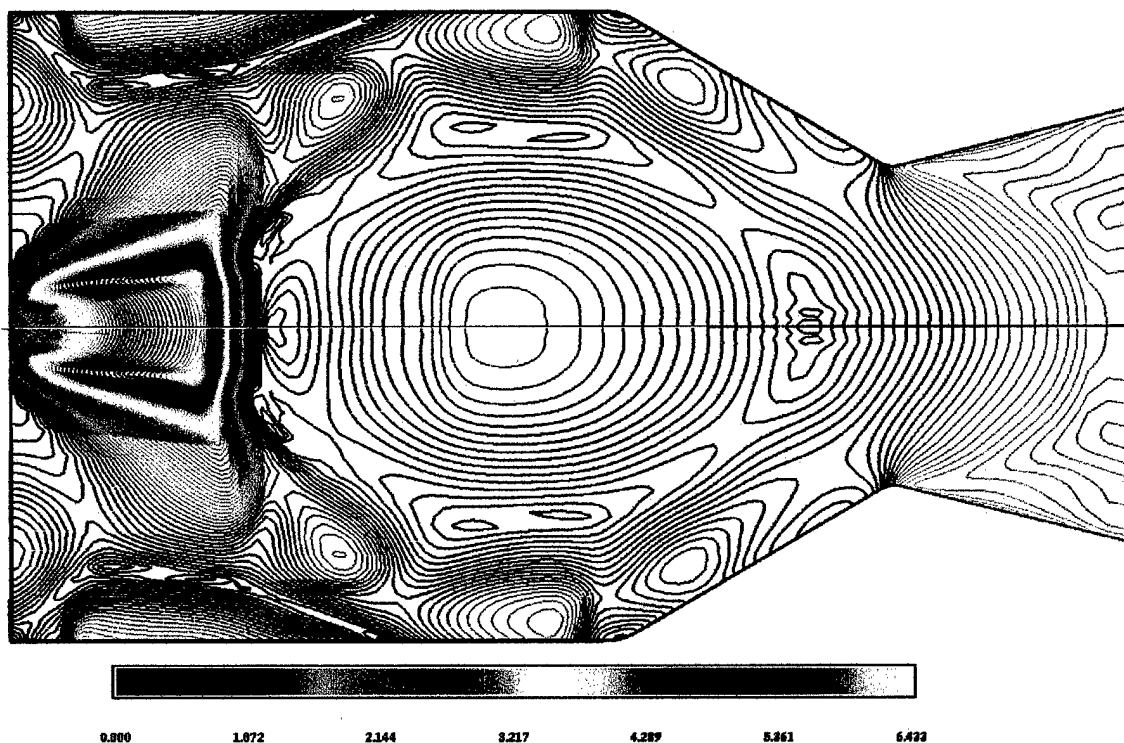


Figure 24. Inviscid Mach Number Contours.

Recirculation zones formed in the regions outside the expansion layers and in the center of the chamber, downstream of the normal shock. The recirculation zone velocity vectors just downstream of the normal shock were directed back towards the igniter faceplate.

Figure 25 shows the centerline Mach number profile. The flow decelerated to zero velocity at the end of the Mach disk, re-expanded to supersonic conditions, and then shocked to almost zero velocity inside the converging nozzle section. At the flow centerline of the throat, the flow was subsonic.

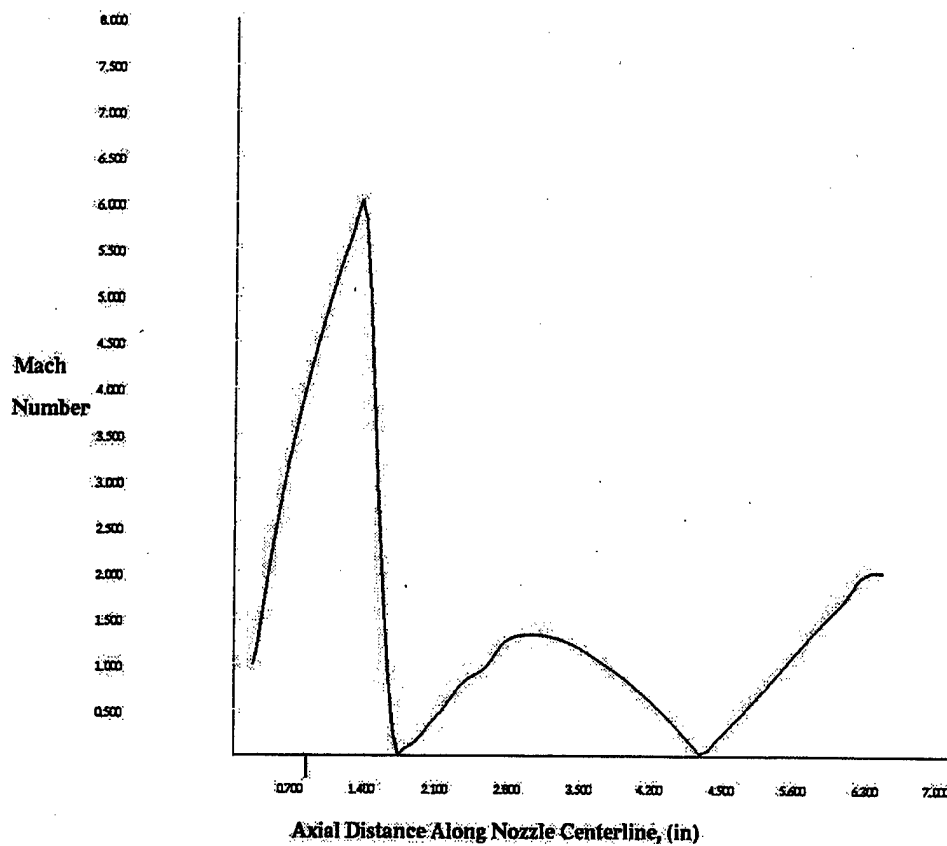


Figure 25. Inviscid Centerline Mach Number Profile.

As can be seen from Figure 26, there was a region of supersonic flow near the throat walls. Physically, this would not occur since viscosity and an adiabatic wall boundary would form a boundary layer at the throat wall, which would decrease the velocity in the boundary layer. The majority of the flow at the throat was subsonic.

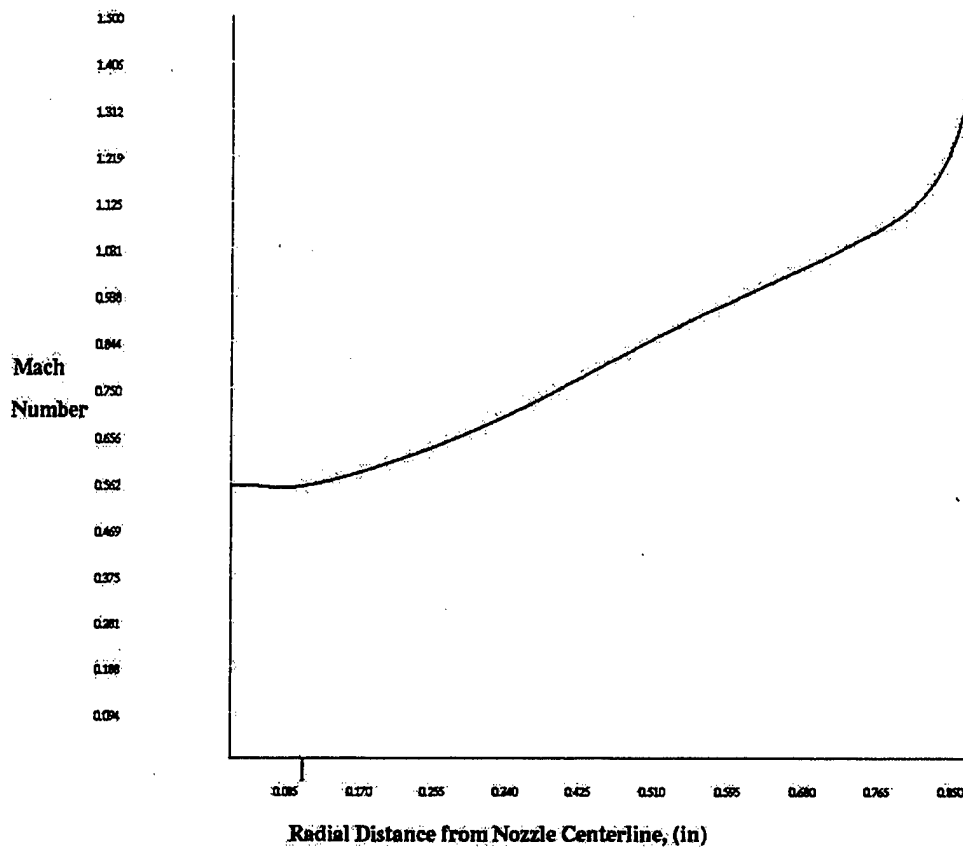


Figure 26. Inviscid Throat Radial Mach Number Profile.

c. Static Temperature Contours

The corresponding normalized static temperature contours are shown in Figure 27. Almost all of the wall surfaces inside the main chamber were above 80 percent of the inlet stagnation temperature.

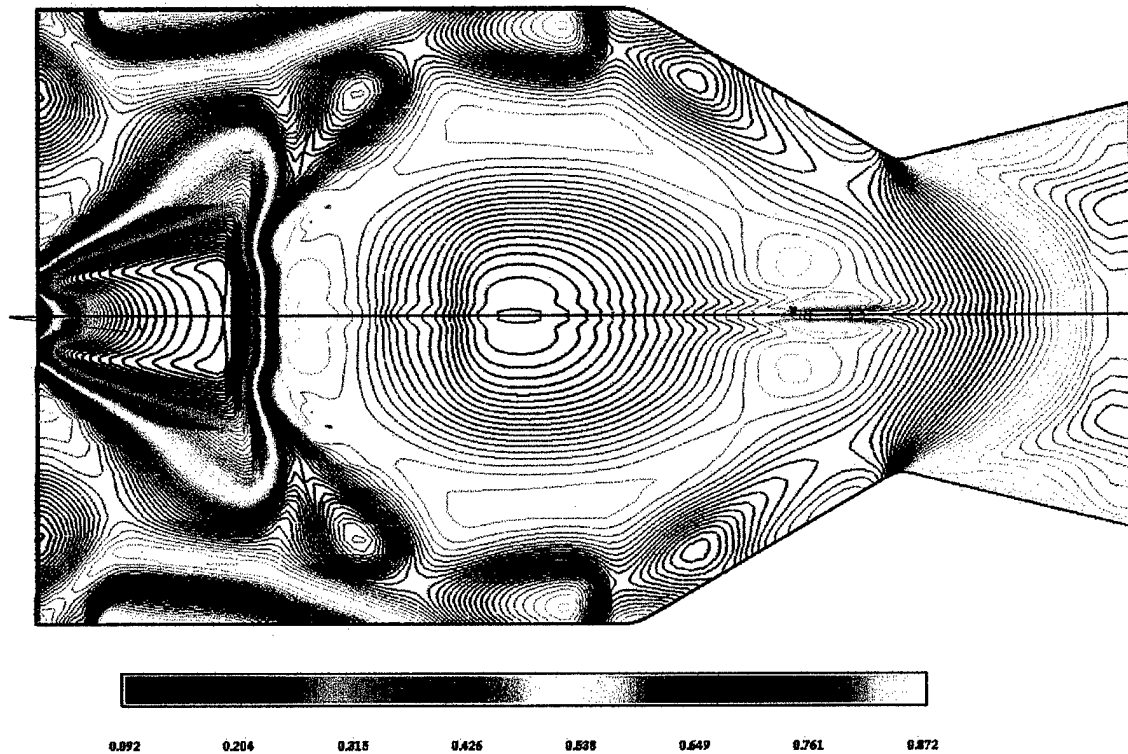


Figure 27. Inviscid Normalized Static Temperature Contours, (5598° R = 1.0).

3. Spalart-Allmaras Turbulence Model Results

a. Convergence History

Figure 28 shows the convergence history using the Spalart-Allmaras turbulence model. The density residual dropped almost nine orders of magnitude before rising again, leveling off and then oscillating periodically. The contours and profiles of Mach number and static temperature that follow were taken from the leveled portion of the solution.

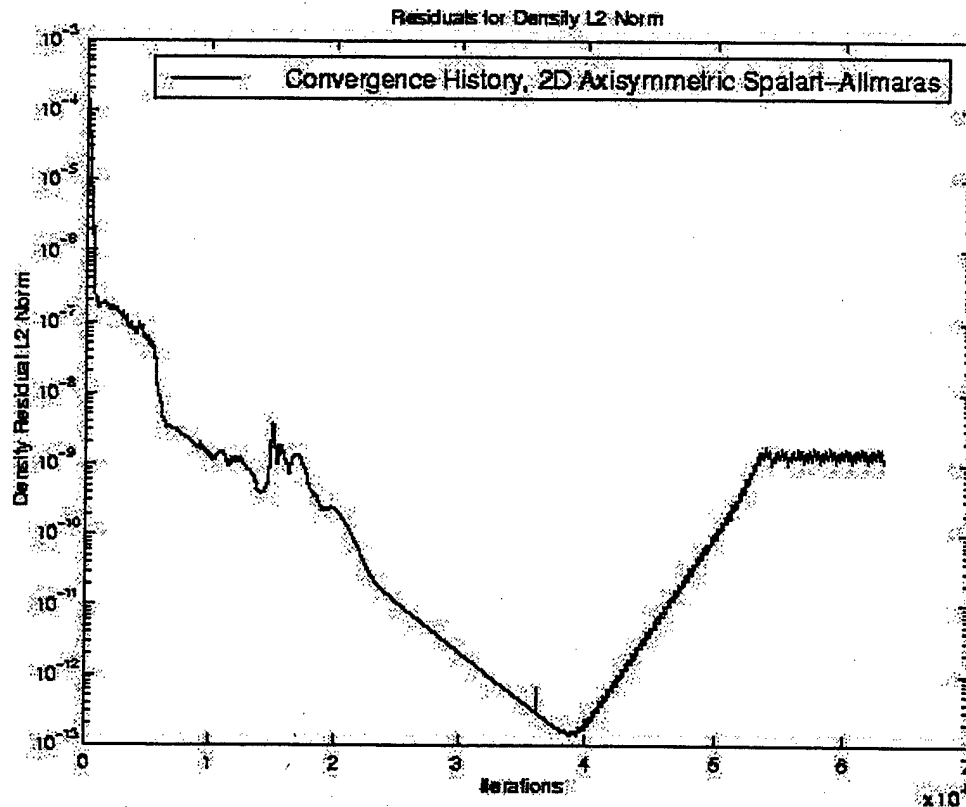


Figure 28. Spalart-Allmaras Convergence History.

b. Mach Number Contours and Centerline Profiles

The Mach number contours for this model were very similar to those of the underexpanded freejet. Figure 29 shows that the barrel shock structure with Mach disk and shock layer regions were well defined. Recirculation predominated the region of the flow outside the barrel shock and shock layer regions. This flow was directed back towards the injector faceplate and appeared to be almost sonic. There was also a subsonic layer between the outer recirculating flow and the barrel shock/shock layer regions. The maximum Mach number achieved was also greater than that of the inviscid solution.

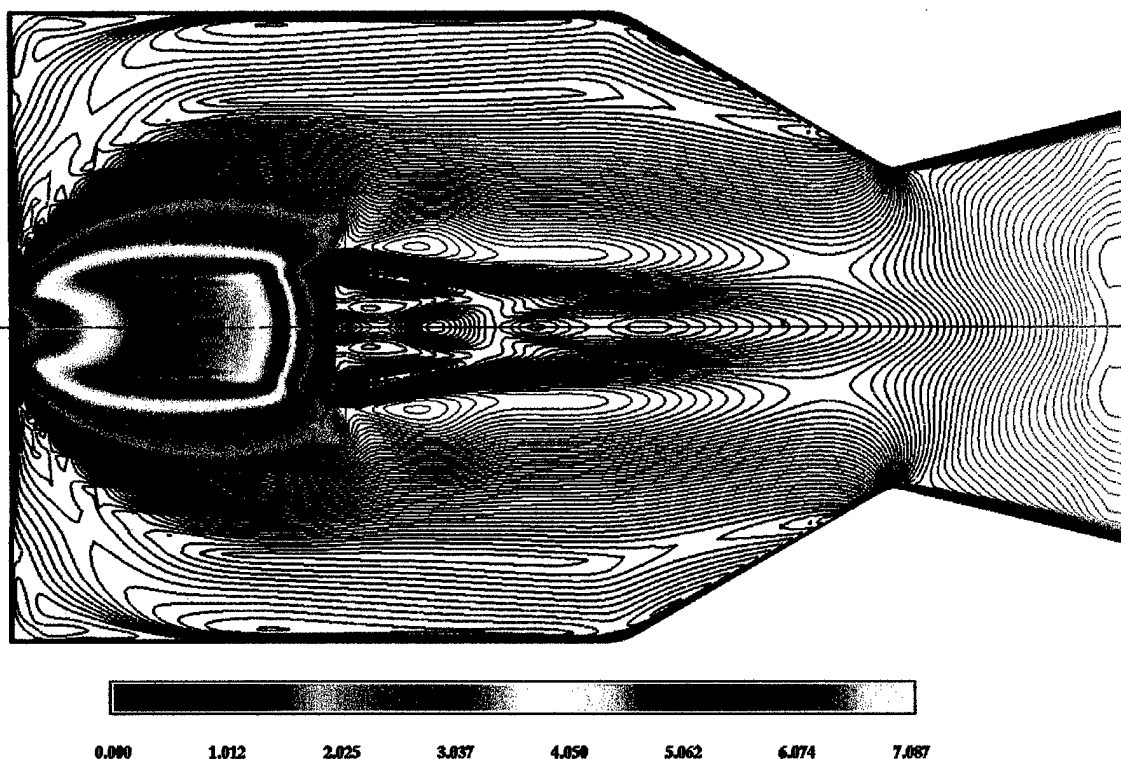


Figure 29. Spalart-Allmaras Mach Number Contours.

The centerline Mach number profile is shown in Figure 30. This profile was quite different from that of the inviscid solution. The location of the Mach disk was slightly downstream of the inviscid solution's position. The subsonic portion of the flow downstream of the Mach disk was evident and oscillated subsonically until expanding to near sonic conditions at the throat.

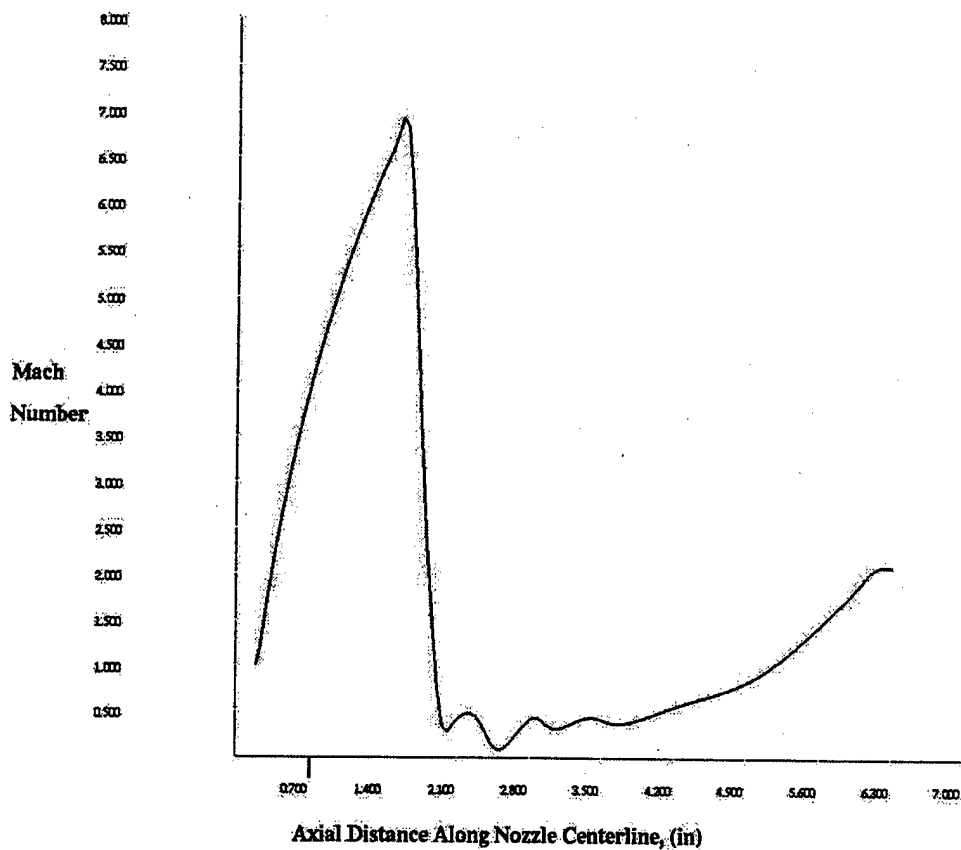


Figure 30. Spalart-Allmaras Centerline Mach Number Profile.

The corresponding radial Mach number profile at the throat is shown in Figure 31. At the centerline, the flow was almost sonic with a region becoming supersonic, returning to subsonic and finally zero at the throat wall. In a one-dimensional sense the flow was essentially choked.

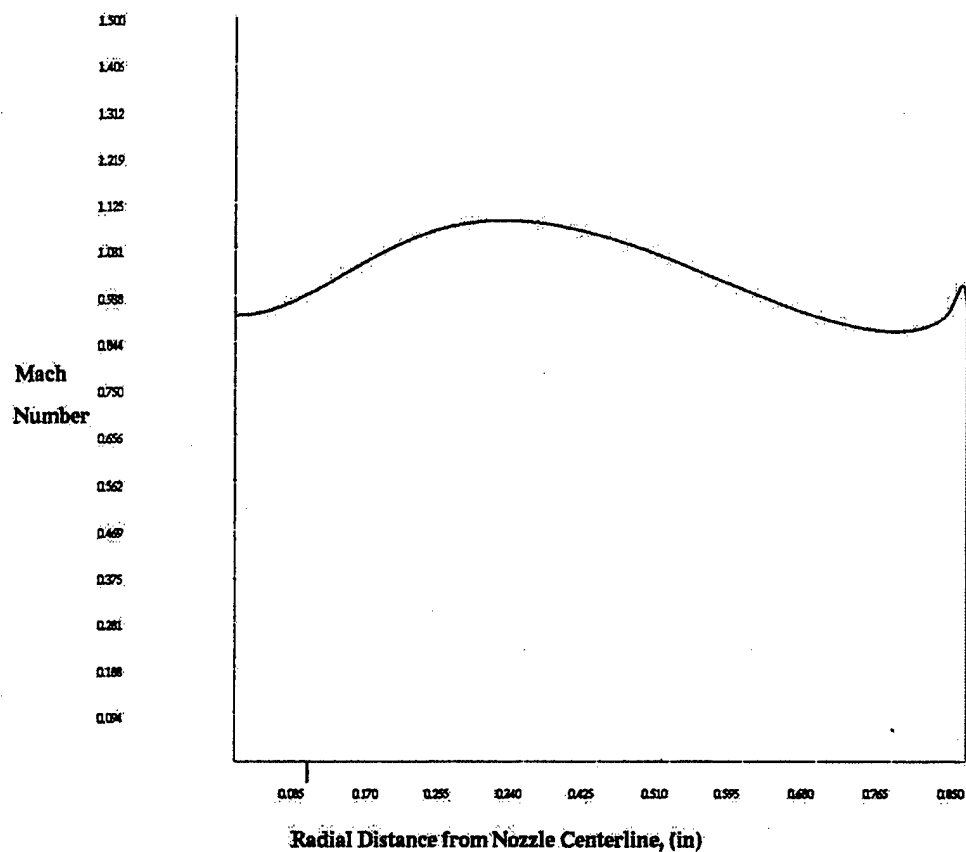


Figure 31. Spalart-Allmaras Throat Radial Mach Number Profile.

c. Static Temperature Contours

Figure 32 shows the normalized static temperature contours of this solution. The entire wall surface inside the main chamber and converging nozzle were above 80 percent of inlet stagnation temperature.

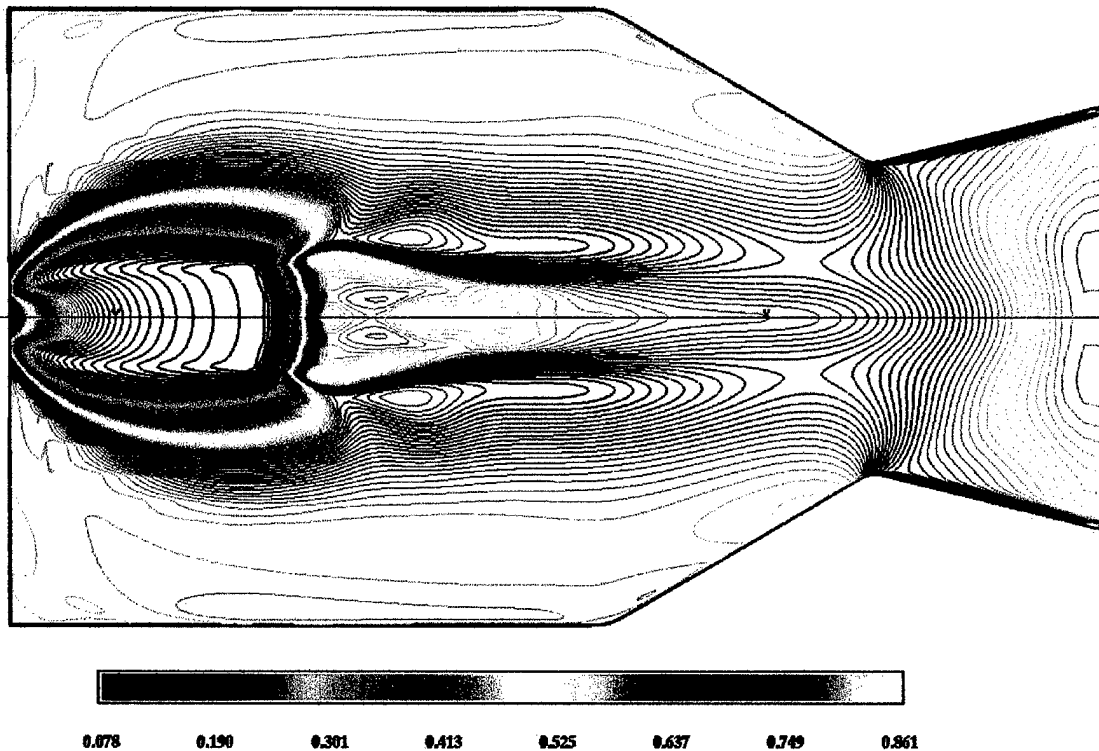


Figure 32. Normalized Static Temperature Contours, (5598° R = 1.0).

4. $k-\omega$ Turbulence Model Results

a. *Convergence History*

As with the residual convergence of the FLUENT two-equation $k-\epsilon$ turbulence model, the convergence of the two equation $k-\omega$ turbulence model residuals was also the best of the three intra-solver solutions. Figure 33 shows the convergence history computed using this turbulence model. After 70,000 iterations the residuals still continued to drop with no oscillation.

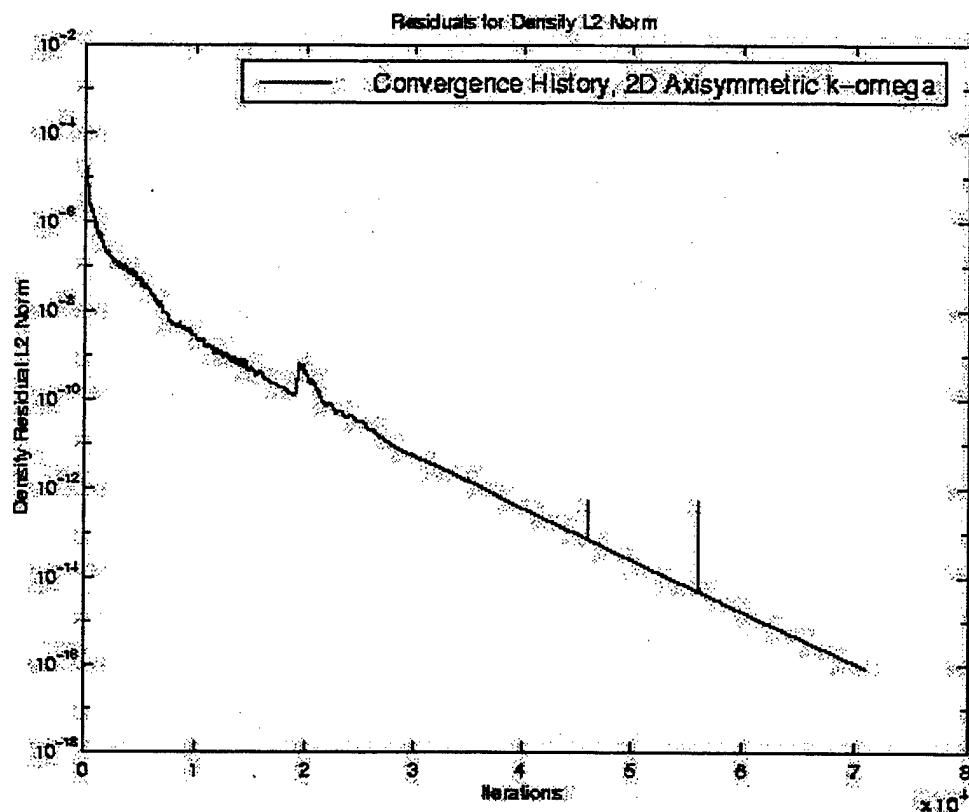


Figure 33. k - ω Convergence History.

b. Mach Number Contours and Centerline Profiles

By far the k - ω turbulence model solution displayed the best overall subsonic/supersonic patterns compared with those of Figure 1. Figure 34 shows the Mach contours of this solution. The supersonic mixing layer region extending from the triple point showed a likely expansion/compression pattern. This mixing layer region enclosed the subsonic Mach disk mixing layer region through the throat. Reflected shocks were also shown in the supersonic mixing layer region. The Mach disk structure was very well defined and did not display the distortion evident in the Spalart-Allmaras turbulence model solution. The maximum Mach number was slightly higher, as well.

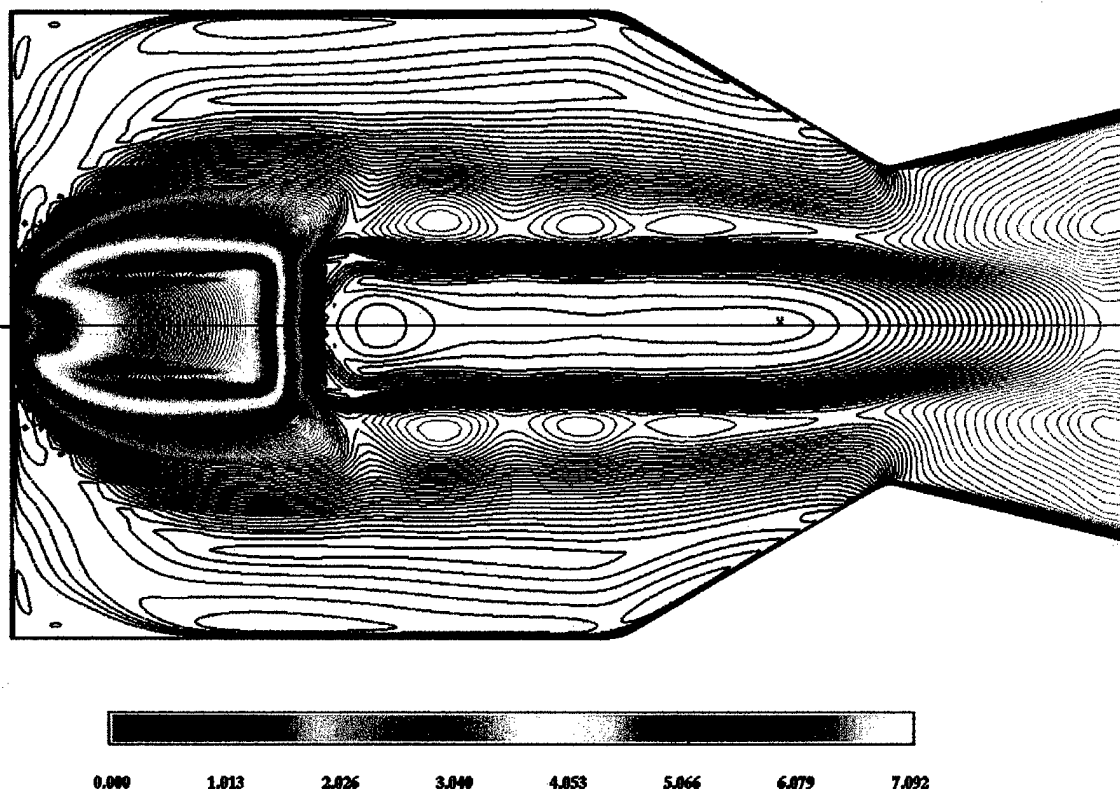


Figure 34. $k-\omega$ Mach Number Contours.

Figure 35 shows the centerline Mach number profile for this solution. The centerline Mach number profile looked similar to the OVERFLOW Spalart-Allmaras solution profile with the exception of the number of subsonic oscillations in Mach number downstream of the Mach disk. The location of the Mach disk was almost coincident with that of the Spalart-Allmaras solution, which was downstream of the location in the inviscid solution.

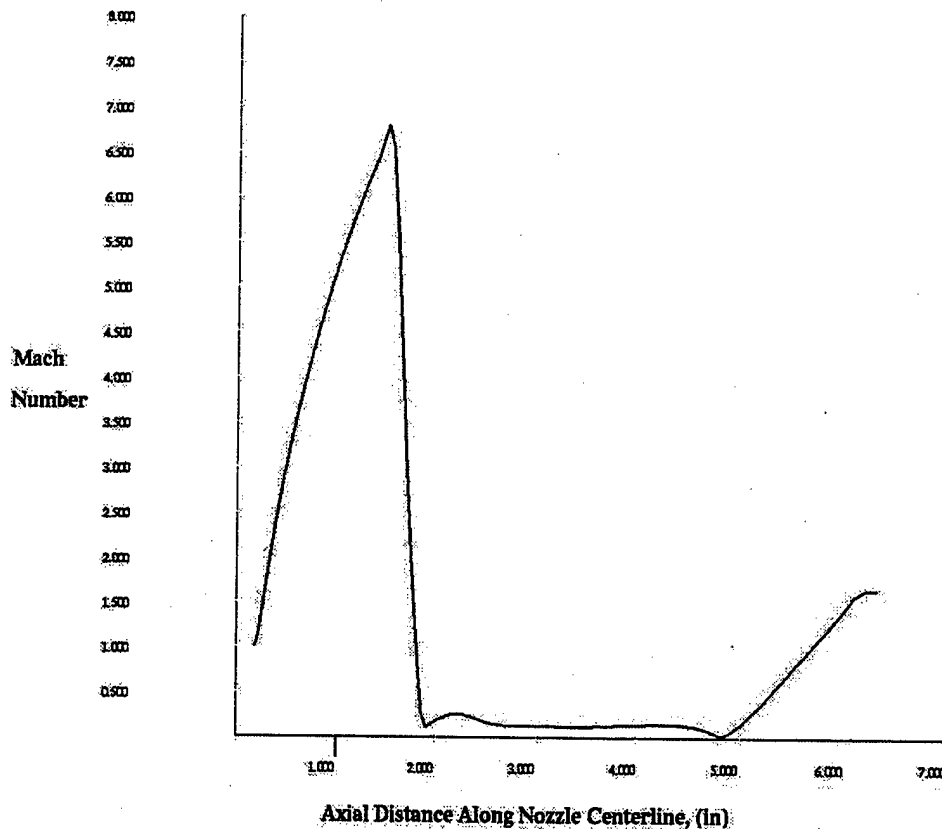


Figure 35. $k-\omega$ Centerline Mach Number Profile.

Figure 36 shows the radial Mach number profile at the throat. The centerline of the flow was at Mach 0.2, but reached sonic conditions less than half a radii from the centerline. The slope representing the rate of change from subsonic to supersonic conditions at the throat was much steeper than the Spalart-Allmaras model's solution. The boundary layer at the throat wall was also thinner than that of the Spalart-Allmaras model.

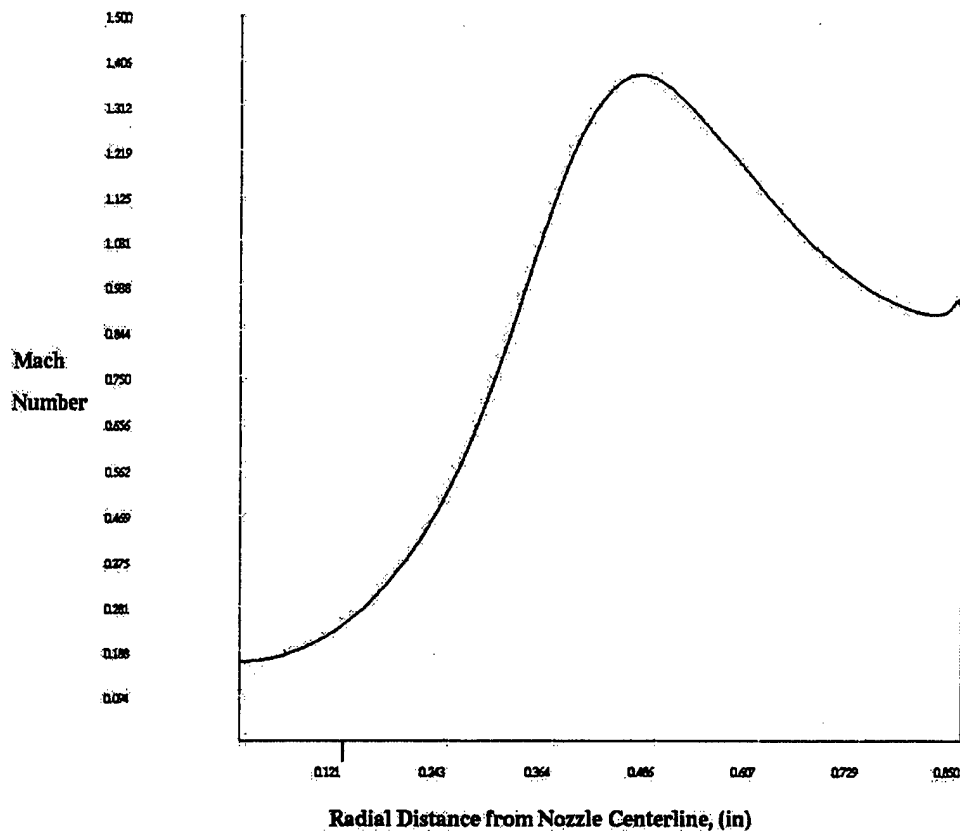


Figure 36. $k-\omega$ Throat Radial Mach Number Profile.

c. Static Temperature Contours

The corresponding normalized static temperature contours for this flow are given in Figure 37. Once again, almost the entire surface of the main chamber walls and converging nozzle were above 80 percent of inlet stagnation temperature.

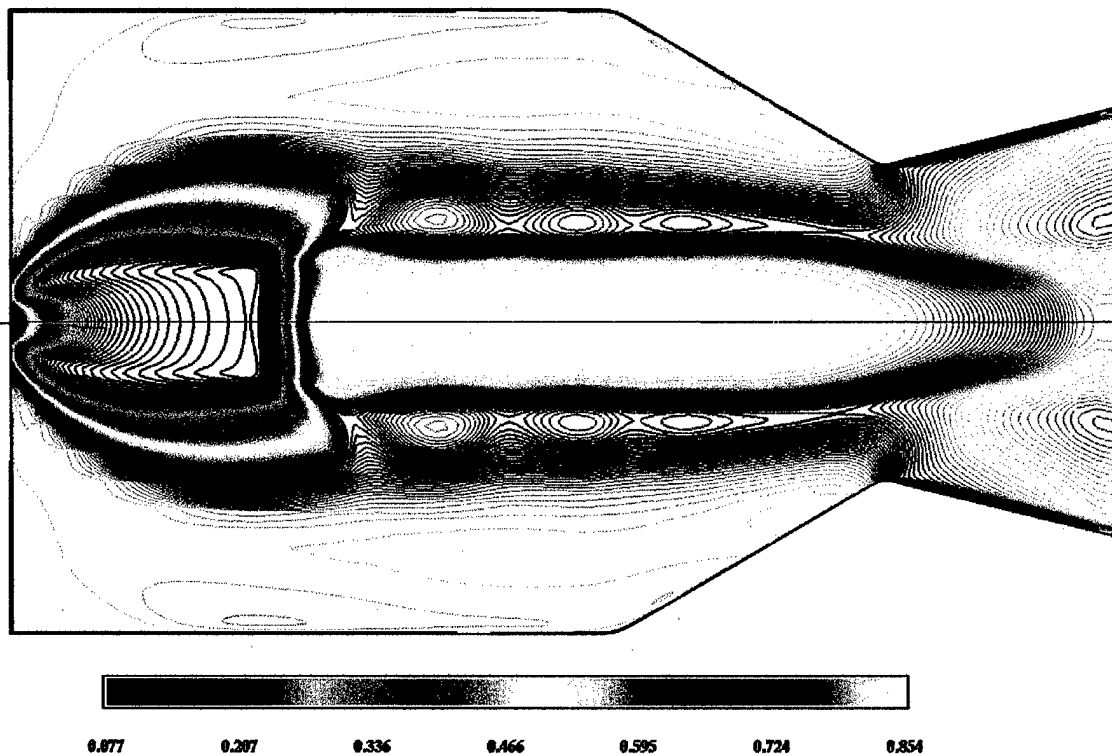


Figure 37. Normalized Static Temperature Contours, (5598° R = 1.0).

C. COMPARISON OF FLOW SOLVER RESULTS FOR TWO-DIMENSIONAL MODELS

Overall the solutions for the OVERFLOW models were definitely better than those of the FLUENT models. Using the FLUENT solver a converged inviscid solution could not be obtained. Perhaps, with more time and computational resources this would not have been the case.

The upwind-differencing scheme used in FLUENT may also have contributed to solution convergence difficulties, not only for the inviscid solution, but also for the turbulence model solutions as well. A Roe upwind-differencing scheme was also used, briefly, within OVERFLOW, but a converged solution could not be obtained even at high levels of dissipation.

For the OVERFLOW inviscid model the central-differencing scheme still had minor convergence problems as a small time step, $DT = 0.1$, had to be used to get through the rise that occurred after approximately 10,000 iterations. Also upon leveling out, the inviscid solution became non-physical. Appendix C shows Mach number contours at various iterations. From 5,000 to 8,000 iterations the Mach disk structure was well maintained, but then after approximately 10,000 iterations the recirculating flow immediately downstream of the Mach disk seemed to push the shock layer region radially outward, enlarging the Mach disk and destroying the barrel shock. This formed the large normal shock in the chamber shown in Figure 24.

The solution computed using the FLUENT Spalart-Allmaras turbulence model also seemed somewhat non-physical. The flow downstream of the Mach disk immediately expanded to supersonic conditions and was never again subsonic. From Figure 17, the distance between the end of the Mach disk shock and the point where the flow became supersonic was about one-quarter of an inch in length. Comparison with the FLUENT k- ϵ models and the two turbulence models used within OVERFLOW would suggest that there was a region of subsonic flow downstream of the Mach disk and that the flow does not expand to sonic conditions until much further downstream. Perhaps with better convergence of the FLUENT Spalart-Allmaras model, the region of subsonic flow would elongate downstream.

The Mach disk shock location was further upstream in the solution computed using the FLUENT Spalart-Allmaras model than it was in its OVERFLOW counterpart. Comparing Figure 17 with Figure 30 shows that the difference in location was almost half an inch.

The convergence history of the OVERFLOW Spalart-Allmaras solution was interesting in that it dropped almost nine orders of magnitude before rising and leveling to a constant oscillating pattern. Values of the Mach number were evaluated at the trough of this convergence and found to differ by only approximately 0.02 from the values at the leveled portion. There were no differences in shock location either, but there were slight differences in the amplitude of the oscillations following the Mach disk.

The solution computed using the FLUENT $k-\epsilon$ turbulence model showed the most promising convergence history. After 2,500 iterations it still continued to drop. This was unlike the inviscid and Spalart-Allmaras solutions. A general trend for solutions computed using both FLUENT and OVERFLOW was that the Mach number increased with increasing residual convergence; the $k-\epsilon$ model may have converged to the same levels as the $k-\omega$ model given enough iterations. When compared to the flow structure of similar types of flows, the overall flow structure of the $k-\epsilon$ model was the most similar of the FLUENT models. There was, however, no formation of the recirculation regions outside the barrel shock as there were in the solutions computed using the turbulence models within OVERFLOW. This may have been a product of the upwind-differencing scheme or of the grid resolution of the FLUENT model. Both of the turbulence models used in OVERFLOW clearly showed flow recirculating in the subsonic layers outside the barrel shock, heading back upstream towards the lower pressure of the Prandtl-Meyer expansion region.

The lengths of the subsonic Mach disk layer were also very different for the $k-\epsilon$ and $k-\omega$ turbulence models. Both of these models were the most sophisticated models for their respective solver. The $k-\epsilon$ model's subsonic region downstream of the Mach disk reached supersonic conditions approximately three inches downstream of the disk. The $k-\omega$ model did not reach supersonic conditions until it was well outside the throat or approximately four inches downstream of the disk. This difference in length may be accounted for by the strength of the normal shock in the Mach disk; the $k-\omega$ model shocked from Mach 7.09 while the $k-\epsilon$ shocked from Mach 5.61. The location of the Mach disk for each model was also different.

Acceleration of the flow downstream of the Mach disk in the $k-\epsilon$ model oscillated in similar fashion to the OVERFLOW Spalart-Allmaras model. The $k-\omega$ model did not show the same magnitude of oscillation. It oscillated once and then was constant until it almost reached the throat where it decelerated slightly before expanding.

Comparing the overall results of the two solvers indicated that the solutions computed in OVERFLOW showed much better convergence. The OVERFLOW models

also showed much better flow development in terms of Mach disk structure and regions of subsonic and supersonic flow. It should also be noted that the two-equation turbulence models used within each solver produced the best numerical solutions.

D. OVERFLOW THREE-DIMENSIONAL SINGLE-BLOCK MODEL RESULTS

Three-dimensional grids were created for the main chamber and also for a portion of the torch igniter. This was done as a precursor to modeling the flow using multiple grid blocks in which the two single-block grids would be connected using the Chimera scheme. One of the objectives of this multi-block approach was to produce more physically realistic solutions; the effects of the boundary layer inside the igniter chamber could be modeled. Only the results of the main chamber model are discussed at length. Results for the igniter are given in Appendix B.

1. Boundary Conditions

The boundary conditions used for the two-dimensional models were duplicated for the three-dimensional models. The input files used for the three-dimensional models are given in the Appendix E. While the boundary conditions were held the same as the two-dimensional model boundary conditions, the three-dimensional computations did not converge in the same manner as the two-dimensional computations. Each of the three-dimensional models converged to a point, whereupon a negative density arose. This may have indicated a problem with the grid; however, several grids with different spacing along the flow axis were tried and all of them performed in the same manner. It was thought that by using the symmetry plane boundary conditions that each plane would be a duplicate of the other so that, in effect, the three-dimensional models would perform in the same manner as the two-dimensional models. This was not the case; however, all of the three-dimensional models, inviscid, Spalart-Allmaras and $k-\omega$ turbulence models, showed reasonable convergence and were very similar to the two-dimensional computations in terms of Mach number contours.

2. Inviscid Model Results

a. Convergence History

Figure 38 shows the density residual convergence of the solution computed using the inviscid model. The solution dropped approximately two and a half orders of magnitude in 5,000 iterations. This was just short of the point where negative densities were computed.

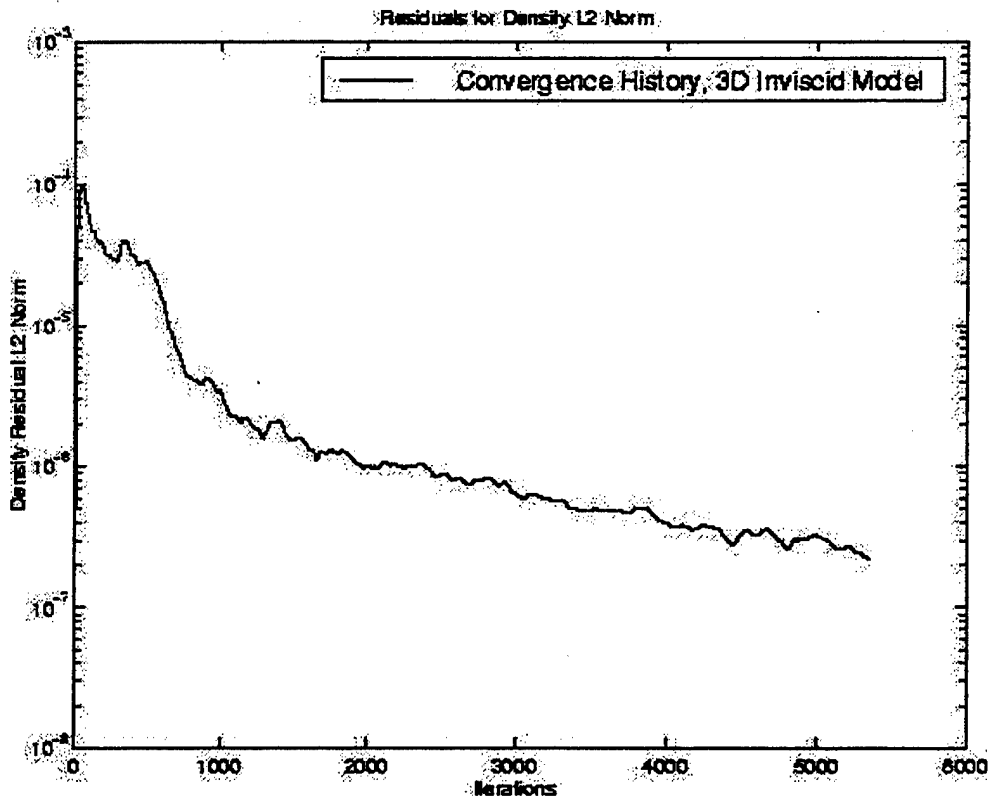


Figure 38. 3D Inviscid Convergence History.

b. Mach Number Contours and Centerline Profiles

Figure 39 shows the Mach number contours for this solution. The contour lines plotted were of two separate planes normal to each other. This was done to show the non-axisymmetry of the solution. As can be seen, the solution contours were not axisymmetric. The Mach disk structure starting at the centerline and extending radially outward was not entirely normal to the direction of flow. The maximum Mach number

was 6.74, which was 4.7 percent greater than the two-dimensional inviscid model's maximum Mach number; however, the two-dimensional solution also became nonphysical. Further iterations of this model would probably have resulted in a non-physical solution.

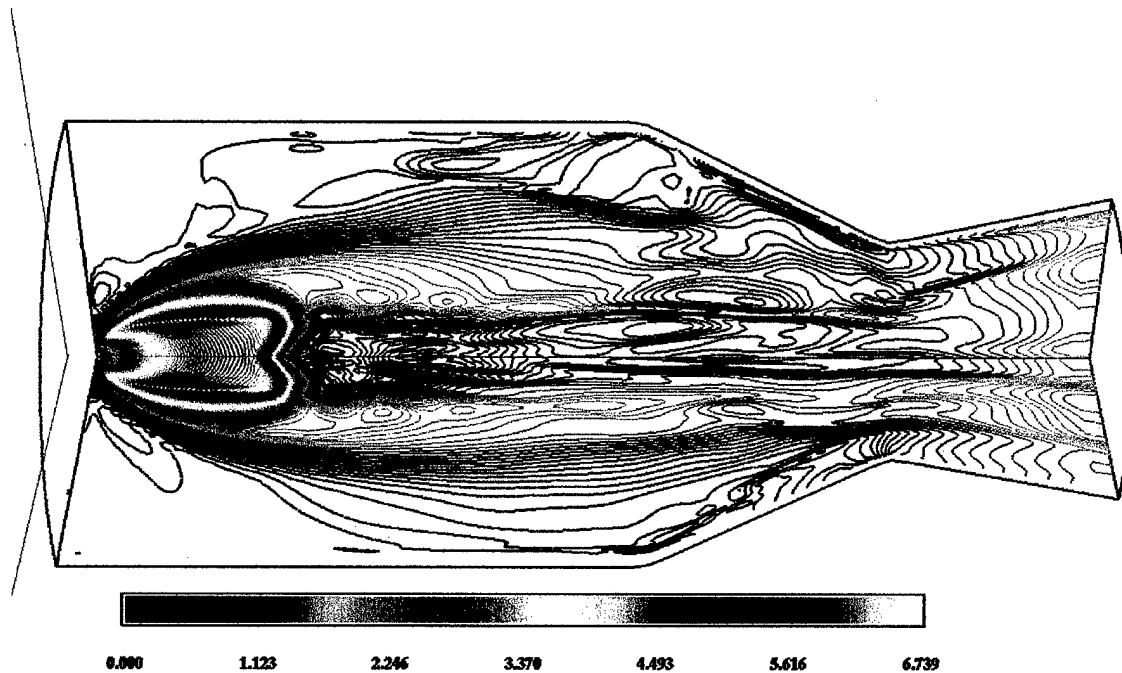


Figure 39. 3D Inviscid Mach Number Contours.

In Figure 40 the Mach number oscillated as the flow re-accelerated and decelerated downstream of the Mach disk. Further downstream the profile rose as the flow reached supersonic conditions, and then at the throat station, which was at a distance of five inches along nozzle centerline on the above figure, the flow decelerated slightly until re-accelerating again out the diverging portion of the nozzle. Comparing Figure 40 with Figure 25 shows that the location of the Mach disk was further downstream for the solution computed using the three-dimensional model.

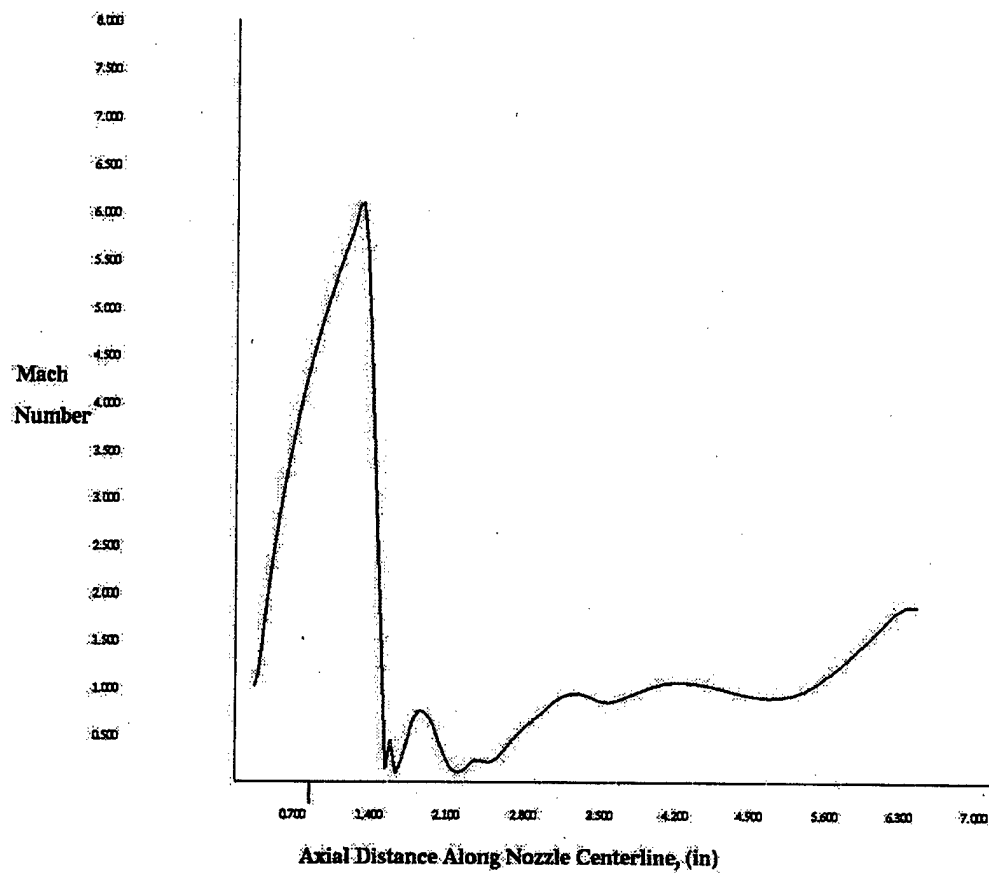


Figure 40. 3D Inviscid Centerline Mach Number Profile.

Figure 41 shows the Mach number profile at the throat. This did not resemble the inviscid two-dimensional solution's profile and looked somewhat erratic.

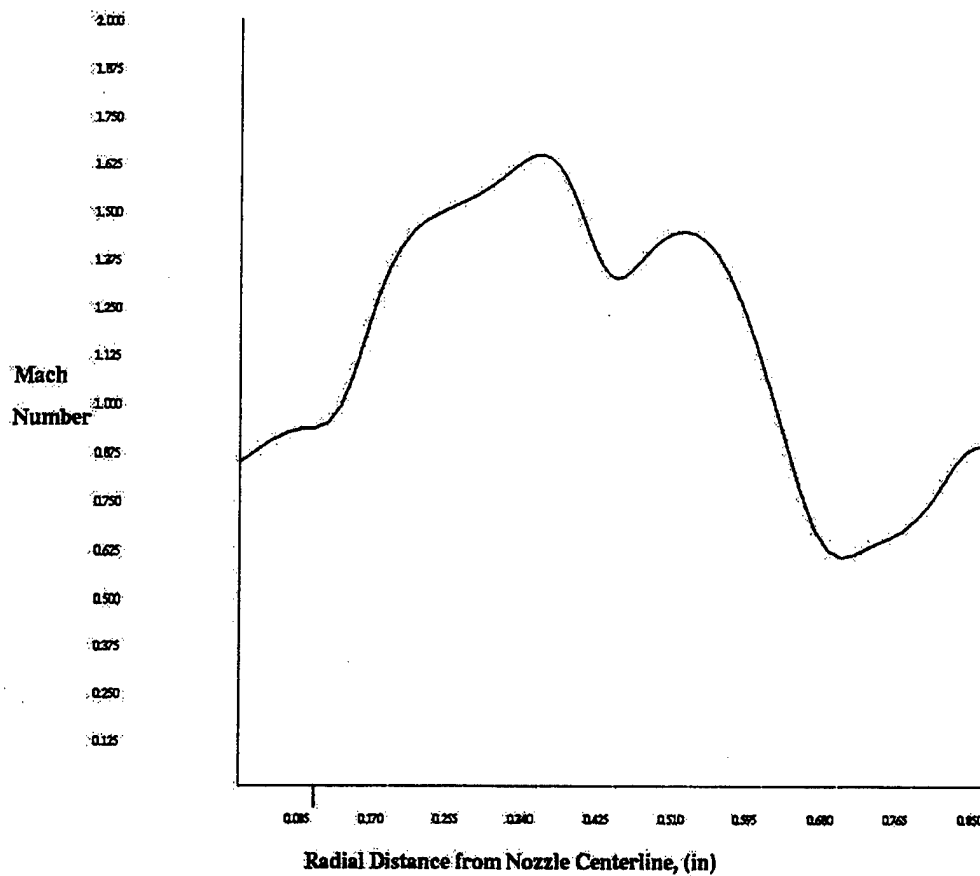


Figure 41. 3D Inviscid Throat Radial Mach Number Profile.

3. Spalart-Allmaras Turbulence Model Results

a. *Convergence History*

Figure 42 shows the density residual convergence history after almost 5,000 iterations. The density residual dropped almost five orders of magnitude, which was approximately the same order of magnitude as the two-dimensional model. The full multi-grid option was used for the first several hundred iterations, which was why the residuals dropped very rapidly after 400 iterations. This was the only three-dimensional model that ran well using the full multi-grid capability of OVERFLOW. This computation was stopped just short of computation of a negative density.

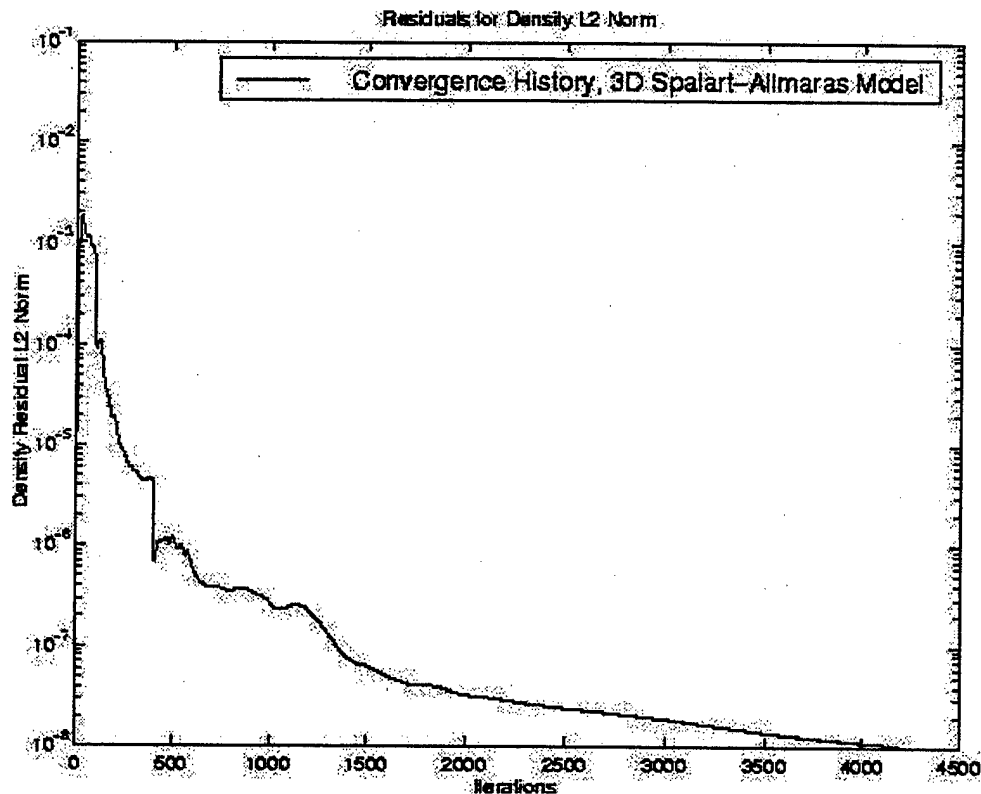


Figure 42. 3D Spalart-Allmaras Convergence History.

b. Mach Number Contours and Centerline Profiles

Figure 43 shows Mach number contours for two grid planes normal to each other. The differences in contours between the two planes was very slight. The contours showed the planar structure of the Mach disk with better resolution than its two-dimensional counterpart. The maximum Mach number was 1.8 percent higher than the two-dimensional solution. This was the most axisymmetric of the three-dimensional models.

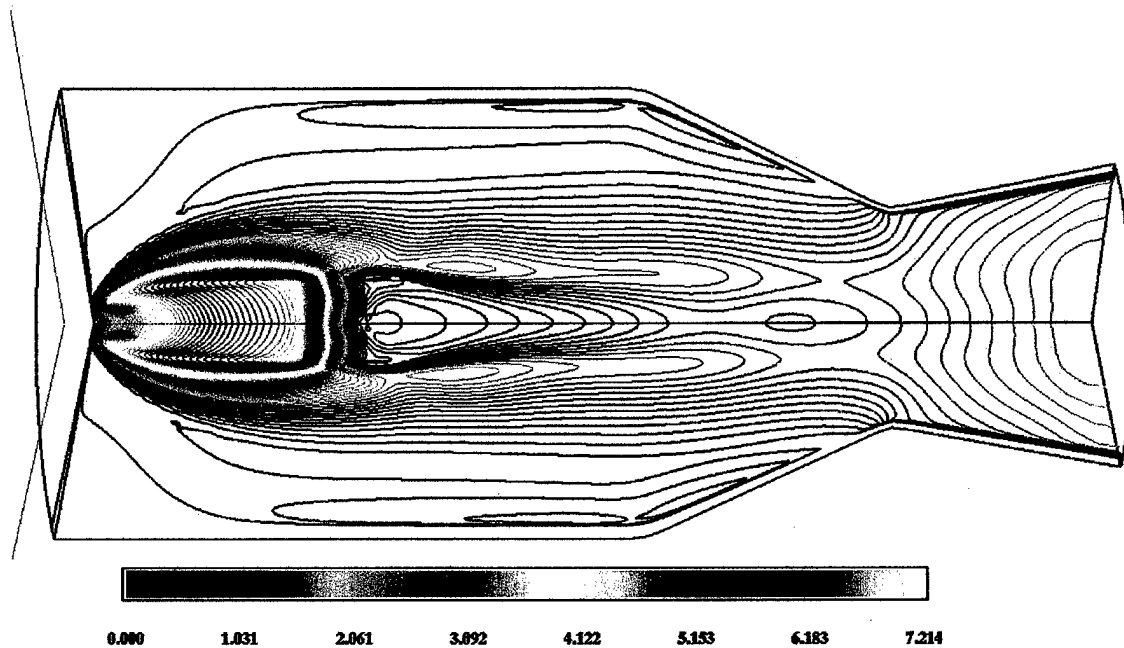


Figure 43. 3D Spalart-Allmaras Mach Number Contours.

Figure 44 shows the Mach number along the nozzle centerline. The flow decelerated to zero velocity at the point where the curve touches the abscissa. The flow then re-accelerated until it was halfway inside the converging nozzle, x equals 4.2 inches. It then decelerated slightly, probably due to the influence of the converging nozzle, until it was at x equals 4.6 inches where it expanded through the throat. The Mach disk was at the same approximate location as the two-dimensional counterpart.

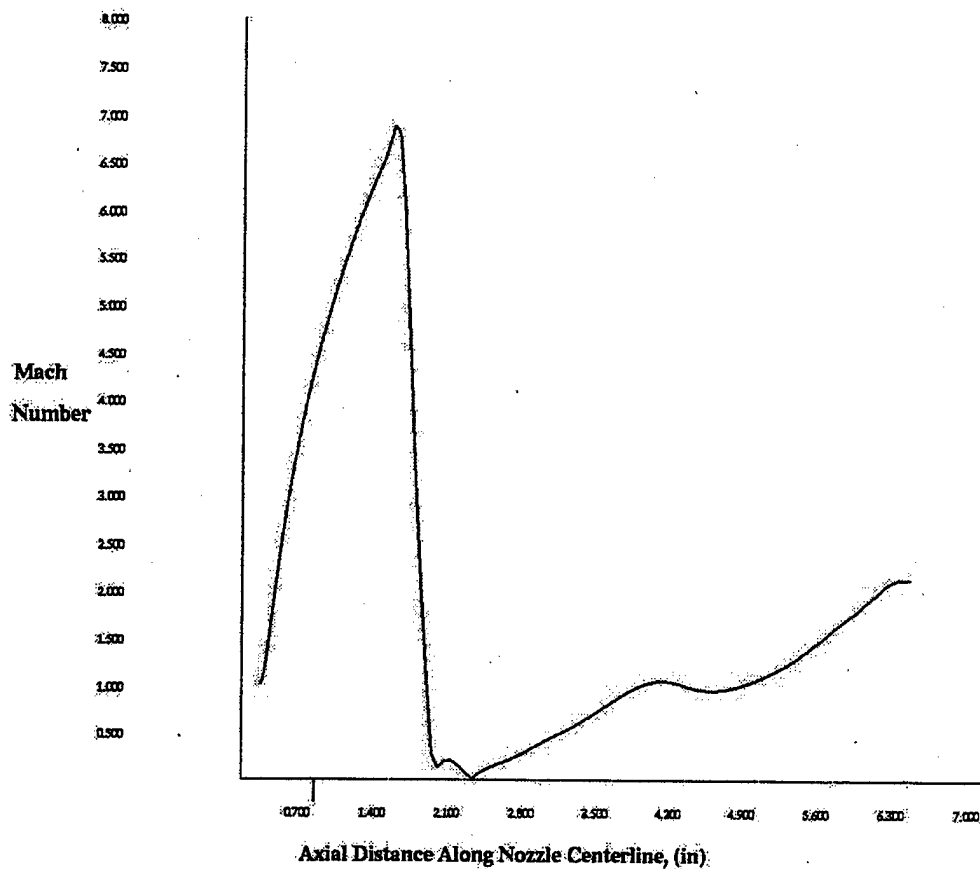


Figure 44. 3D Spalart-Allmaras Centerline Mach Number Profile.

Figure 45 shows the profile of Mach number at the throat. This was different than its two-dimensional counterpart. The Mach number was supersonic along the nozzle centerline at the throat for this model, but was not for the two-dimensional model. The Mach number peaked at the same approximate location as its two-dimensional counterpart, x equals 0.34 inches. The average Mach number was approximately 1.0.

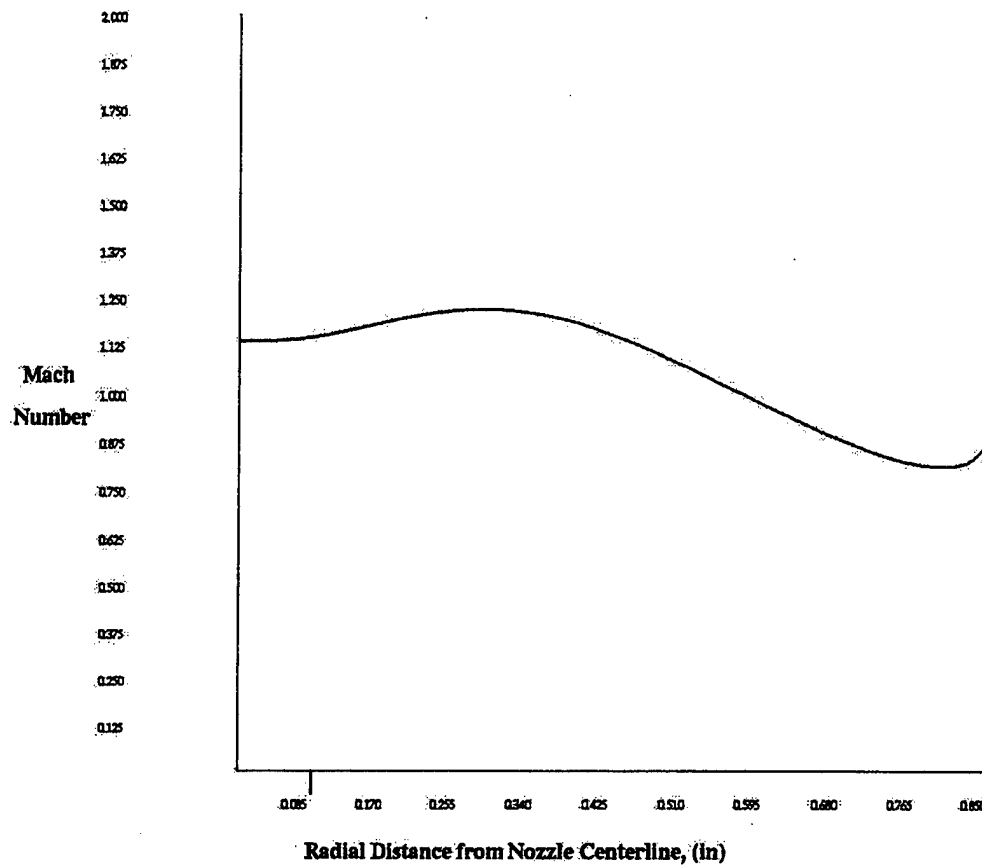


Figure 45. 3D Spalart-Allmaras Throat Radial Mach Number Profile.

4. $k-\omega$ Turbulence Model Results

a. Convergence History

The $k-\omega$ turbulence model density residual convergence history is shown in Figure 46. This was stopped just short of computation of a negative density. The solution only dropped four orders of magnitude, unlike its two-dimensional counterpart that dropped eleven orders of magnitude and was still dropping.

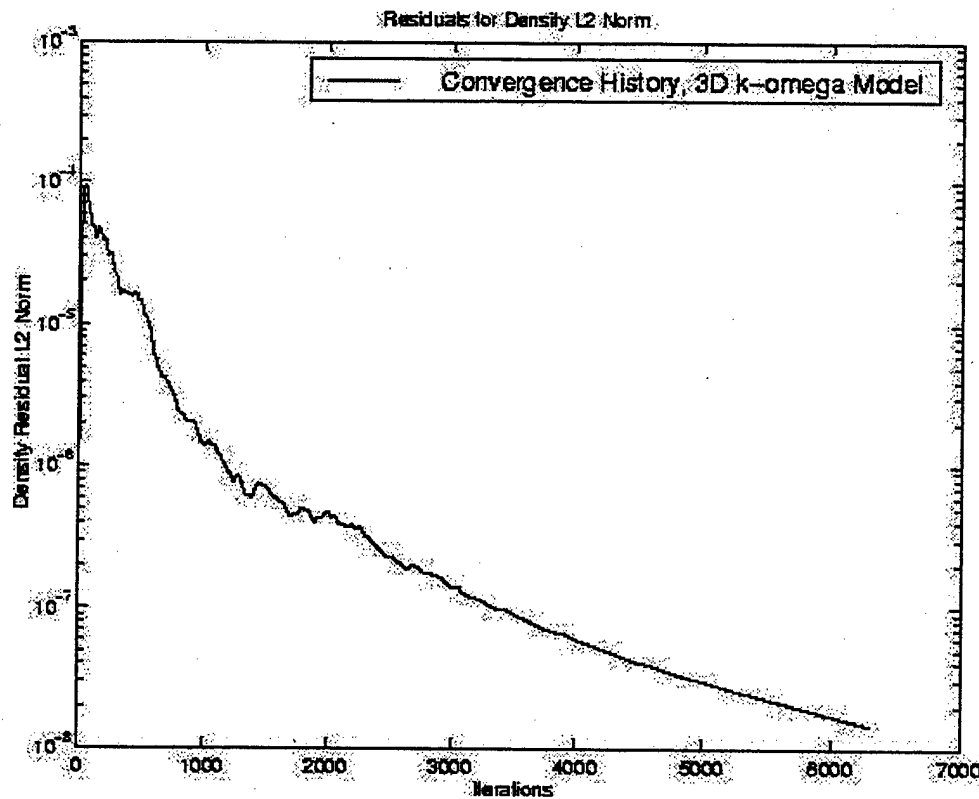


Figure 46. k- ω Convergence History.

b. Mach Number Contours and Centerline Profiles

Figure 47 shows the Mach number contours for this solution. The non-axisymmetry of each of the planes was apparent. The Mach disk structure was well defined and normal to the flow direction. The maximum Mach number was 2.6 percent greater than its two-dimensional counterpart.

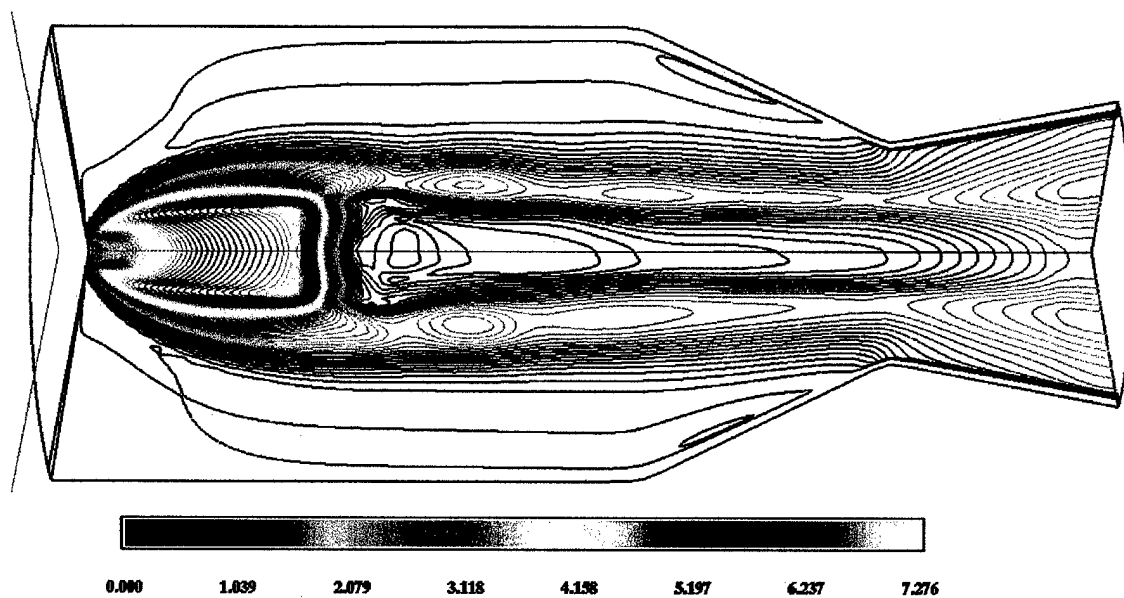


Figure 47. 3D $k-\omega$ Mach Number Contours.

Figure 48 shows the corresponding Mach number along the nozzle centerline. Immediately downstream of the Mach disk, which was in the same approximate location as its two-dimensional counterpart, the flow abruptly accelerated, but did not reach supersonic conditions. It remained level until it was near the throat station where it accelerated and expanded through the divergent nozzle.

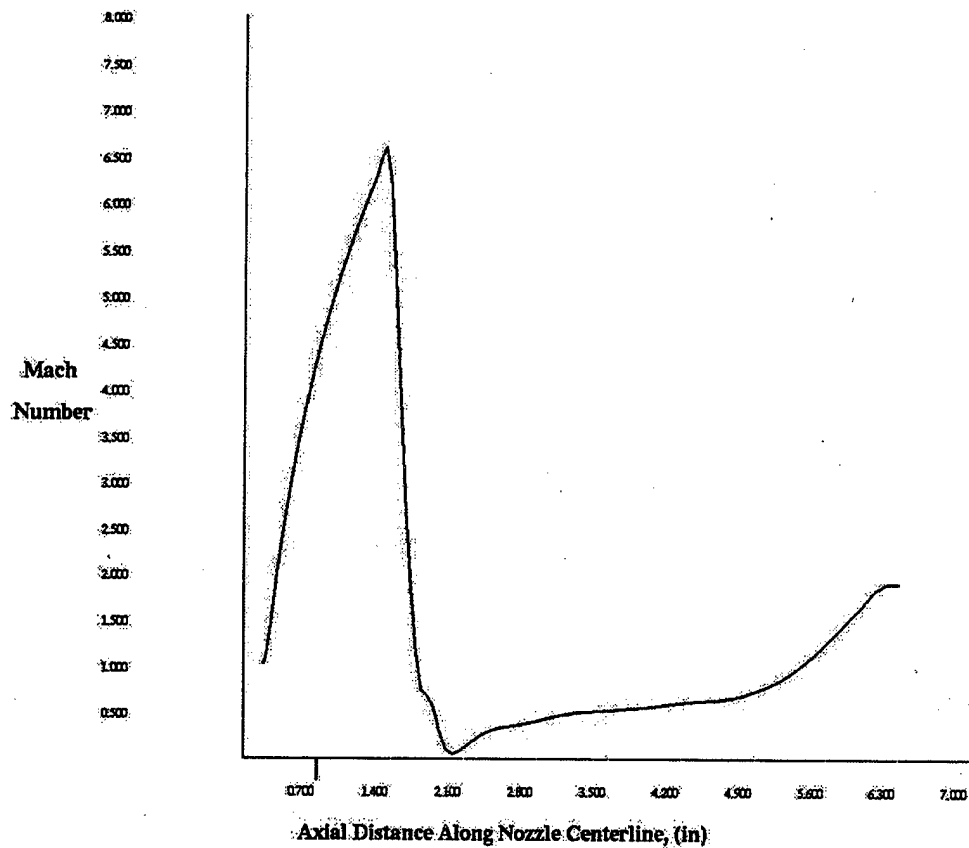


Figure 48. 3D k- ω Centerline Mach Number Profile.

Figure 49 shows the Mach number profile at the throat. The maximum Mach number was higher than its two-dimensional counterpart, but occurred at the same approximate radial location, x equals 0.48 inches from centerline. The ring-shaped region of supersonic flow was approximately 0.4 inches wide at the throat, which was slightly larger than the two-dimensional model's. The boundary layer also looked smaller than its two-dimensional counterpart.

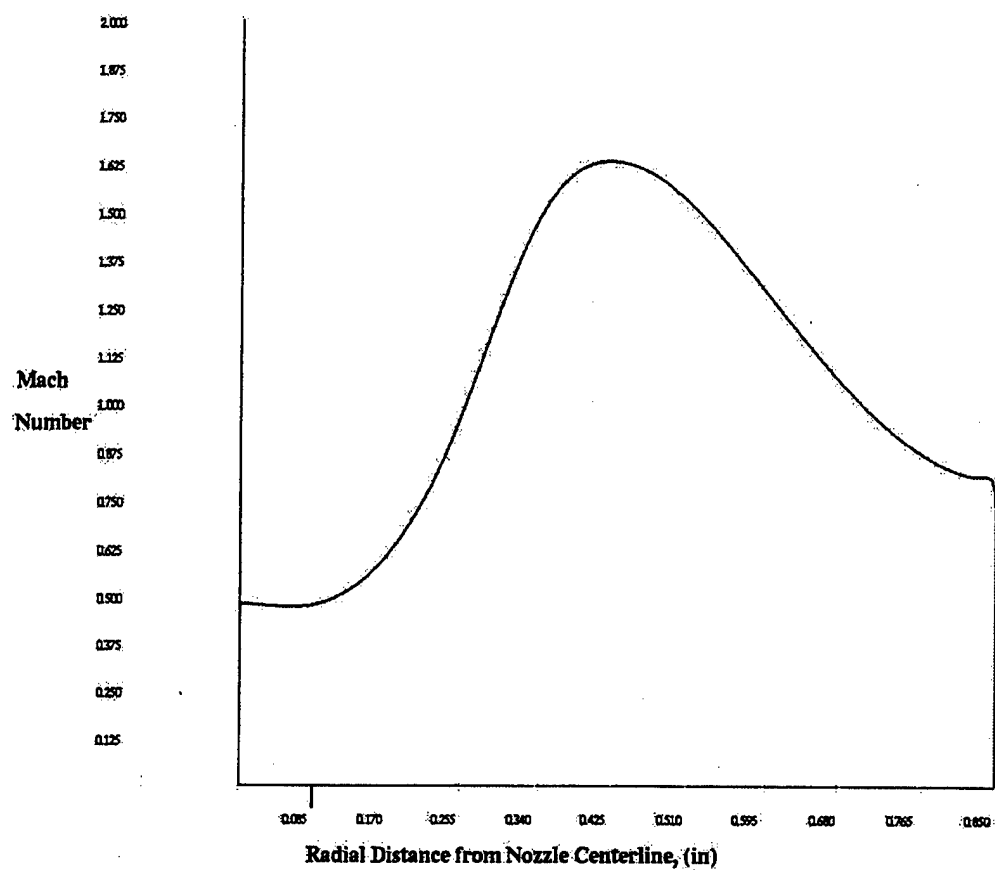


Figure 49. 3D k- ω Throat Radial Mach Number Profile.

E. OVERFLOW THREE-DIMENSIONAL MULTI-BLOCK MODEL RESULTS

In general, the results computed using the $k-\omega$ turbulence model were considered to be the best results. For the three-dimensional multi-block model solutions were computed using an inviscid model and the two turbulence models used for the two- and three-dimensional cases. Only the results computed using the $k-\omega$ turbulence model are discussed here. The results computed using the inviscid model and the Spalart-Allmaras turbulence model are given in Appendix H.

1. Boundary Conditions

The boundary conditions were modified slightly from those of the single-block main chamber model. This was done to adjust for the interpolation done by PEGSUS on the surface representing the igniter inlet in the single-block model (boundary conditions 40 and 41 in the input file). The inlet boundary condition on this surface for the single-block model had to be deleted within the OVERFLOW input file for the multi-block model to permit proper interpolation between the main chamber grid and the torch igniter grid. This was key to generating an accurate solution as both grids had to properly communicate with each other. The OVERFLOW input file is provided in Appendix F.

The freestream Mach number was set to 0.3, but was defined at the inlet boundary into the igniter chamber instead of the inlet boundary into the main chamber. Freestream temperature was also reset to 5846 °R from the previous 5598 °R. This temperature was based on the thermodynamic equilibrium combustion temperature of GOX and ethanol given by TEP (mixture ratio 1.8 and igniter chamber pressure of 150 psi) inside the igniter chamber; the temperature previously used was based on the thermodynamic equilibrium combustion temperature of GOX and ethanol at the exit of the igniter, see Appendix K.

2. k - ω Turbulence Model Results

a. *Convergence History*

Convergence history for the k - ω turbulence model is shown in Figure 54. This density residual dropped approximately three orders of magnitude before computation of a negative density. This was an order of magnitude less than its single-block counterpart; however, it appeared to be leveling out and showed no oscillation. The density residual for the igniter chamber dropped six orders of magnitude and was still decreasing.

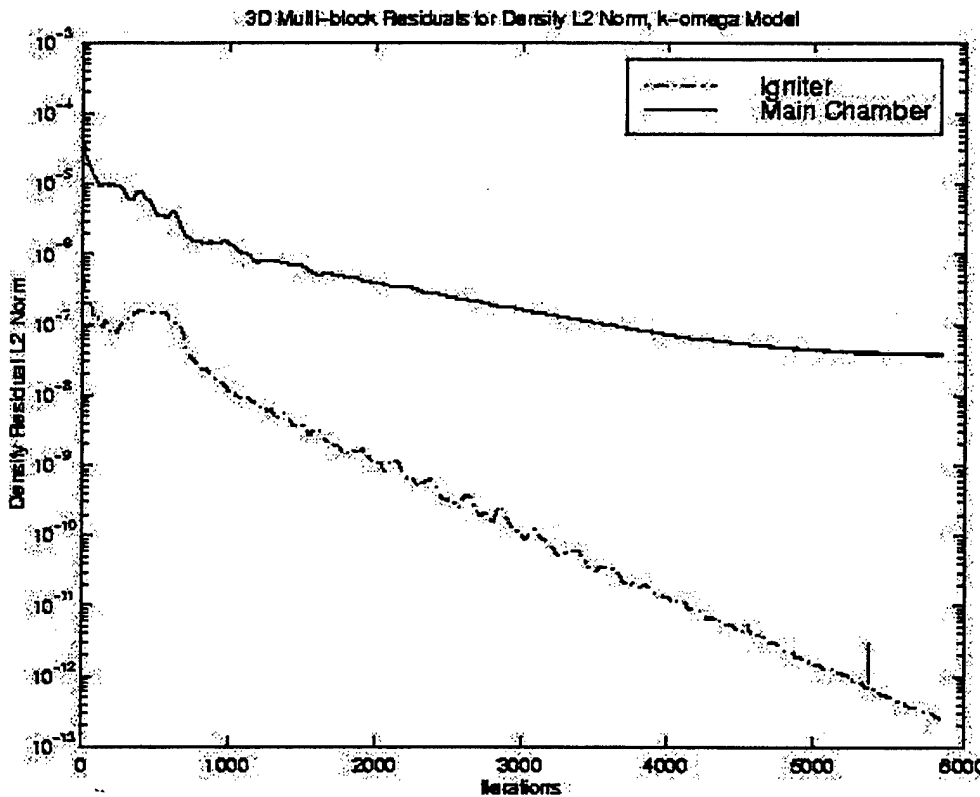


Figure 54. Multi-block k - ω Convergence History.

b. *Mach Number Contours and Centerline Profiles*

Figure 55 shows that axisymmetry was well maintained for this model. The Mach disk structure appeared to be slightly distorted as the normal shock along the centerline appeared to be slightly oblique, slanting in the flow direction from the

centerline to triple point. The overall length of the subsonic layer following the Mach disk was much shorter than the single-block model. The maximum Mach number was also a Mach number less than the single-block model. The effects of interpolation between the two grids and the boundary layer formation inside the igniter most likely affected the computation.

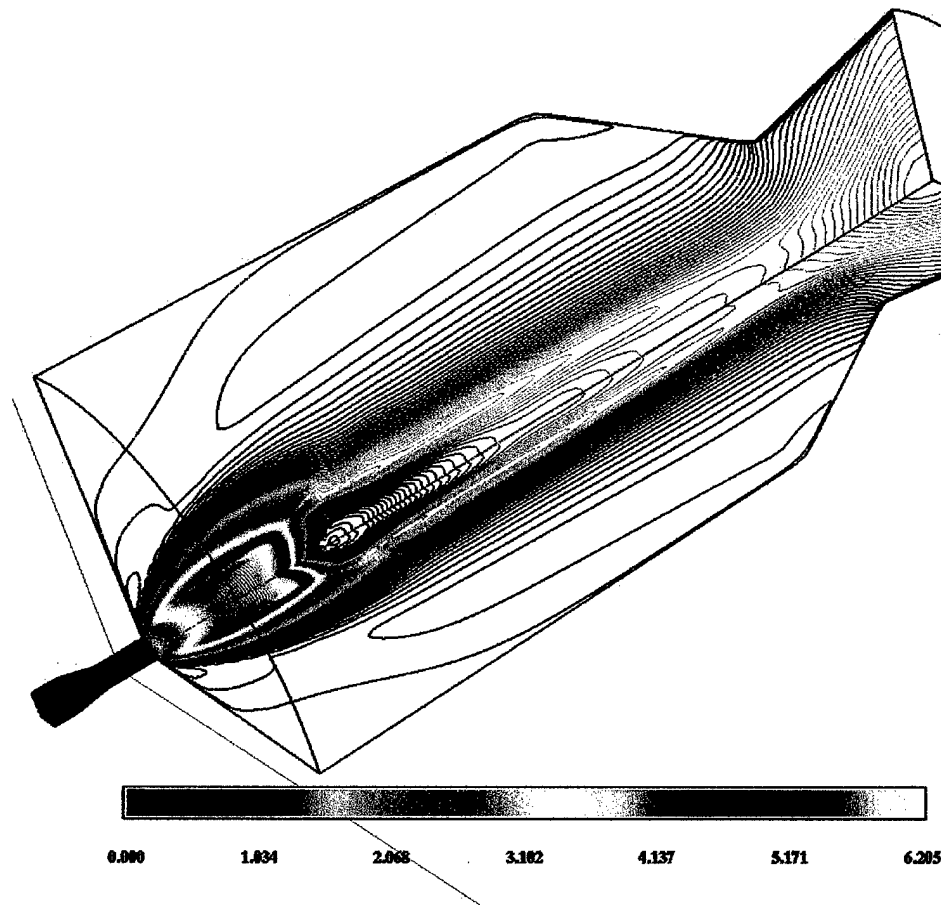


Figure 55. Multi-block $k-\omega$ Mach Number Contours.

Figure 56 shows a close-up view of the igniter chamber and the contours of Mach number running from inside the igniter chamber to the main chamber. The interpolation, which connects the igniter chamber grid to the main chamber grid, created a smooth transition in Mach number through the exit plane of the igniter. Boundary layers

created by the viscous wall boundaries of the $k-\omega$ turbulence model were visible within the constant area section of the igniter.

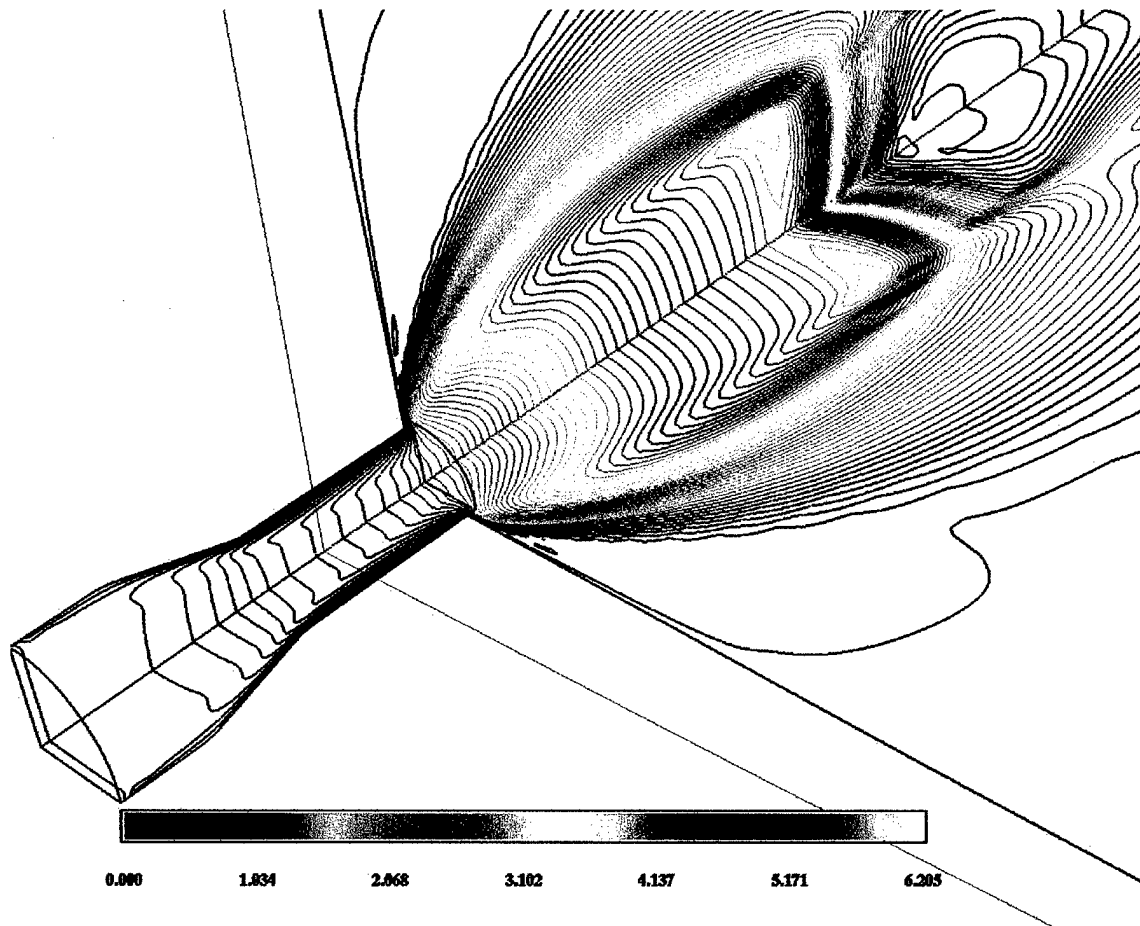


Figure 56. Multi-block $k-\omega$ Close-up of Igniter Chamber Exit.

Figure 57 shows the variation in centerline Mach number along the flow axis for both the single-block and multi-block $k-\omega$ turbulence model solutions in terms of station location. The dashed line is the single-block's solution and the solid line is the multi-block's solution.

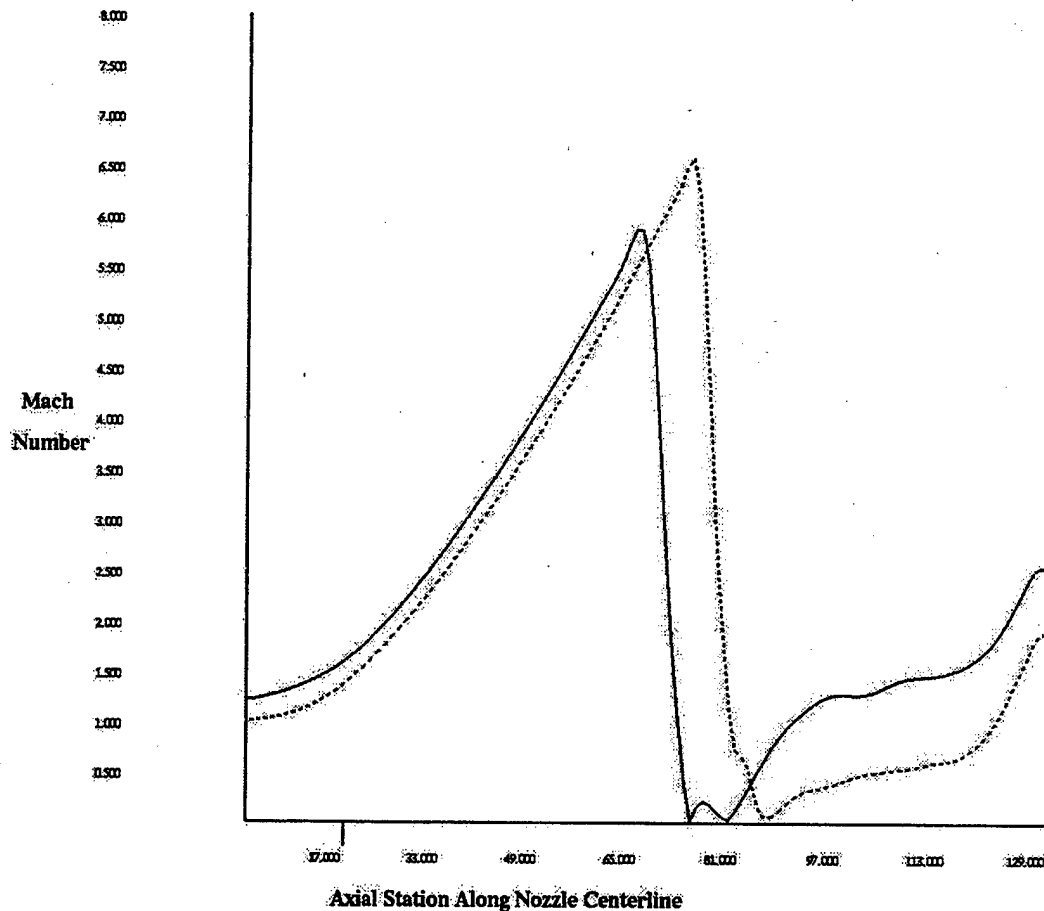


Figure 57. Multi-block $k-\omega$ Centerline Mach Number Profile.

Due to the interpolation between the two grids for the multi-block model, it was not possible to plot distance along the flow axis in terms of its actual physical distance as was done for the two- and three-dimensional models; instead, distance was plotted in terms of station location along the centerline. Keep in mind that the station locations represented grid point spacing, and since the points were not spaced equidistant from each other, the visible distance along the abscissa in Figure 58 was not to scale with the physical distance. Station 65 corresponded to a physical distance of approximately 1.0 inches down the axis from the igniter exit plane. In the figure, this was where the multi-block model's flow reached its maximum Mach number and began to shock. For the multi-block model the flow shocked to almost zero Mach at station 73, which

corresponded to a distance of 1.3 inches down the flow axis. At station 89 the flow was again sonic for the multi-block model's solution. This station corresponded to a distance of 2.5 inches down the axis. The nozzle throat was at station 118 and as can be seen from the figure, the flow was supersonic at this location. See Figure 48 for more correlation of the physical distances with the station locations.

At the igniter exit location (station 0), the multi-block model's Mach number profile had already reached supersonic conditions. The single-block model's solution was holding the inlet boundary condition (freestream Mach number = 1.0) at this location. Both flows expanded with similar slopes, but the single-block's expanded to a higher Mach number.

The result of the higher maximum expansion Mach number for the single-block model would have moved the Mach disk location further downstream than the Mach disk location for the multi-block model. And since the multi-block model's Mach disk was weaker, the flow downstream of the Mach disk would have to expand more rapidly than the single-block's to adjust to the outlet (nozzle exit) plane's very low pressure boundary condition. Consequently the exit plane Mach number would be higher for the multi-block model's solution than for the single-block model's solution. Physically, there would also be a stagnation pressure loss in the igniter chamber, occurring due to the losses created by the effects of friction on the igniter chamber walls, which would also have served to decrease the strength of the Mach disk for the multi-block model's solution.

Figure 58 shows that the Mach number was just above 1.6 at the centerline of the throat. This figure is given in terms of station location, as well. Station 81 corresponded to a radial distance of 0.85 inches from the centerline. In contrast to the single-block's solution, the flow was supersonic at the centerline, and gradually decreased to subsonic conditions. Near the throat walls the profile leveled until reaching the boundary layer where it rapidly decelerated to meet the viscous adiabatic wall boundary condition.

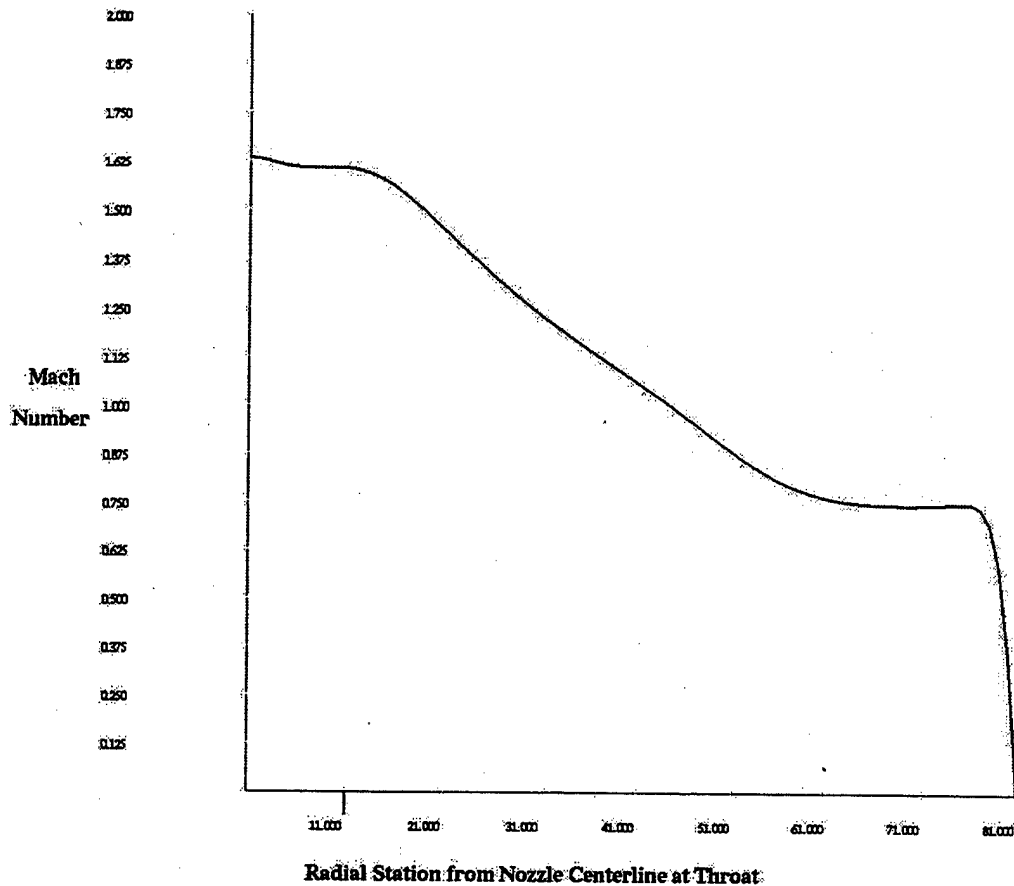


Figure 58. Multi-block $k-\omega$ Throat Radial Mach Number Profile.

F. MAIN CHAMBER THRUST PROFILES

One of the output files supplied by OVERFLOW consisted of computed coefficients of drag and mass flow rate for each boundary of the solution domain at each iteration. The thrust produced by this engine would be the integrated force of the chamber wall surfaces, and can be computed based on the coefficients of drag given by OVERFLOW. The value of the mass flow rate coefficient can also be used in an independent calculation to check the accuracy of the thrust calculated by using the drag coefficients.

Thrust values were plotted for all of the OVERFLOW models. The values for the inviscid model and Spalart-Allmaras model are given in Appendix I, while the $k-\omega$ values

are discussed here. The steps used to compute thrust based on the drag coefficients is given below.

The coefficients of drag due to pressure and skin friction calculated by OVERFLOW were multiplied by the freestream dynamic pressure and projected chamber wall surface area normal to the direction of flow to obtain the drag force on the chamber walls. See Reference 5 for the method used to normalize values in OVERFLOW. The negative of this drag force represented the thrust. It should be noted that the thrust values determined for the two-dimensional and single-block models did not account for the pressure and viscous forces that would exist on the igniter chamber walls. For the multi-block model, the thrust values accounted for the pressure and viscous forces on the circumferential walls of the igniter chamber, but not on the igniter's back wall (wall normal to the direction of flow). The reason for this was that the surface that would be the back wall of the igniter chamber was set as the pressure inlet boundary for the multi-block model.

Figure 59 shows the thrust profiles for the final 5,000 iterations of the two-dimensional computation, 6,000 iterations of the three-dimensional single-block computation and all iterations of the multi-block computation for the $k-\omega$ turbulence model. After almost 5,000 iterations of the three-dimensional single-block model the thrust had almost leveled to the same value as the two-dimensional model. These values should be the same since the wall surface areas were the same.

The multi-block model's thrust profile also leveled-out to the same value as the two- and three-dimensional model's thrust values. There should be a negative contribution to the thrust created by the pressure and viscous forces acting on the walls of the convergent section of the igniter chamber. There would also be a positive contribution to the thrust created by the pressure force acting on the back of the igniter chamber wall. The first contribution was accounted for in the calculation, however, its value was small. The second contribution was not accounted for since that surface was not modeled computationally as a chamber wall.

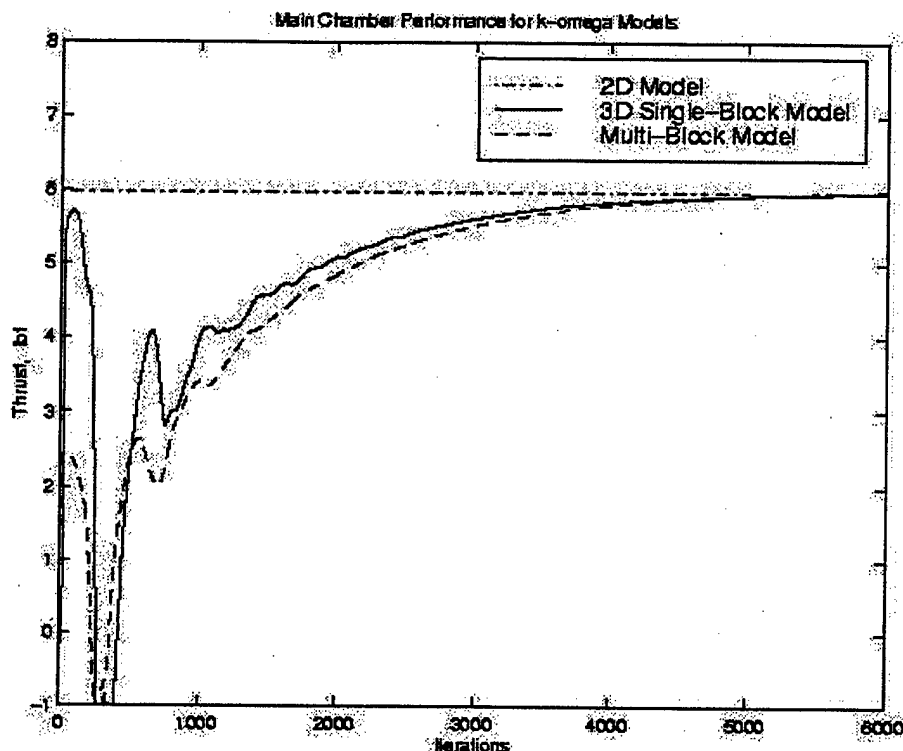


Figure 59. Thrust Profiles for $k-\omega$ Turbulence Model Computations.

For the independent calculation used to confirm the drag coefficient thrust values, mass flow rate (adjusted for an igniter chamber stagnation pressure of 150 psi) and exit plane velocity were used to calculate an ideal thrust, assuming that the nozzle exit pressure equaled the outlet pressure, which for this case was taken as zero psi. A sample of this calculation is given in Appendix J.

The calculation was done by plotting the velocity magnitude coefficient, which was a computed value, at the exit plane of the main chamber nozzle, determining an average value for the velocity magnitude coefficient, multiplying the average velocity magnitude coefficient by the freestream velocity to dimensionalize it, and then multiplying the computed mass flow rate by the average velocity magnitude at the exit plane. The thrust values calculated by using the computed mass flow rate and average exit plane velocity compared favorably with the thrust values calculated from the drag coefficients. Velocity magnitude profiles are also included in Appendix J for each of the two-dimensional models.

IV. CONCLUSIONS AND RECOMMENDATIONS

The objectives of this thesis were accomplished. A qualitative and quantitative prediction of the performance of the dual mode thruster under the specified fluid and boundary conditions was performed. The analysis was developed through the use of several computational models. The results of the solutions computed using OVERFLOW compared favorably with one another while those using FLUENT 5.1 were not as favorable when compared with each other or with the OVERFLOW results.

The quantitative analysis showed the internal flow characteristics and the associated wall regions where very high temperatures will likely occur. Based on the static temperature contours from the OVERFLOW solutions, all of the walls inside the main chamber will reach approximately 80 percent of inlet stagnation temperature.

The adequacy of this model to analyze different methods of cooling has yet to be evaluated. In order to model the influence of the like-on-like orifices on the injector faceplate the three-dimensional grid would need to be used. Although a three-dimensional grid was developed and tested, showing favorable results with a separate two-dimensional model, more evaluation and possible modification of the three-dimensional structured grid used in OVERFLOW may be needed. Favorably, the use of different spacing along the flow axis for the two- and three-dimensional models showed that the solutions were not grid dependant.

Numerically this problem was best solved with central-differencing, which was not available in FLUENT 5.1. This conclusion was based on the inability to obtain a solution using Roe upwind-differencing in OVERFLOW, and the difficulty of obtaining one within FLUENT 5.1.

The effects of viscosity for the turbulence models were very important; most likely the two-dimensional inviscid model used in OVERFLOW became non-physical due to the absence of viscosity. The effects of the level of sophistication of the turbulence models were evident from differences between the solutions of the two turbulence models used in OVERFLOW. Consistently, the $k-\omega$ turbulence model

solutions showed less oscillation for density residual convergence histories and centerline Mach number profiles.

Even though the three-dimensional model and multi-block model solutions all computed a negative density value, the thrust profiles had leveled off. The Mach number contours also appeared reasonable for these models.

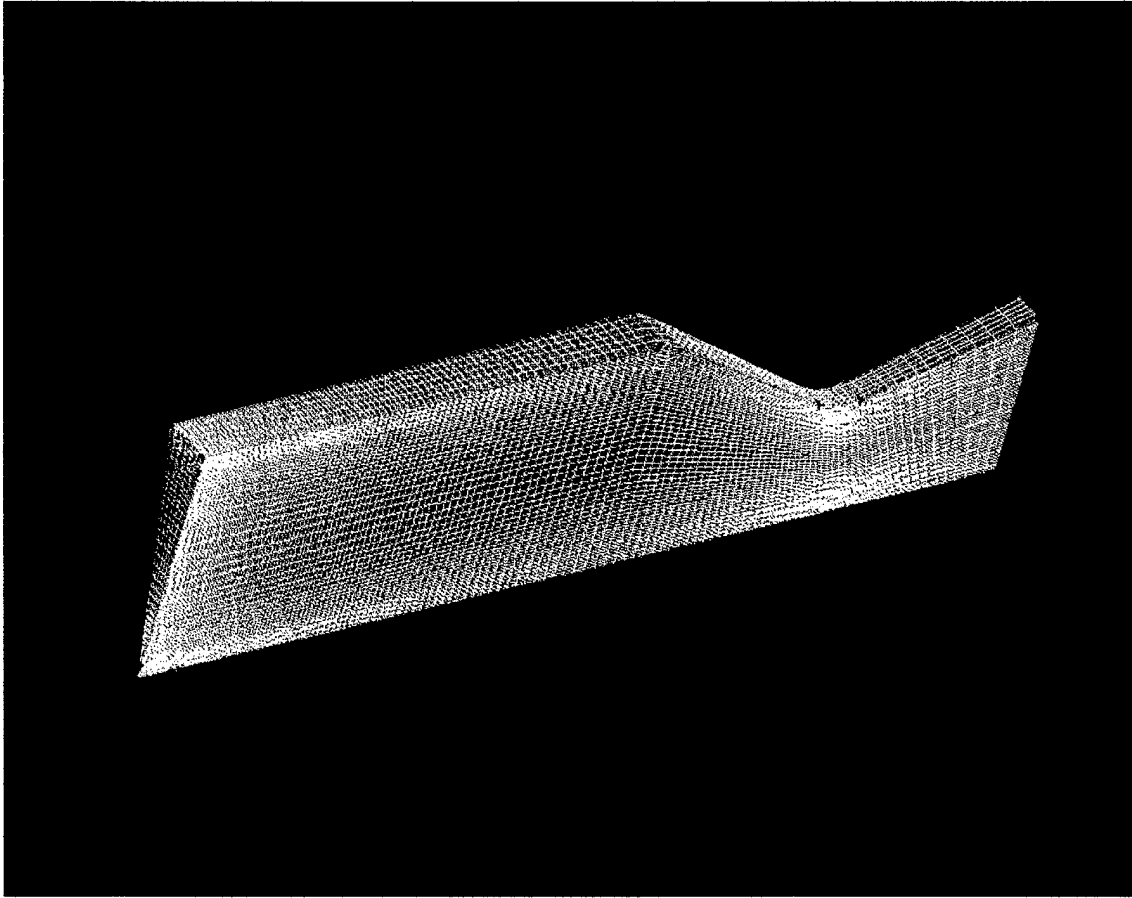
The Mach number contours and profiles of centerline Mach number also compared well with current data for similar types of flows. The presence of the chamber walls did not seem to effect the flow very much; however, the presence of the converging nozzle section seemed to slow the re-expansion of the flow after passage through the Mach disk. At the throat station, this resulted in a mixture of both subsonic and supersonic flow, so prediction of the flow conditions at the throat tended toward a mixture of subsonic and supersonic flow. All of the OVERFLOW models compared favorable on this. The effect this will have on the performance of the engine may result in a slight increase in flow exhaust velocity at the nozzle exit and a resulting increase in specific impulse for a fixed mass flow rate.

There is much room for further study of this problem. Given the current OVERFLOW grids, performance in the torch igniter only mode could be further evaluated for different inlet temperatures, molecular weights and ratios of specific heats. Real gas effects for variable ratios of specific heats may also be implemented within OVERFLOW. Further study of the three-dimensional model is needed to address the computation of negative densities.

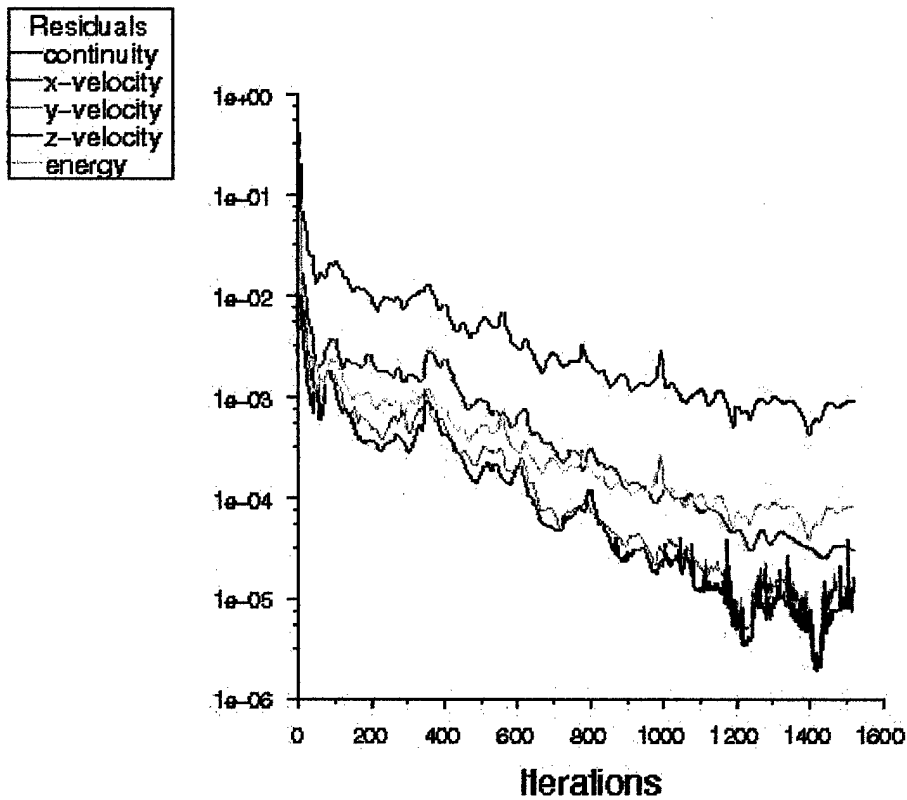
Combustion modeling would not be possible within OVERFLOW as it is not currently capable of this. FLUENT 5.1 is, however, capable of some combustion modeling. If central differencing were used within the FLUENT code then it may better be used for future modeling of the internal aerodynamics and the effects of combustion. More computational resources would be desirable to run the FLUENT computations in a timely manner.

APPENDIX A. FLUENT 3D GRID AND RESULTS

The three-dimensional grid is presented along with an inviscid solution and solutions computed using the Spalart Allmaras and $k-\epsilon$ turbulence models.



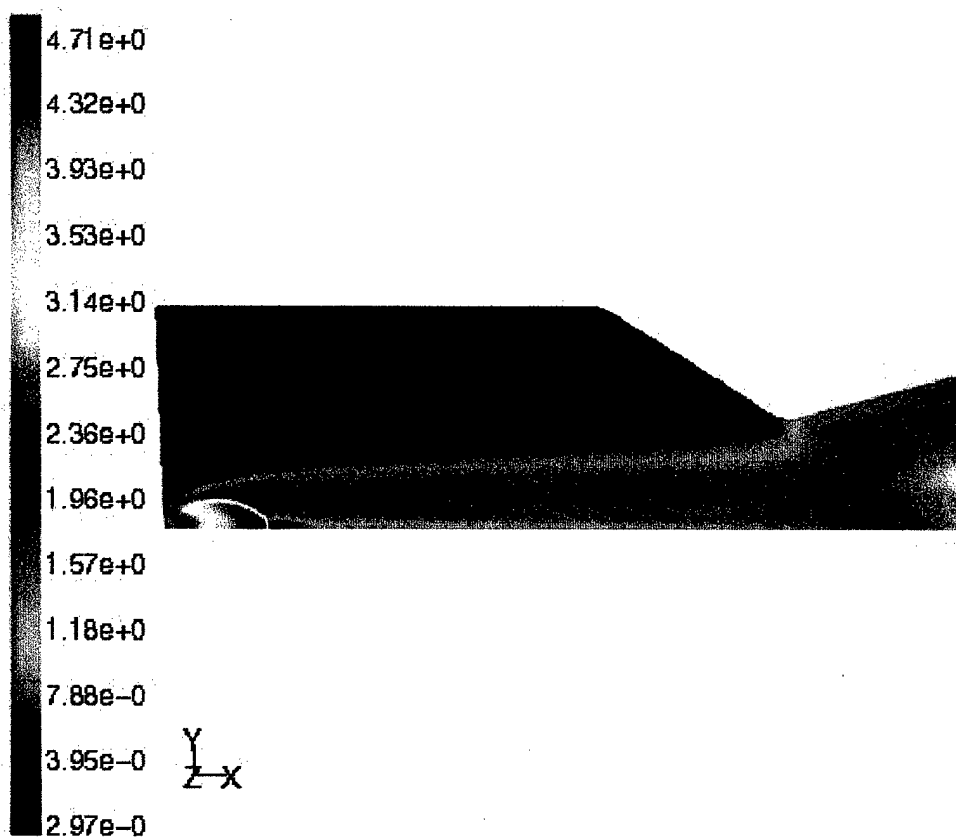
FLUENT Three-dimensional Grid



Scaled Residuals

Jul 03, 1999
FLUENT 5.1 (3d, coupled imp)

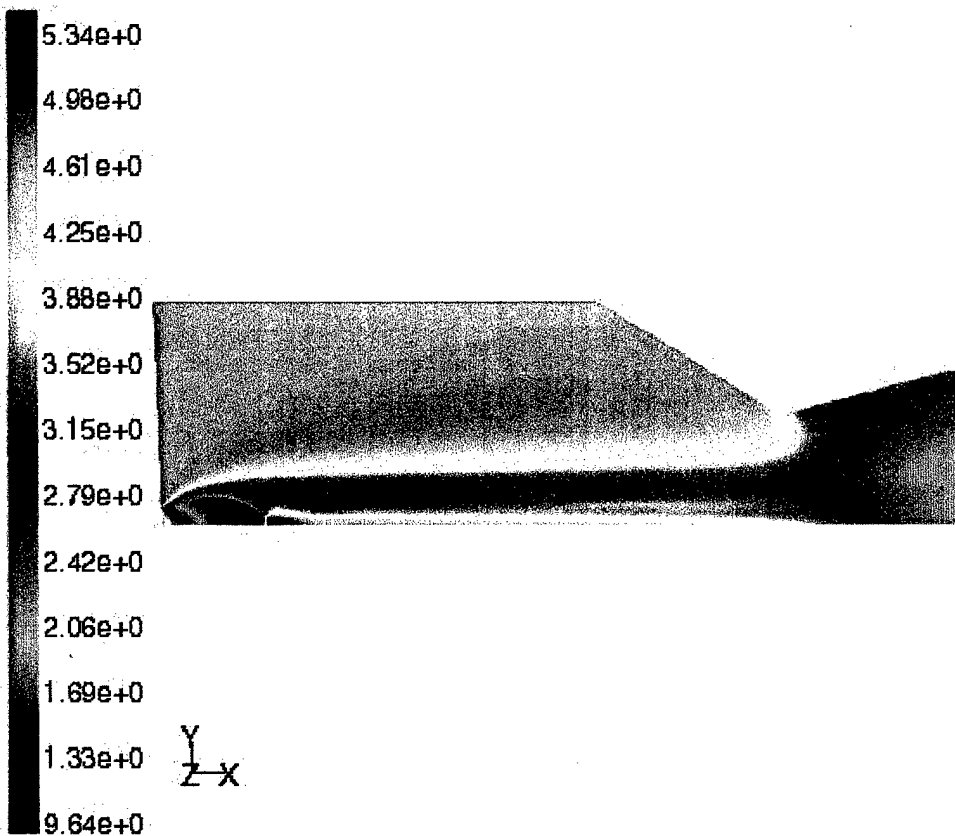
Inviscid Model Convergence History



Contours of Mach Number

Jul 03, 1999
FLUENT 5.1 (3d, coupled imp)

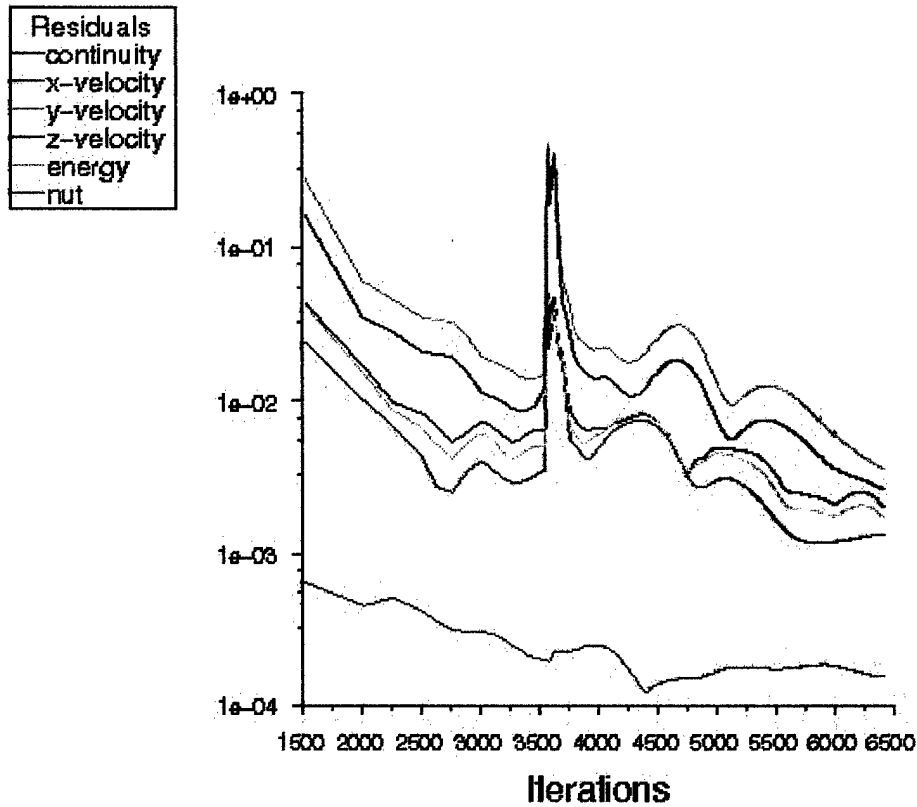
Inviscid Model Mach Number Contours



Contours of Static Temperature (r)

Jul 03, 1999
FLUENT 5.1 (3d, coupled imp)

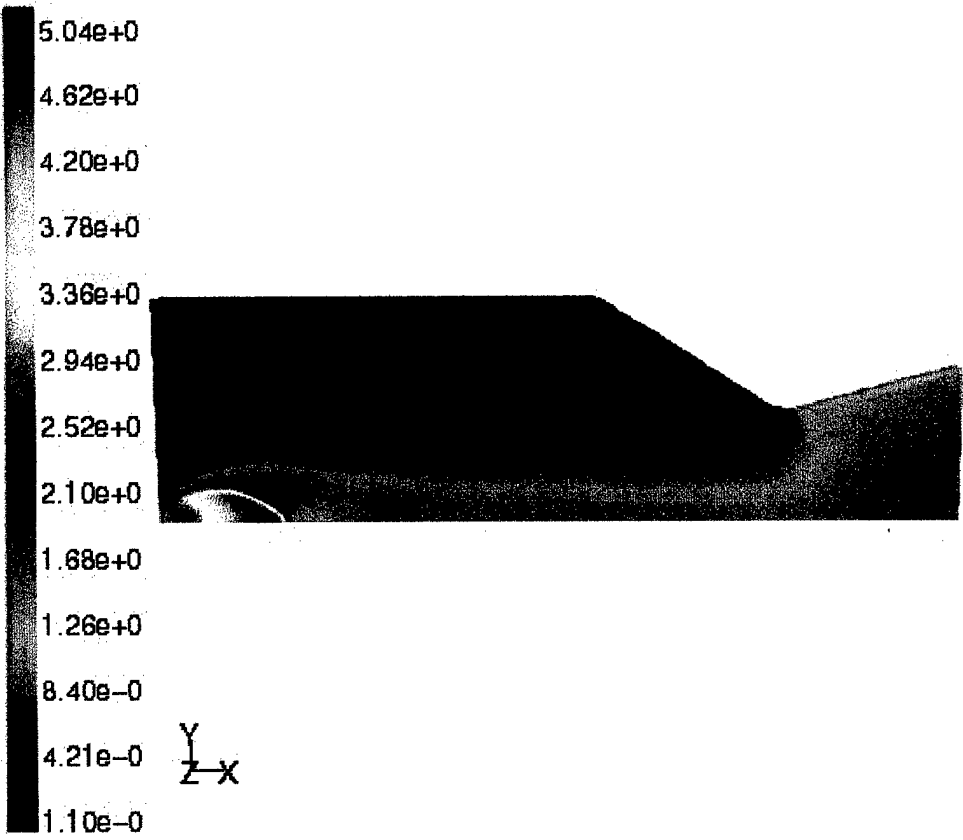
Inviscid Model Static Temperature Contours



Scaled Residuals

Jul 03, 1999
FLUENT 5.1 (3d, coupled imp, S-A)

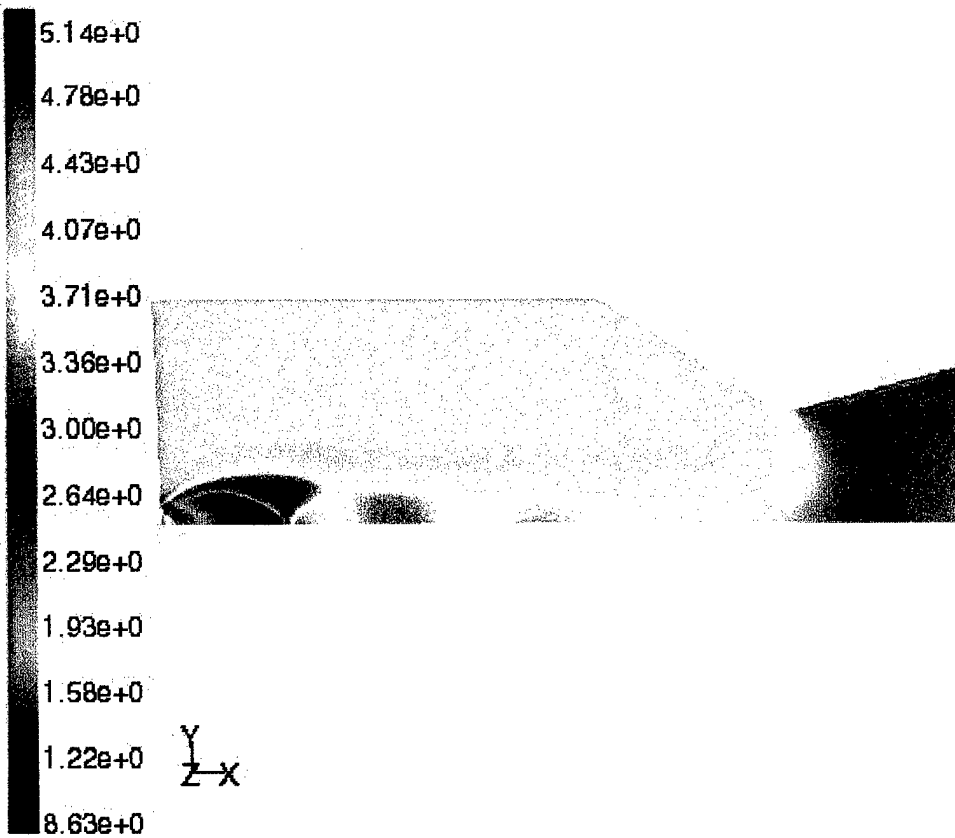
Spalart-Allmaras Model Convergence History



Contours of Mach Number

Jul 03, 1999
FLUENT 5.1 (3d, coupled imp, S-A)

Spalart-Allmaras Mach Number Contours

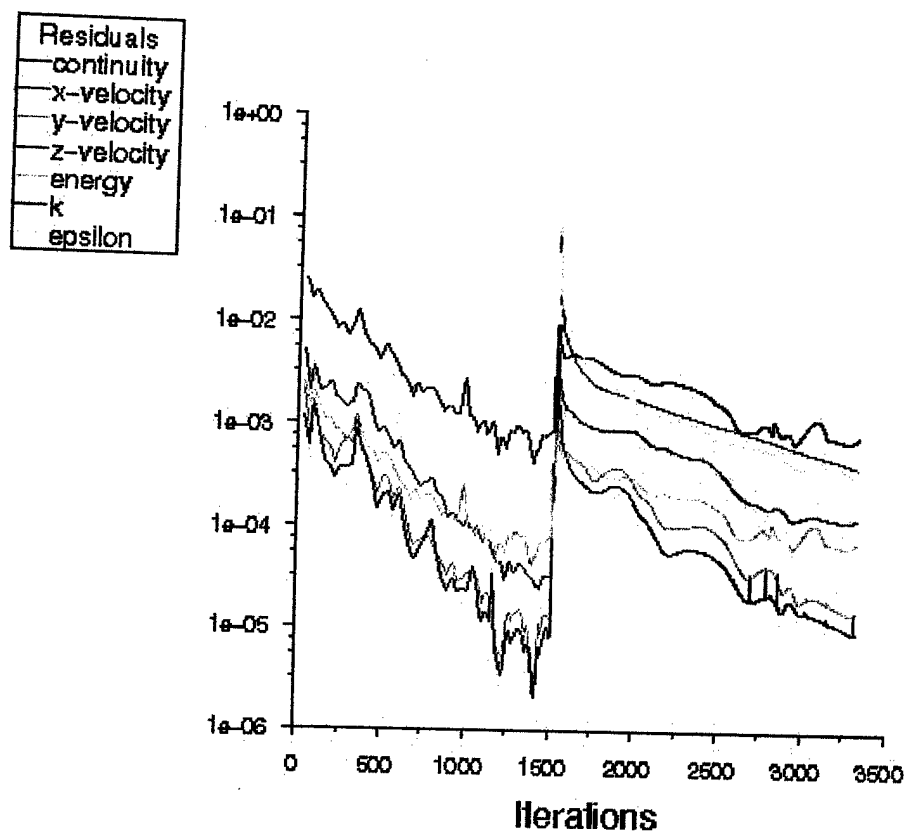


Contours of Static Temperature (r)

Jul 03, 1999

FLUENT 5.1 (3d, coupled imp, S-A)

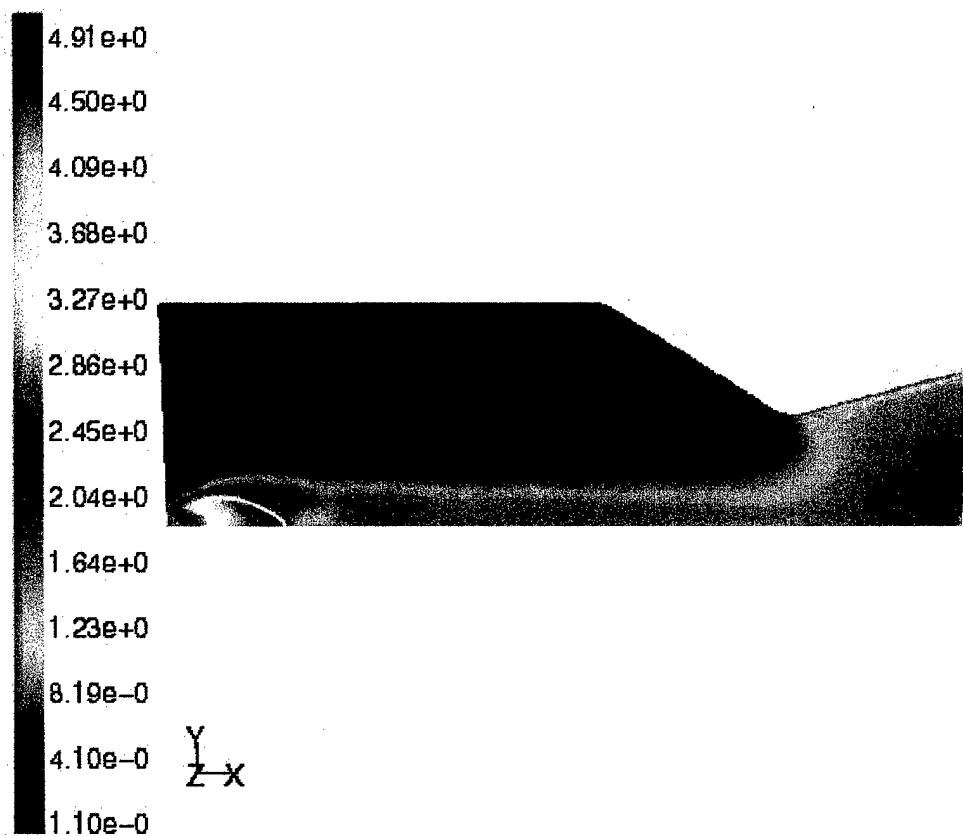
Spalart-Allmaras Static Temperature Contours



Scaled Residuals

Jul 03, 1999
FLUENT 5.1 (3d, coupled imp, ke)

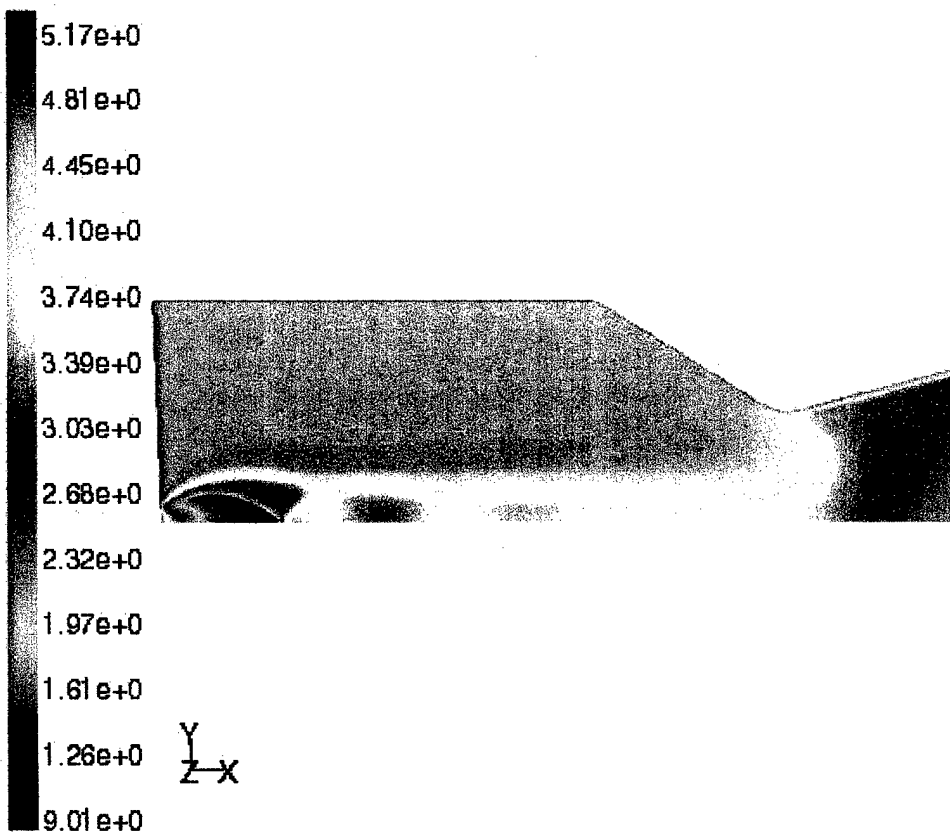
k- ϵ Convergence History



Contours of Mach Number

Jul 03, 1999
FLUENT 5.1 (3d, coupled imp, ke)

k-ε Mach Number Contours



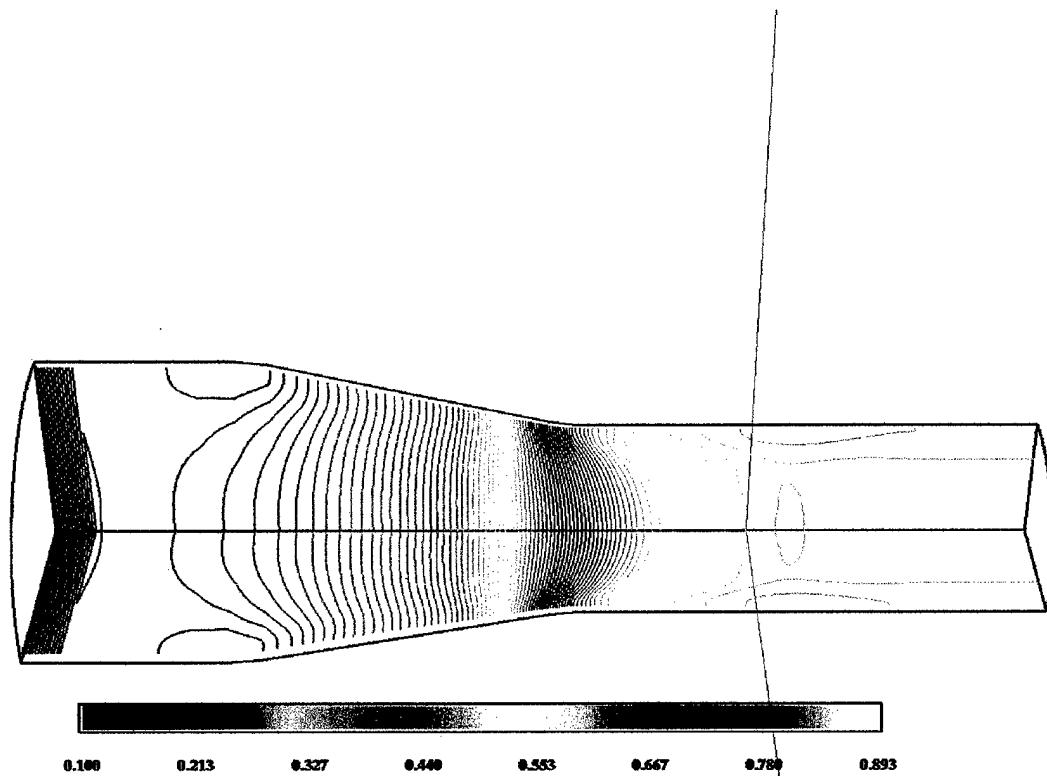
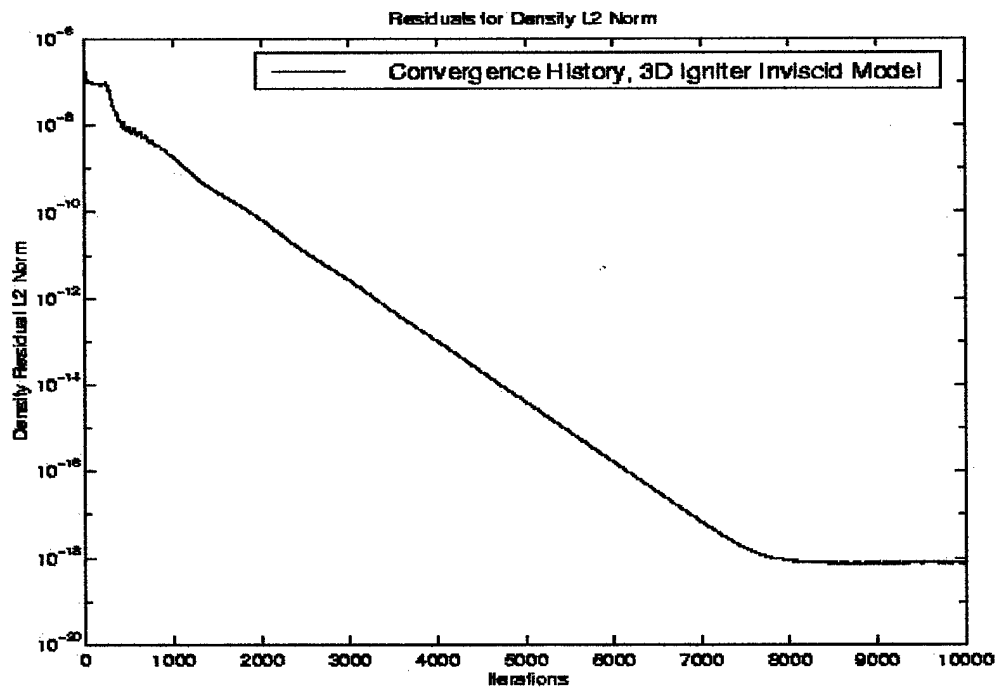
Contours of Static Temperature (r)

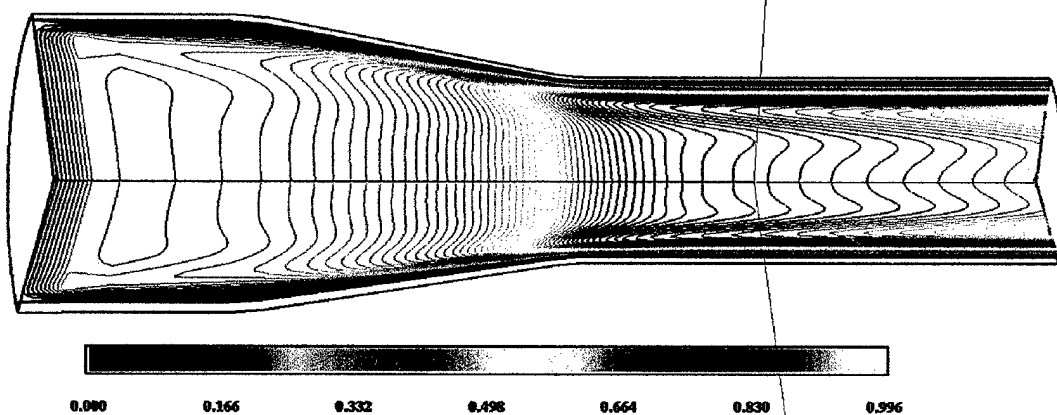
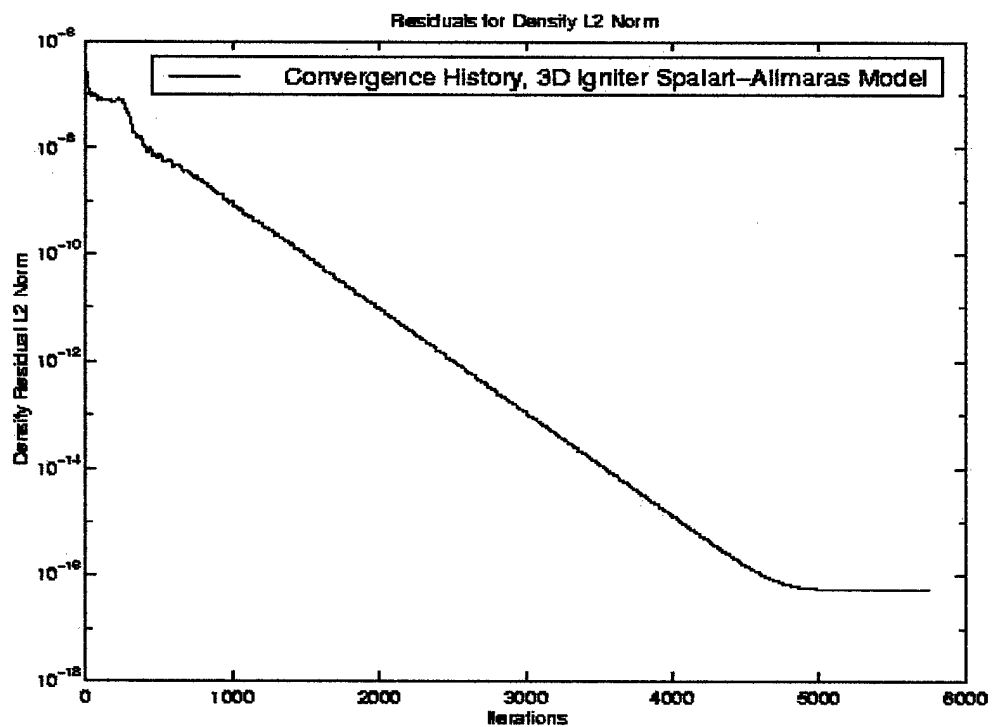
Jul 03, 1999

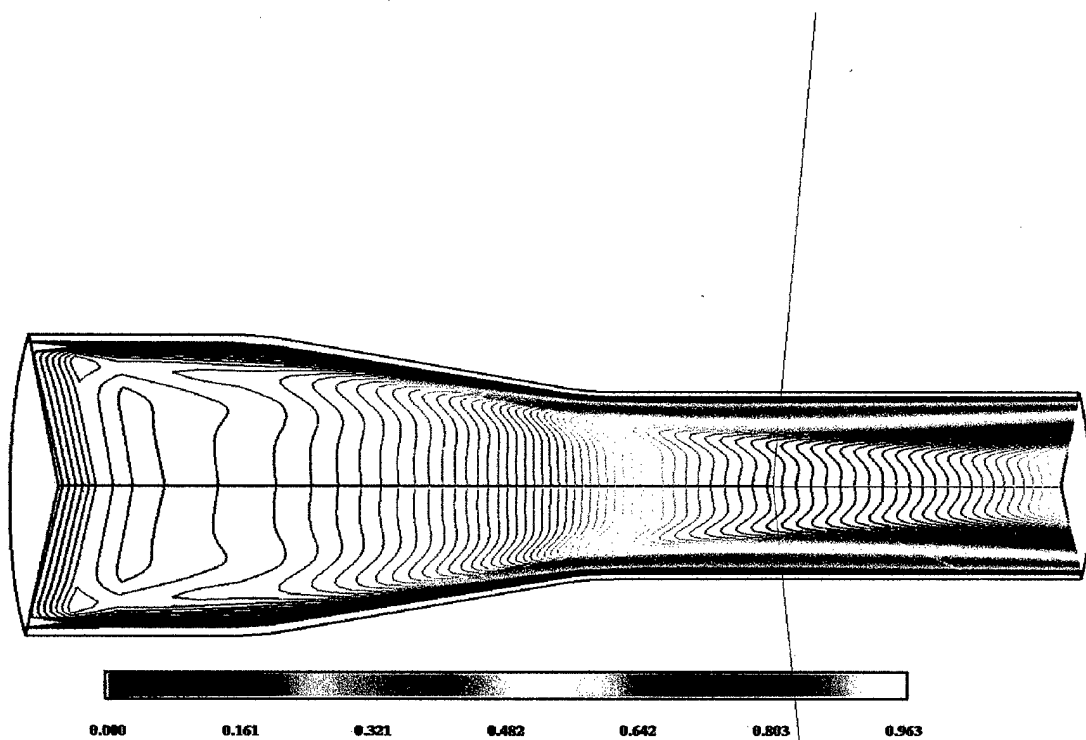
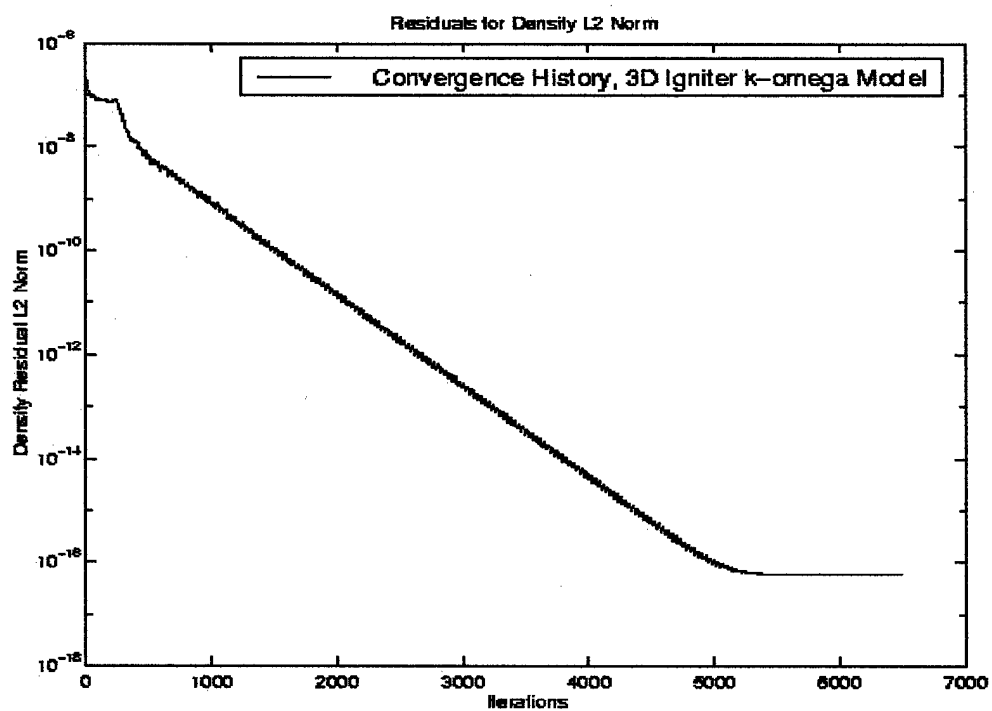
FLUENT 5.1 (3d, coupled imp, ke)

k-ε Static Temperature Contours

APPENDIX B. OVERFLOW SINGLE-BLOCK IGNITER RESULTS

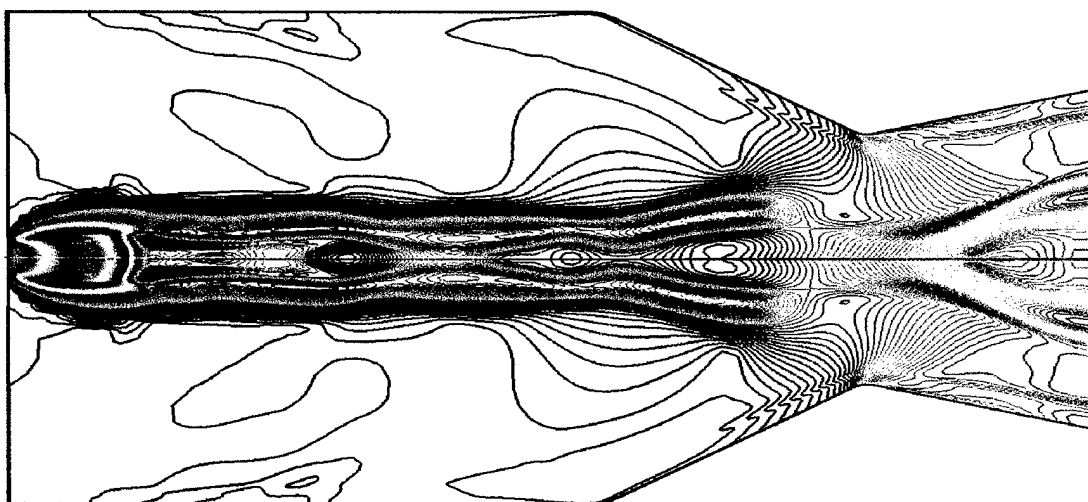




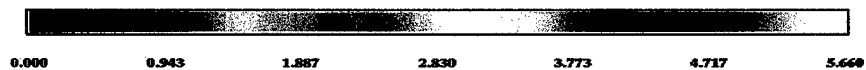
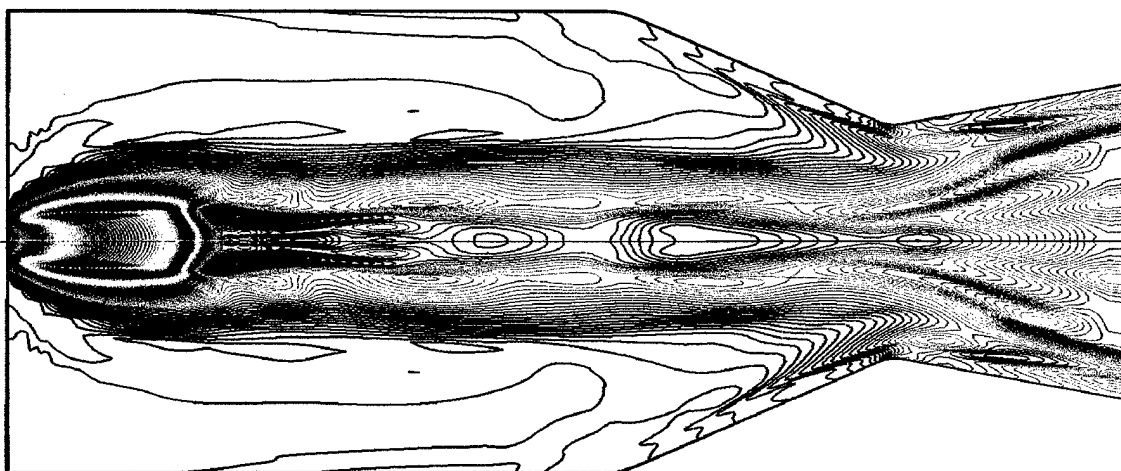


APPENDIX C. 2D INVISCID MACH NUMBER CONTOUR CHRONOLOGY

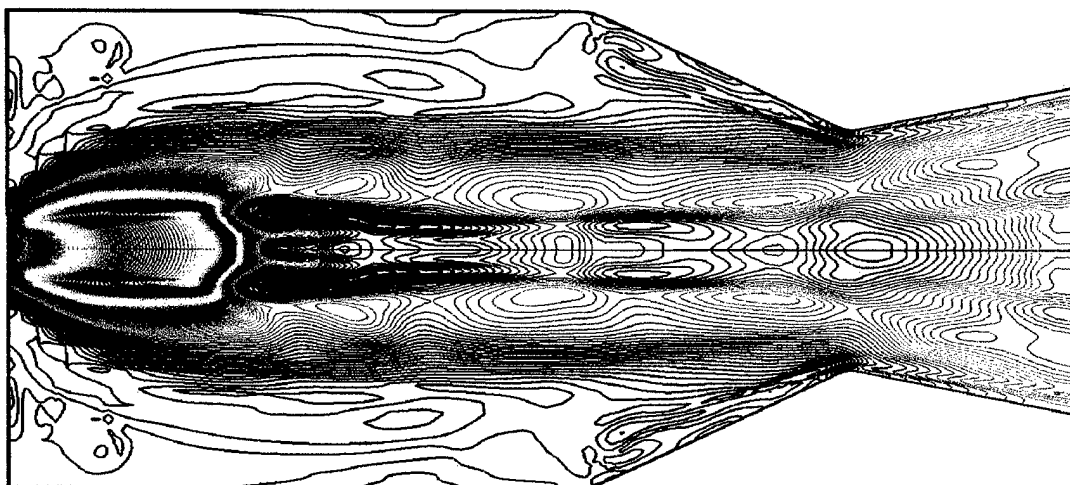
A Mach number contour chronology is presented at 5,000 iterations, 8,000 iterations, 10,000 iterations, 20,000 iterations, and 30,000 iterations.



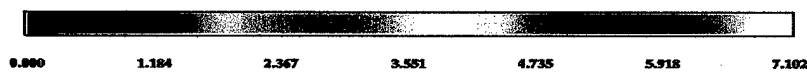
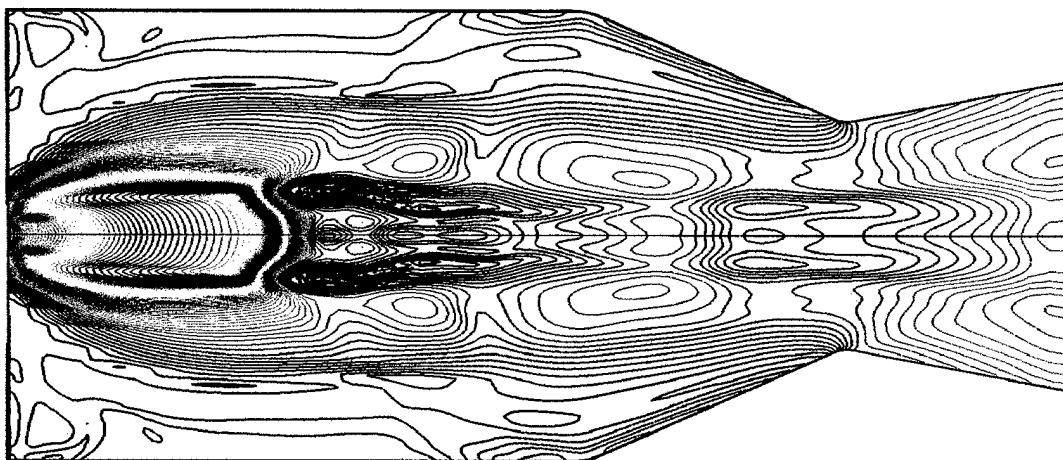
5,000 iterations



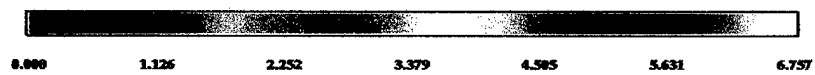
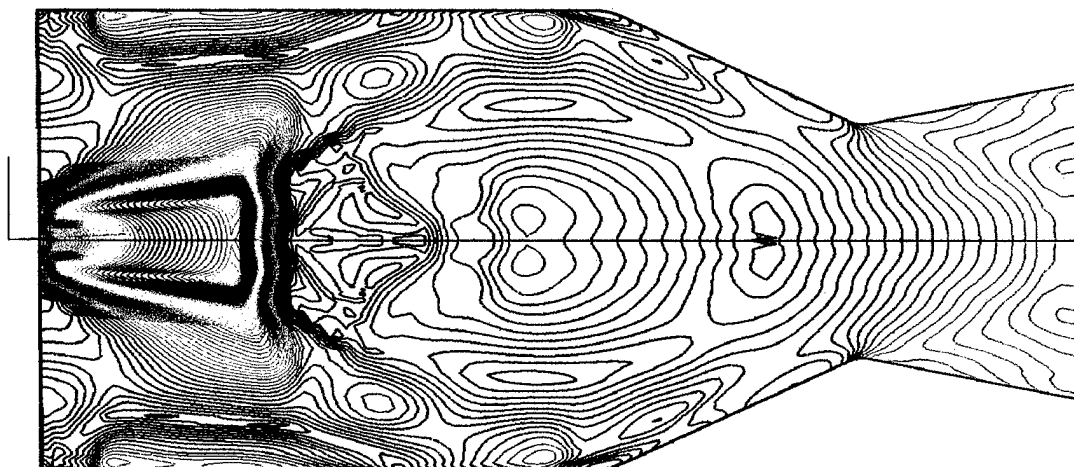
8,000 iterations



10,000 iterations



20,000 iterations



30,000 iterations

APPENDIX D. 2D MODEL OVERFLOW INPUT FILES

2D Inviscid Model Input:

\$GLOBAL

CHIMRA= .F., NSTEPS=5000, RESTR= .T., NSAVE =1,
 NQT = 0, MULTIG=.F., FMG=.F., FMGCYC= 300,300,
 \$END

\$FLOINP

FSMACH= 1.00, REY= 3.42e5, TINF= 5598.0, GAMINF= 1.4, ALPHA= 0.0,
 XKINF=0.0001, RETINF=0.1,
 \$END

\$VARGAM

\$END

\$GRDNAM

NAME = '2D nozzle, 81 x 3 x 129 grid',

\$END

\$NITERS \$END

\$METPRM \$END

\$TIMACU DT = 0.2, CFLMIN = 1.0, \$END

\$SMOACU \$END

\$VISINP

VISC = .F.,
 CFLT=2,
 ITERT = 3,
 \$END

\$BCINP

NBC	=	8,							
IBTYP	=	1,	1,	22,	15,		41,	33,	32, 40,
IBDIR	=	3,	-1,	2,	1,		3,	-3,	-3, 3,
JBCS	=	30,	-1,	1,	1,		1,	1,	1, 1,
JBCE	=	-1,	-1,	-1,	1,		30,	-1,	-1, 30,
KBCS	=	1,	1,	1,	1,		1,	1,	1, 1,
KBCE	=	-1,	-1,	1,	-1,		-1,	-1,	-1, -1,
LBCS	=	1,	1,	1,	1,		1,	-1,	-1, 1,
LBCE	=	1,	-1,	-1,	-1,		1,	-1,	-1, 1,

BCPAR1(6)= 0.0001,
 \$END

\$SCEINP

\$END

2D Spalart-Allmaras Turbulence Model Input:

\$GLOBAL

CHIMRA= .F., NSTEPS=5000, RESTRT= .T., NSAVE =10,
 NQT = 102, MULTIG=.F., FMG=.F., FMGCYC= 300,300,
 \$END

\$FLOINP

FSMACH= 1.00, REY= 3.42e5, TINF= 5598.0, GAMINF= 1.4, ALPHA= 0.0,
 XKINF=0.0001, RETINF=0.1,
 \$END

\$VARGAM

\$END

\$GRDNAM

NAME = '2D nozzle, 81 x 3 x 129 grid',

\$END

\$NITERS \$END

\$METPRM \$END

\$TIMACU DT = 0.5, CFLMIN = 1.0, \$END

\$SMOACU \$END

\$VISINP

VISC = .T.,
 CFLT=2,
 ITERT = 3,
 \$END

\$BCINP

NBC	=	8,							
IBTYP	=	5,	5,	22,	15,	41,	33,	32,	40,
IBDIR	=	3,	-1,	2,	1,	3,	-3,	-3,	3,
JBCS	=	30,	-1,	1,	1,	1,	1,	1,	1,
JBCE	=	-1,	-1,	-1,	1,	30,	-1,	-1,	30,
KBCS	=	1,	1,	1,	1,	1,	1,	1,	1,
KBCE	=	-1,	-1,	1,	-1,	-1,	-1,	-1,	-1,
LBCE	=	1,	1,	1,	1,	1,	-1,	-1,	1,
LBCE	=	1,	-1,	-1,	-1,	1,	-1,	-1,	1,

BCPAR1(6)= 0.0001,

\$END

\$SCEINP

\$END

2D k- ω Turbulence Model Input:

\$GLOBAL

CHIMRA= .F., NSTEPS=5000, RESTRT= .T., NSAVE =10,
 NQT = 202, MULTIG=.F., FMG=.F., FMGCYC= 300,300,
 \$END

\$FLOINP

FSMACH= 1.00, REY= 3.42e5, TINF= 5598.0, GAMINF= 1.4, ALPHA= 0.0,
 XKINF=0.0001, RETINF=0.1,
 \$END

\$VARGAM

\$END

\$GRDNAM

NAME = '2D nozzle, 81 x 3 x 129 grid',

\$END

\$NITERS \$END

\$METPRM \$END

\$TIMACU DT = 0.4, CFLMIN = 1.0, \$END

\$SMOACU \$END

\$VISINP

VISC = .T.,
 CFLT=2,
 ITERT = 3,
 \$END

\$BCINP

NBC = 8,
 IBTYP = 5, 5, 22, 15, 41, 33, 32, 40,
 IBDIR = 3, -1, 2, 1, 3, -3, -3, 3,
 JBCE = 30, -1, 1, 1, 1, 1, 1, 1,
 JBCE = -1, -1, -1, 1, 30, -1, -1, 30,
 KBCS = 1, 1, 1, 1, 1, 1, 1, 1,
 KBCE = -1, -1, 1, -1, -1, -1, -1, -1,
 LBCE = 1, 1, 1, 1, 1, -1, -1, 1,
 LBCE = 1, -1, -1, -1, 1, -1, -1, 1,
 BCPAR1(6)= 0.0001,

\$END

\$SCEINP

\$END

APPENDIX E. 3D MODEL OVERFLOW INPUT FILES

3D Inviscid Model Input:

```

$GLOBAL
  CHIMRA= .F.,   NSTEPS=90,   RESTRT= .T.,   NSAVE =100,
  NQT = 0,      MULTIG = .F., FMG = .F.,      FMGCYC = 100,300,
  $END
$FLOINP
  FSMACH= 1.00,  REY= 3.42e5, TINF= 5598.0, GAMINF= 1.4, ALPHA= 0.0,
  XKINF=0.0001,  RETINF=0.1,
  $END
$VARGAM
  $END
$GRDNAM
  NAME = '3D nozzle, 81 x 29 x 129 grid',
$END
$NITERS $END
$METPRM $END
$TIMACU DT = .3, CFLMIN = 1.0, $END
$SMOACU $END
$VISINP
  VISC = .F.,
  CFLT=2,
  ITERT = 3,
  $END
$BCINP
  NBC = 9,
  IBTYP = 1, 1, 12, 15, 13, 41, 33, 32, 40,
  IBDIR = 3, -1, -2, 1, 2, 3, -3, -3, 3,
  JBCE = 30, -1, 1, 1, 1, 1, 1, 1, 1,
  JBCE = -1, -1, -1, 1, -1, 30, -1, -1, 30,
  KBCS = 1, 1, -1, 1, 1, 1, 1, 1, 1,
  KBCE = -1, -1, -1, -1, 1, -1, -1, -1, -1,
  LBCE = 1, 1, 1, 1, 1, 1, -1, -1, 1,
  LBCE = 1, -1, -1, -1, -1, 1, -1, -1, 1,
  BCPAR1(7)= 0.0001,
  $END
$SCEINP
$END

```

3D Spalart-Allmaras Turbulence Model Input:

\$GLOBAL

CHIMRA= .F., NSTEPS=90, RESTR= .T., NSAVE =100,
NQT = 102, MULTIG = .F., FMG = .F., FMGNCYC = 100,300,
\$END

\$FLOINP

FSMACH= 1.00, REY= 3.42e5, TINF= 5598.0,GAMINF= 1.4, ALPHA= 0.0,
XKINF=0.0001, RETINF=0.1,
\$END

\$VARGAM

\$END

\$GRDNAM

NAME = '3D nozzle, 81 x 29 x 129 grid',

\$END

\$NITERS \$END

\$METPRM \$END

\$TIMACU DT = .3, CFLMIN = 1.0, \$END

\$SMOACU \$END

\$VISINP

VISC = .T.,
CFLT=2,
ITERT = 3,
\$END

\$BCINP

NBC	=	9,							
IBTYP	=	5,	5,	12,	15,	13,	41,	33,	32, 40,
IBDIR	=	3,	-1,	-2,	1,	2,	3,	-3,	-3, 3,
JBCS	=	30,	-1,	1,	1,	1,	1,	1,	1, 1,
JBCE	=	-1,	-1,	-1,	1,	-1,	30,	-1,	-1, 30,
KBCS	=	1,	1,	-1,	1,	1,	1,	1,	1, 1,
KBCE	=	-1,	-1,	-1,	-1,	1,	-1,	-1,	-1, -1,
LBCS	=	1,	1,	1,	1,	1,	1,	-1,	-1, 1,
LBCE	=	1,	-1,	-1,	-1,	-1,	1,	-1,	-1, 1,

BCPAR1(7)= 0.0001,

\$END

\$SCEINP

\$END

3D k- ω Turbulence Model Input:

\$GLOBAL

CHIMRA= .F., NSTEPS=800, RESTRT= .T., NSAVE =100,
 NQT = 202, MULTIG = .F., FMG = .F., FMGCYC = 300,300,
 \$END

\$FLOINP

FSMACH= 1.00, REY= 3.42e5, TINF= 5598.0, GAMINF= 1.4, ALPHA=0.0,
 XKINF=0.0001, RETINF=0.1,
 \$END

\$VARGAM

\$END

\$GRDNAM

NAME = '3D nozzle, 81 x 29 x 129 grid',

\$END

\$NITERS \$END

\$METPRM \$END

\$TIMACU DT = 0.2, CFLMIN = 1.0, \$END

\$SMOACU DIS2 = 2.0, \$END

\$VISINP

VISC = .T.,
 CFLT=2,
 DIS2T = 2.0,
 ITERT = 3,
 \$END

\$BCINP

NBC = 9,
 IBTYP = 5, 5, 12, 15, 13, 41, 33, 32, 40,
 IBDIR = 3, -1, -2, 1, 2, 3, -3, -3, 3,
 JBCE = 30, -1, 1, 1, 1, 1, 1, 1, 1,
 JBCE = -1, -1, -1, 1, -1, 30, -1, -1, 30,
 KBCS = 1, 1, -1, 1, 1, 1, 1, 1, 1,
 KBCE = -1, -1, -1, -1, 1, -1, -1, -1, -1,
 LBCE = 1, 1, 1, 1, 1, 1, -1, -1, 1,
 LBCE = 1, -1, -1, -1, -1, 1, -1, -1, 1,
 BCPAR1(7)= 0.0001,
 \$END

\$SCEINP

\$END

APPENDIX F. MULTI-BLOCK MODEL OVERFLOW INPUT FILES

3D Multi-block Chamber with Torch Igniter Inviscid Input:

```

$GLOBAL
  CHIMRA= .T.,    NSTEPS=200,    RESTRT= .F.,    NSAVE =50,
  NQT = 0,      MULTIG = .F., FMG = .F.,      FMGCRYC = 100,100,
  $END
$FLOINP
  FSMACH= 0.3,   REY= 3.42e5, TINF= 5846.0,   GAMINF= 1.4, ALPHA= 0.0,
  XKINF=0.0001, RETINF=0.1,
  $END
$VARGAM
  $END

$GRDNAM
  NAME = 'IGNITOR',
$END
$NITERS $END
$METPRM $END
$TIMACU DT = 0.2, CFLMIN = 1.0, $END
$SMOACU $END
$VISINP
  VISC = .F.,
  CFLT=2,
  ITERT = 3,
  $END
$BCINP
  NBC   =      6,
  IBTYP =      1,   12,   15,   13,           41,           40,
  IBDIR =     -1,   -2,    1,    2,           3,           3,
  JBCE  =     -1,    1,    1,    1,           1,           1,
  JBCE  =     -1,   -1,    1,   -1,          -1,          -1,
  KBCE  =      1,   -1,    1,    1,           1,           1,
  KBCE  =     -1,   -1,   -1,    1,          -1,          -1,
  LBCE  =      1,    1,    1,    1,           1,           1,
  LBCE  =     57,   57,   57,   57,           1,           1,
  $END
$SCEINP
$END

$GRDNAM
  NAME = 'CHAMBER',
$END
$NITERS $END
$METPRM $END
$TIMACU DT = 0.2, CFLMIN = 1.0, $END
$SMOACU $END
$VISINP
  VISC = .F.,
  CFLT=2,
  ITERT = 3,
  $END
$BCINP
  NBC   =      7,
  IBTYP =      1,    1,   12,   15,   13,           33,   32,
  IBDIR =      3,   -1,   -2,    1,    2,           -3,   -3,
  JBCE  =     30,   -1,    1,    1,    1,           1,    1,

```

```
JBCE = -1, -1, -1, 1, -1, -1, -1,  
KBCS = 1, 1, -1, 1, 1, 1, 1,  
KBCE = -1, -1, -1, -1, 1, -1, -1,  
LBCS = 1, 1, 1, 1, 1, -1, -1,  
LBCE = 1, -1, -1, -1, -1, -1, -1,  
BCPAR1(6)= 0.0001,  
$END  
$SCEINP  
$END
```


APPENDIX G. PEGSUS INPUT FILES

```

C          PEGSUS INPUT FILE - RCS Torch Ignitor
C                                     with Main Chamber
C      By : Adam Williams
C      Date: August, 1999
C
C *****
C *****
C          General Information
C
C      This input file is used with the 'INGRID' grid file, produced using
C      RMG2PEG, to create the interpolation stencil 'INTOUT' used by OVERFLOW.
C      Two other output files COMPOUT (composite mesh) and IBPLOT (iblanking info)
C      are concatenated in program MERGE41 into a grid file, which should be named
C      'grid.in'. This file and PEGSUS interpolation information file 'INTOUT'
C      are required for the Chimera overset grid scheme in OVERFLOW.
C
C *****
C *****
C      Note - Start typing in second column!!!
C
$GLOBAL
    FRINGE = 2,
    EPS = 0.005,
$END

CCC---Grid Dimen - CHAMBER (81 x 29 x 129), IGNITOR (30 x 29 x 60)---CCC

$MESH NAME = 'IGNITOR',
    LINK = 'CHAMBER',

    X0 = -0.001625,
    Y0 = 0.0,
    Z0 = 0.0,
$END

$MESH NAME = 'CHAMBER',
    LINK = 'IGNITOR',

    X0 = 0.0,
    Y0 = 0.0,
    Z0 = 0.0,
$END

CCCCCCC--SURFACE BOUNDARY ON SURFACES OF IGNITER--CCCCCCCCCCCC
CCCCCCCCCCCCCCCCCCCCCCCCCCCCCCCCCCCCCCCCCCCCCCCCCCCCCCCCCCCC
$BOUNDARY NAME = 'IGNITOR TO CHAMBER BOUNDARY',
    CLOSED = .TRUE.,
    ISPARTOF = 'IGNITOR',

```

\$END

CC
\$SURFACE ISPARTOF = 'IGNITOR TO CHAMBER BOUNDARY',

JRANGE = 1,30,
KRANGE = 1,29,
LRANGE = 58,60,

\$END

```
CCCCCCCCCCCCCCCCCCCCCCCCCCCCCCCCCCCCCCCCCCCCCCCCCCCCCCCCCCCCCCCC
$SURFACE ISPARTOF = 'IGNITOR TO CHAMBER BOUNDARY',
```

**JRANGE = 30,30,
KRANGE = 1,29,
LRANGE = 55,60,**

\$END

```
CCCCCCCCCCCCCCCC--HOLE BOUNDARY INSIDE OF CHAMBER--CCCCCCCCCCCC
CCCCCCCCCCCCCCCCCCCCCCCCCCCCCCCCCCCCCCCCCCCCCCCCCCCCCCCCCCCC
$REGION  NAME = 'CHAMBER HOLE BOUNDARY',
          ISPARTOF = 'CHAMBER',
          TYPE = 'HOLE',
```

\$END

```

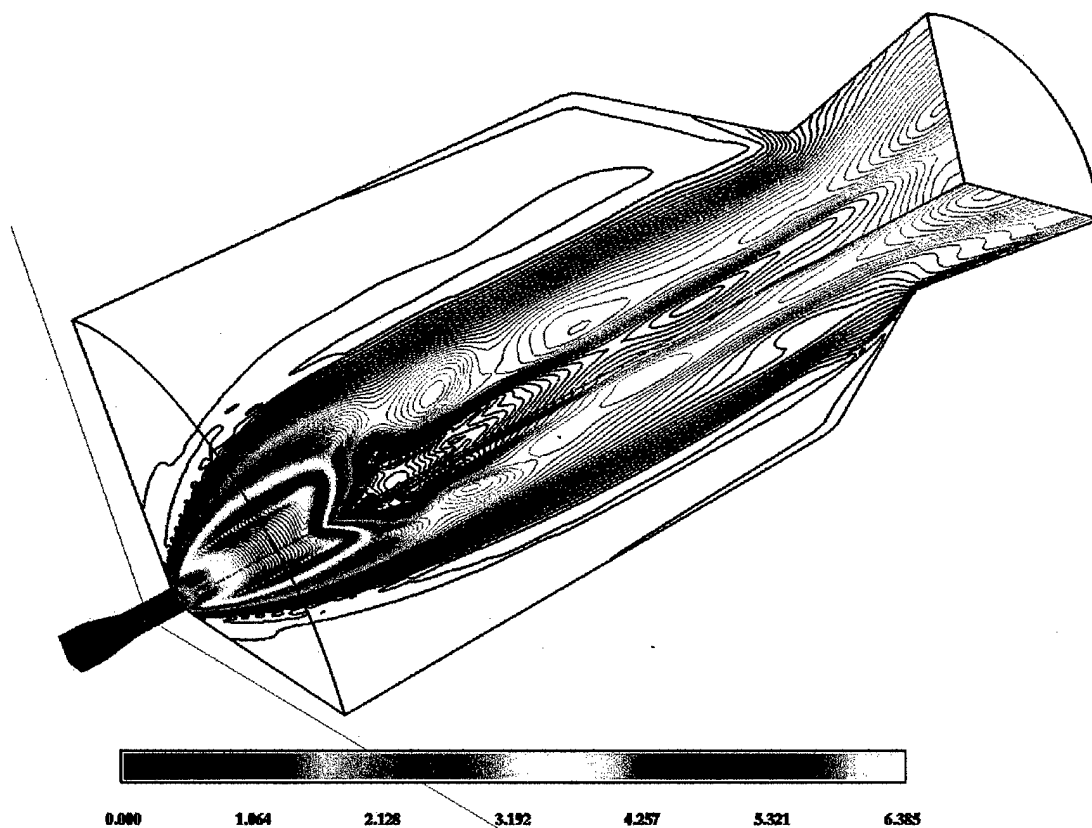
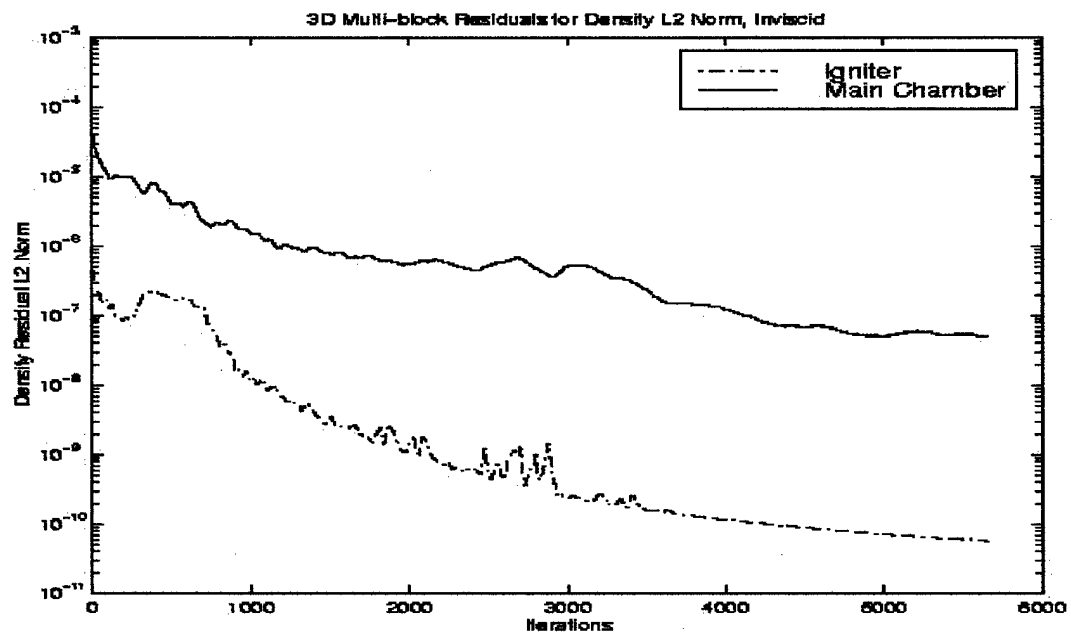
CCCCCCCCCCCCCCCCCCCCCCCCCCCCCCCCCCCCCCCCCCCCCCCCCCCCCCCCCCCCCCCCCCCC
$VOLUME ISPARTOF = 'CHAMBER HOLE BOUNDARY',

```

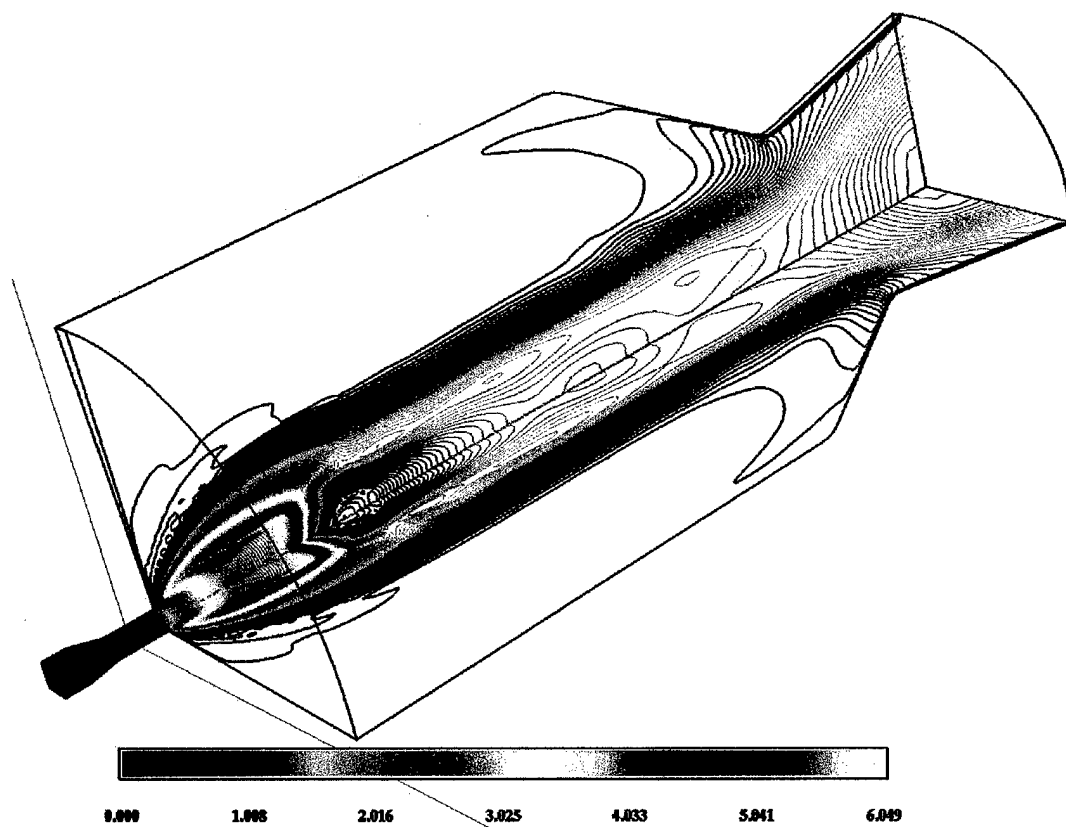
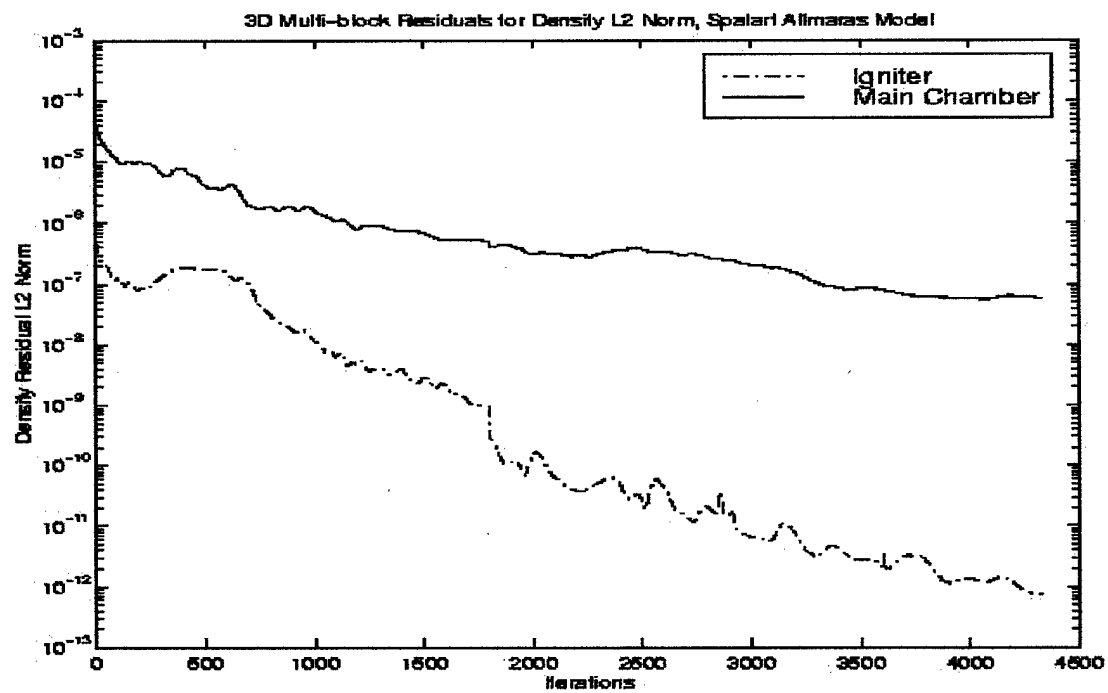
JRANGE = 1,27,
KRANGE = 1,29,
LRANGE = 1,1,

\$END

APPENDIX H. MULTI-BLOCK MODEL RESULTS

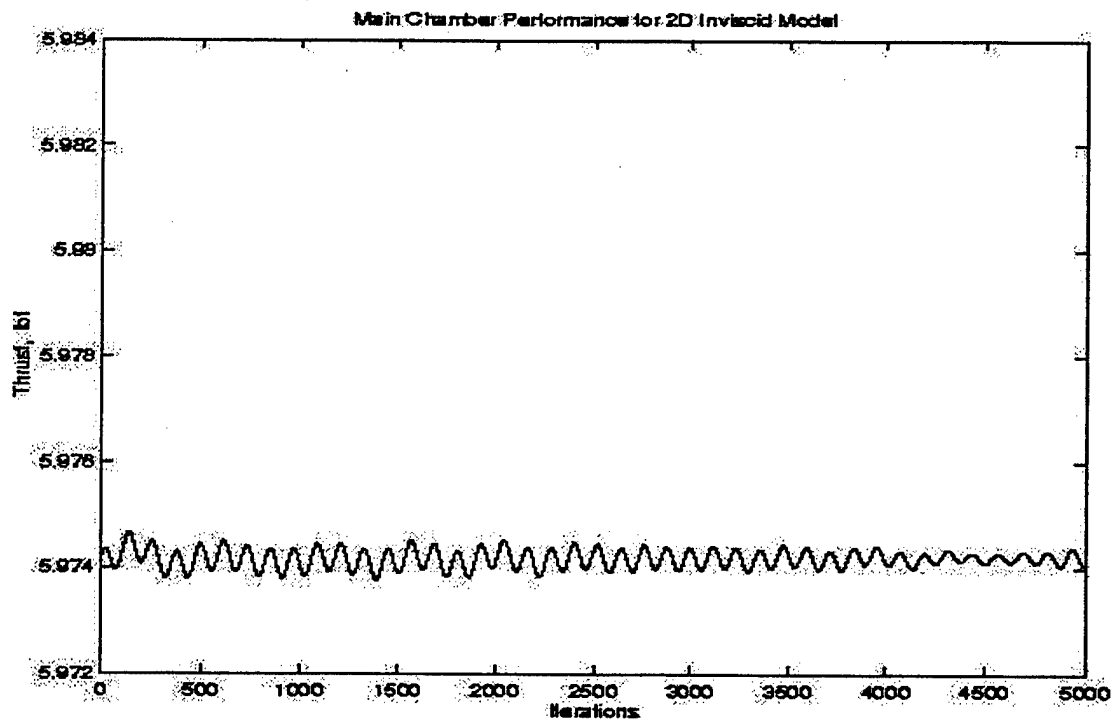


Multi-block Inviscid Model Mach Number Contours

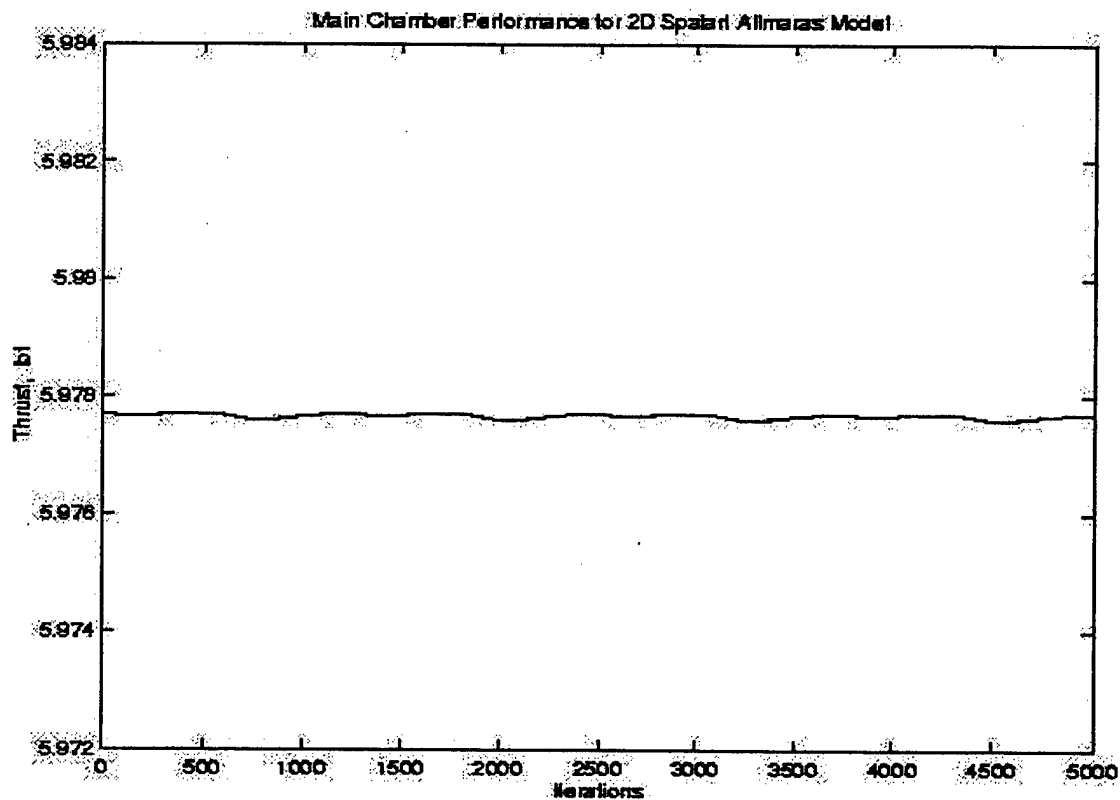


Multi-block Spalart Allmaras Mach Number Contours

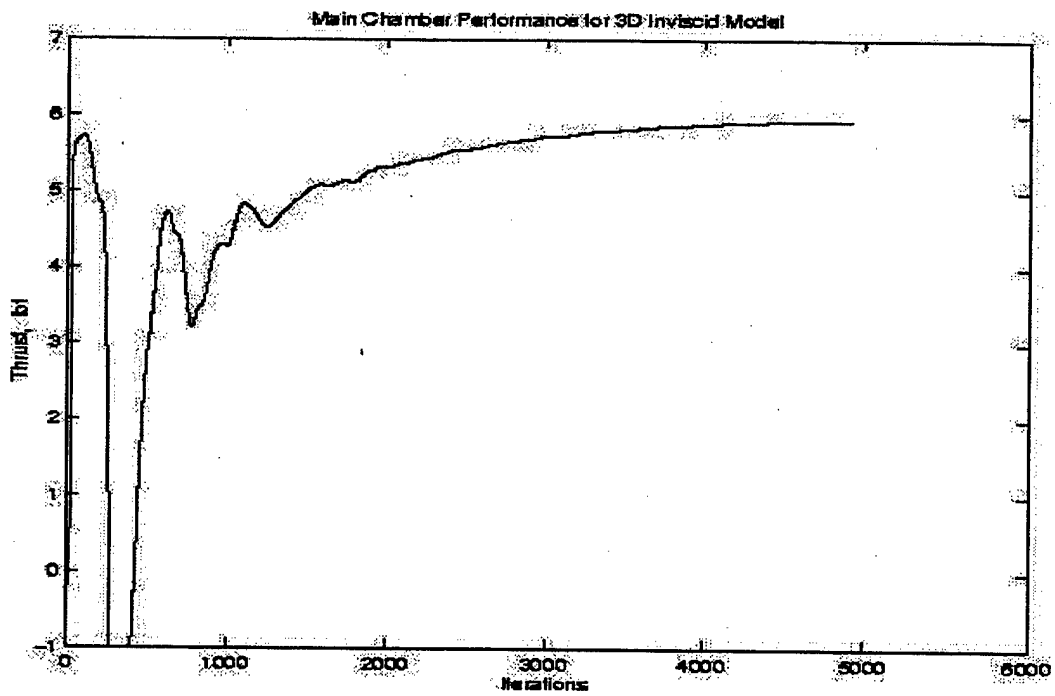
APPENDIX I. THRUST PROFILES



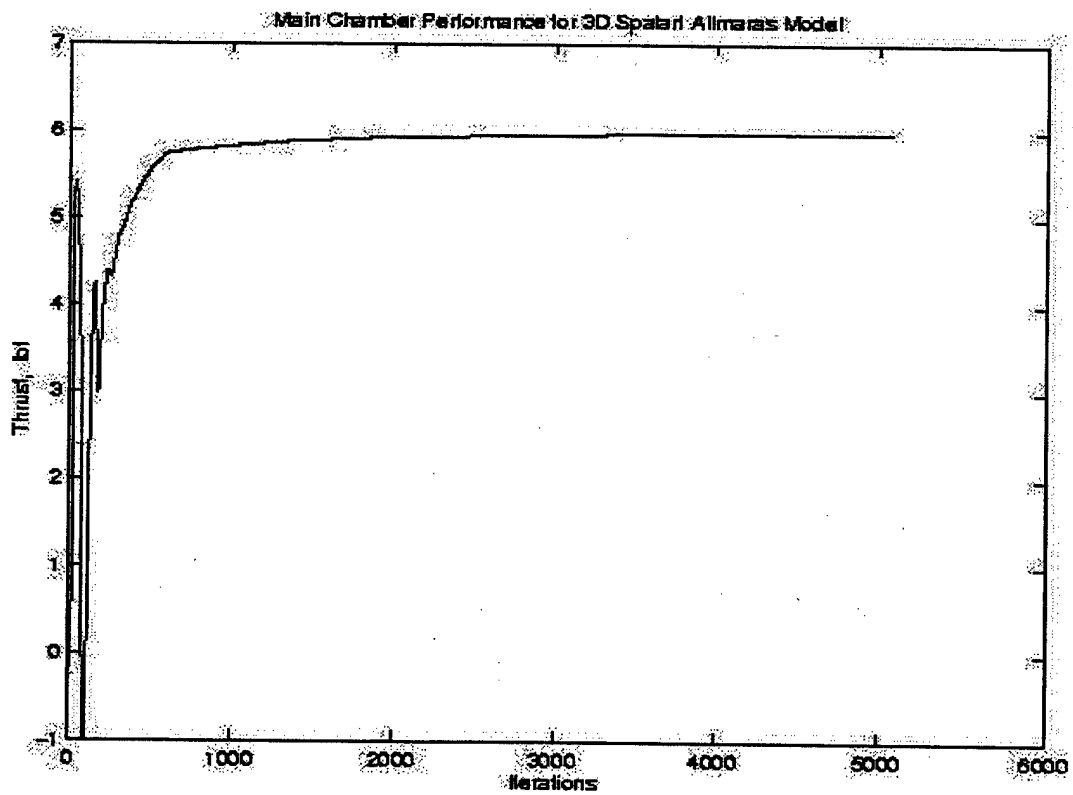
2D Inviscid Main Chamber Thrust



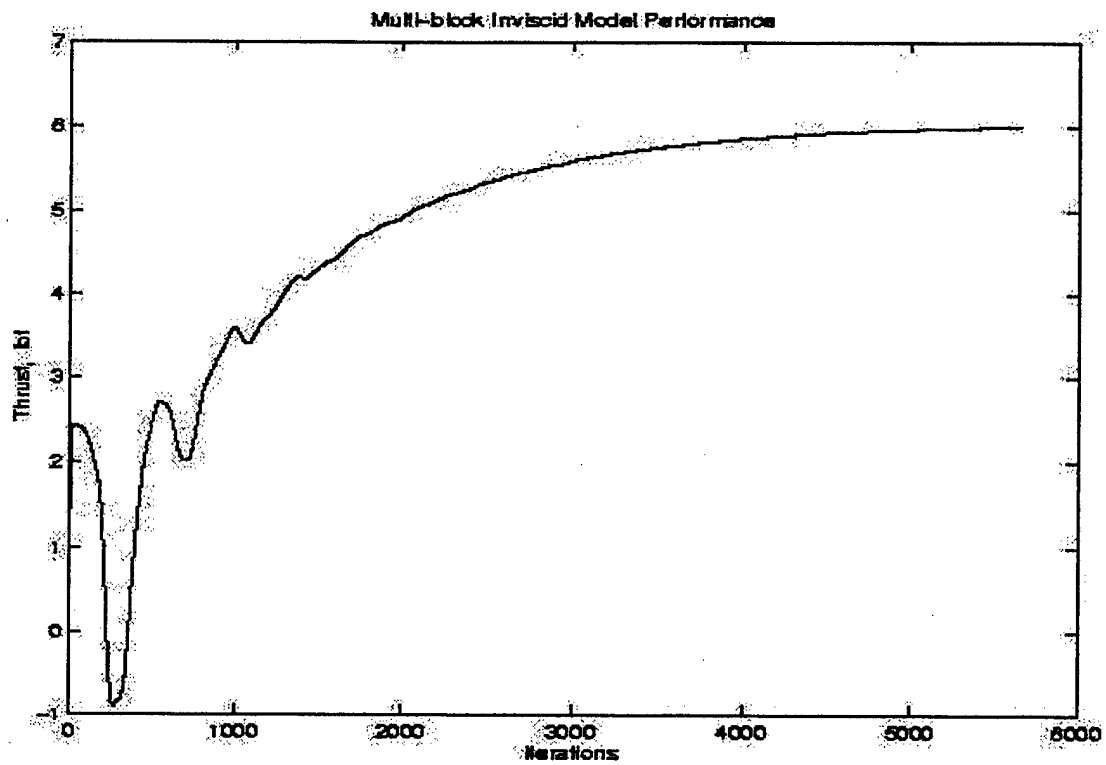
2D Spalart-Allmaras Main Chamber Thrust



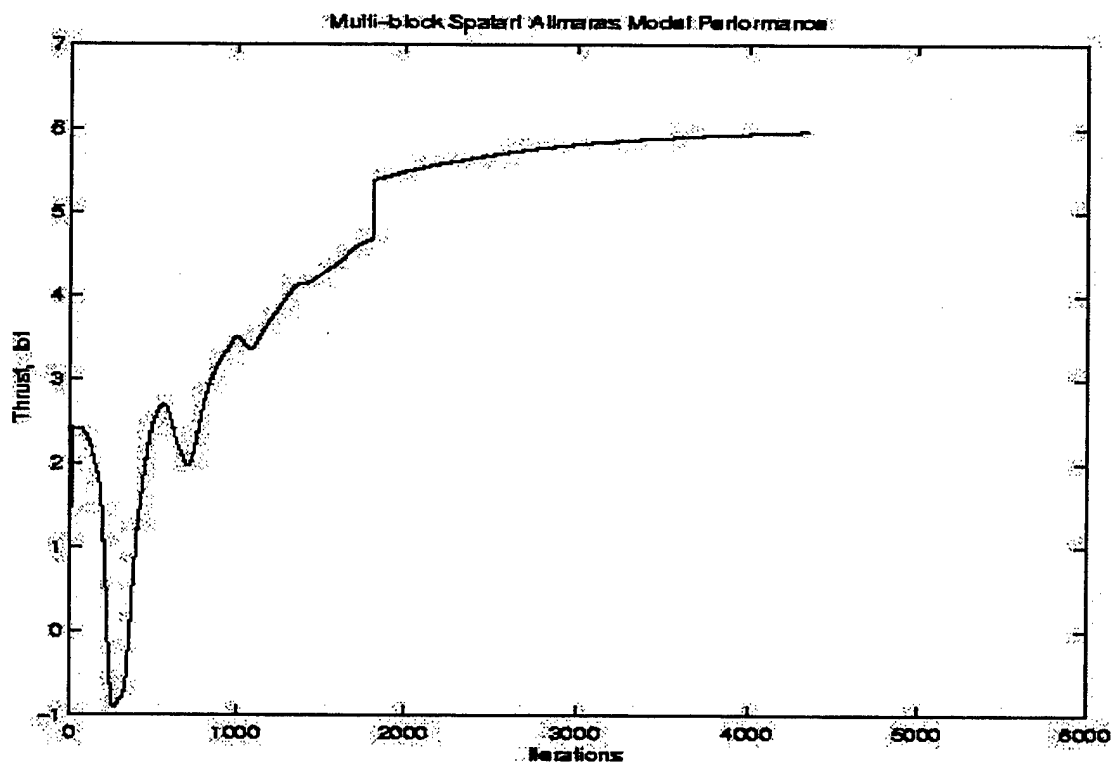
3D Inviscid Main Chamber Thrust



3D Spalart-Allmaras Main Chamber Thrust



Multi-Block Inviscid Thrust



Multi-Block Spalart-Allmaras Thrust

**APPENDIX J. 2D MAIN CHAMBER MODEL VELOCITY COEFFICIENTS
WITH SAMPLE THRUST CALCULATION**

Let C_{mdot} = Computed Mass Flow Rate Coefficient from OVERFLOW fomio.out file,

ρ_{∞} = normalized freestream density,

V_{∞} = normalized freestream velocity,

A_{inlet} = igniter inlet into main chamber area, $\pi^2 = \pi(0.1)^2 \text{ in}^2 = 0.0314 \text{ in}^2$

\dot{m} = mass flow rate,

then

$$\dot{m} = C_{mdot} \rho_{\infty} V_{\infty} A_{inlet}$$

Since OVERFLOW normalizes values based upon freestream values and C_{mdot} is 1.0 at the igniter inlet, the mass flow rate is then

$$\dot{m} = (1.0)(1.0)(1.0)(A_{inlet})$$

$$\dot{m} = 0.00021817 \text{ lbm/sec}$$

Adjusted to a chamber pressure of 150 psi,

$$\dot{m} = (150)(0.00021817) = 0.032726 \text{ lbm/sec}$$

Freestream Velocity can be calculated from inlet total conditions and the freestream Mach number,

$$V_{\infty} = M_{\infty} a_{\infty}$$

$M_{\infty} = 1.0$ (inlet condition), and

$$a_{\infty} = (\gamma R_{\infty} T_{\infty} g_c)^{0.5}$$

In order to dimensionalize a_{∞}

$R_{\infty} = 53.3 \text{ ft-lbf/lbm-}^{\circ}\text{R}$ (air at a ratio of specific heats of $\gamma = 1.4$)

$T_{\infty} = 5598^{\circ}\text{R}$

$g_c = 32.174 \text{ lbm-ft/lbf-sec}^2$

$$a_{\infty} = V_{\infty} = 3667.52 \text{ ft/sec}$$

From the profiles of exit velocity coefficient which follow, the average exit velocity is taken from the plot as approximately 1.65.

$$c = 1.65 V_{\infty} = 6051.41 \text{ ft/sec}$$

So finally from the ideal thrust equation, where

T = thrust,

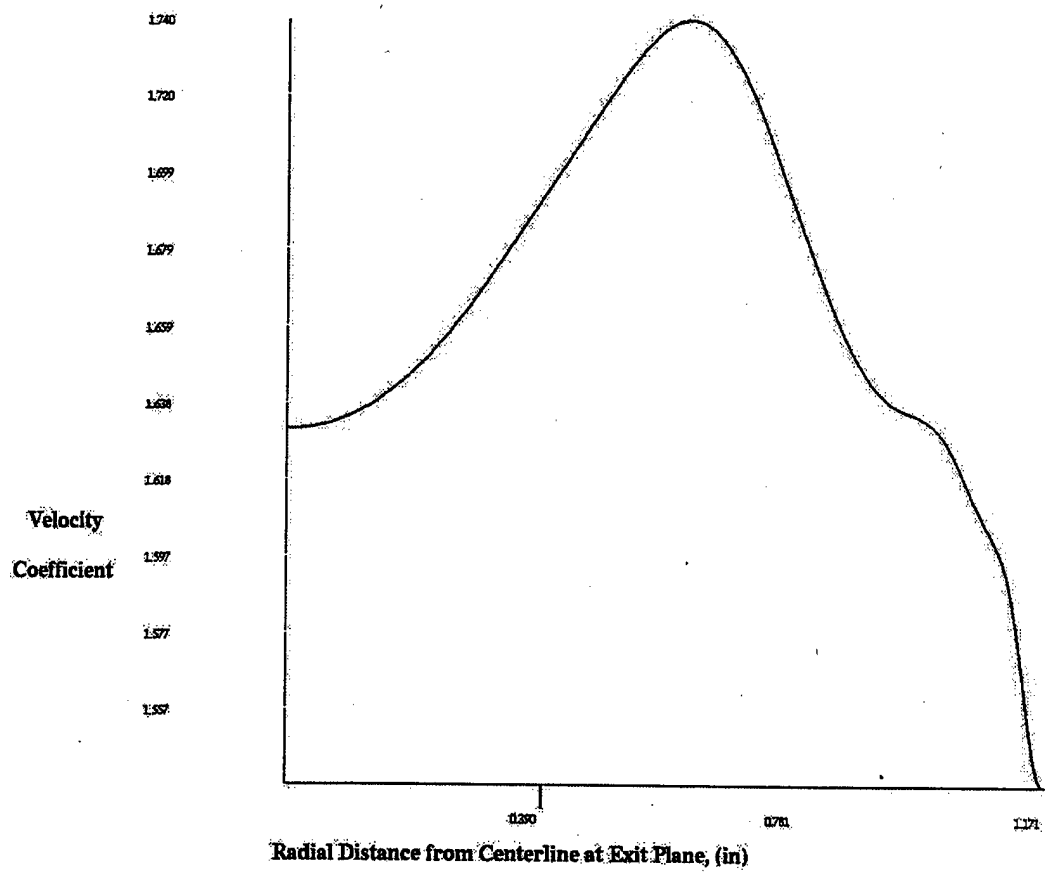
c = exit velocity,

and \dot{m} = mass flow rate

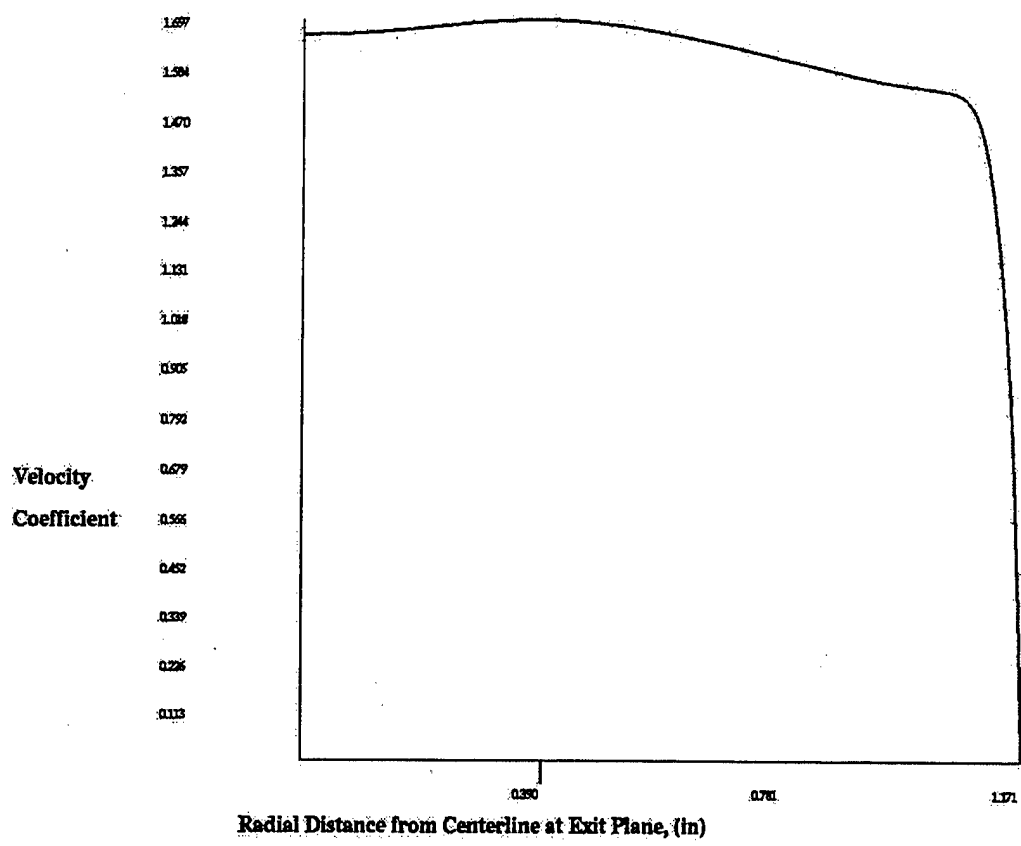
$$T = (\dot{m})(c)/g_c$$

$$T = (0.032726)(6051.41)/32.174$$

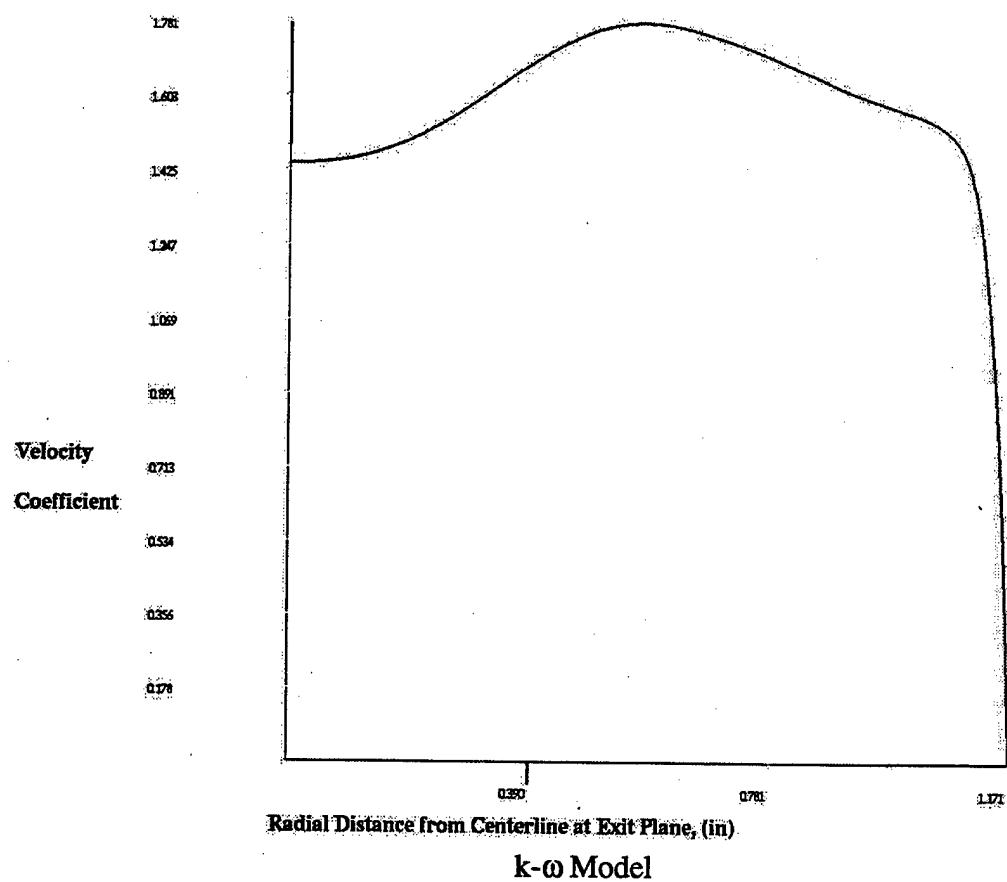
$$T = 6.155 \text{ lbf}$$



Inviscid Model



Spalart-Allmaras Model



APPENDIX K. TEP OUPUT FILE

(KG-MOL) (DEG K)/KG	-0.72543872E+03	0.00000000E+00	-
0.25908527E+03			
OKG-ATOMS/KG	BOP(I,2)	BOP(I,1)	B0(I)
C	0.43412652E-01	0.00000000E+00	0.15504519E-
01			
H	0.13023797E+00	0.00000000E+00	0.46513561E-
01			
O	0.21706326E-01	0.62502339E-01	0.47932334E-
01			

ENTHALPY IN BTU/LBM :

FROM REACTANTS :	-926.1313
FROM DELH() :	0.0000
FROM DELH1() :	0.0000
TOTAL :	-926.1313

1 ZONE = 1
THEORETICAL ROCKET PERFORMANCE ASSUMING EQUILIBRIUM COMPOSITION

DURING EXPANSION

OPC = 150.0 PSIA

ENTHALPY	STATE	TEMP	DENSITY	WT FRACTION
CHEMICAL FORMULA				(SEE NOTE)

CAL/MOL	DEG K	G/CC	
FUEL C 2.00000	H 6.00000	O 1.00000	1.00000
-66370.000	L 298.15	0.0000	
OXIDANT O 2.00000			1.00000
0.000	G 298.15	0.0000	

OO/F=1.8000E+00 PERCENT FUEL=3.5714E+01 EQUIVALENCE RATIO=1.1321E+00 STOIC MIXTURE
RATIO=2.0378E+00 DENSITY=0.0000E+00

	CHAMBER	THROAT	EXIT	EXIT
PC/P	1.0000	1.7202	1.0350	1.7202
P, PSIA	150.0	87.20	144.9	87.20
T, DEG R	5846	5598	5829	5598
H, BTU/LB	-926.1	-1189.9	-943.3	-1189.9
S, BTU/(LB) (R)	2.8608	2.8608	2.8608	2.8608
DEN (LBM/FT3)	5.55E-02	3.41E-02	5.38E-02	3.41E-02

M, MOL WT	23.199	23.525	23.220	23.525
(DLV/DLP)T	-1.04561	-1.04132	-1.04534	-1.04132
(DLV/DLP)P	1.8902	1.8443	1.8875	1.8443
CP, BTU/(LB) (R)	2.0060	1.9725	2.0044	1.9725
CP GAS(SF)	0.5054	0.5035	0.5053	0.5035
GAMMA GAS(SF)	1.2039	1.2014	1.2037	1.2014
GAMMA (S)	1.1196	1.1164	1.1194	1.1164
SON VEL, FT/SEC	3745.3	3634.3	3738.0	3634.3
MU, LBF-S/FT2	1.91E-06	1.85E-06	1.90E-06	1.85E-06
K, LBF/S-DEGR	3.87E-02	3.72E-02	3.86E-02	3.72E-02
PRANDTL NO	0.62242	0.62643	0.62268	0.62643
MACH NUMBER	0.0000	1.0000	0.2480	1.0000

AE/AT	1.0000	2.4885	1.0000
CSTAR, FT/SEC	5600	5600	5600
CF VAC	1.230		1.230
CF	0.649		0.649
IVAC, LBF-S/LBM	214.14		214.14
I, LBF-SEC/LBM	112.96		112.96
MOL WT(MIX)	23.199	23.525	23.220

MOLE FRACTIONS

CO	0.195452	0.187288	0.194949	0.187288
CO2	0.164233	0.177461	0.165060	0.177460
H	0.025498	0.022360	0.025293	0.022360
HCO	0.000003	0.000002	0.000003	0.000002
HO2	0.000100	0.000067	0.000098	0.000067
H2	0.066003	0.062702	0.065791	0.062702
H2O	0.427167	0.443928	0.428246	0.443928
H2O2	0.000006	0.000004	0.000006	0.000004
O	0.015284	0.012475	0.015097	0.012475
OH	0.067111	0.058554	0.066558	0.058554

020.0391410.0351590.0389000.035159

MASS FRACTIONS

CO0.2359900.2229950.2351710.222995

CO20.3115610.3319820.3128490.331982

H0.0011080.0009580.0010980.000958

HCO0.0000040.0000020.0000040.000002

HO20.0001420.0000940.0001390.000094

H20.0057360.0053730.0057120.005373

H2O0.3317200.3399520.3322590.339952

H2O20.0000090.0000060.0000090.000006

O0.0105410.0084840.0104030.008484

OH0.0492000.0423310.0487510.042331

O20.0539880.0478230.0536070.047823

ADDITIONAL PRODUCTS WHICH WERE CONSIDERED BUT WHOSE MOLE FRACTIONS WERE LESS THAN .0000005 FOR ALL ASSIGNED CONDITIONS

CCHCH4C2C2H2C3C4

C(GR)H2O(L)

NOTE

WEIGHT FRACTION OF FUEL IN TOTAL FUELS AND OF OXIDANT IN TOTAL OXIDANTS (SF) STANDS FOR (SHIFTING FROZEN)

1

0

FROZEN TRANSPORT PROPERTIES CALCULATED FROM EQUILIBRIUM

CONCENTRATIONS

STATIONMU

(LBF-SEC/FT**2)

K

(LBF/SEC-DEG R)

PR

CHAMBER1.90672915E-063.87344547E-026.22416377E-01

THROAT1.85043473E-063.72055843E-026.26428485E-01

EXIT1.85043439E-063.72055694E-026.26428604E-01

0VISCOSITY EXPONENT (OMEGA) FOR THE FORM MU=MUREF*(T/TREF)**OMEGA IS0.69272

MUREF FOR INPUT TO BLM=6.13471057E-05 LBM/(FT-SEC)

0SPECIES CONSIDERED IN TRANSPORT PROPERTIES CALCULATIONS

CCHCH4CO

CO2C2C2H2H

H2H2OH2OO

OH02

1

ZONE = 1

THEORETICAL ROCKET PERFORMANCE ASSUMING FROZEN COMPOSITION

DURING EXPANSION

OPC = 150.0 PSIA

WT FRACTION

ENTHALPY STATE TEMP DENSITY

CHEMICAL FORMULA(SEE NOTE)

CAL/MOLDEG KG/CC

FUELC2.00000H6.00000O1.000001.00000

-66370.000L298.150.0000

OXIDANTO2.000001.00000

0.000G298.150.0000

OO/F=1.8000E+00 PERCENT FUEL=3.5714E+01 EQUIVALENCE RATIO=1.1321E+00 STOIC MIXTURE

RATIO=2.0378E+00 DENSITY=0.0000E+00

0CHAMBERTHROATEXITEXIT

PC/P1.00001.77581.03701.7758

P, PSIA150.084.47144.784.47

T, DEG R5846530158105301

H, BTU/LB-926.1-1199.9-944.2-1199.9

S, BTU/(LB) (R)2.86082.86082.86082.8608

DEN (LBM/FT3)5.55E-023.44E-025.38E-023.44E-02

M, MOL WT23.19923.19923.19923.199

CP, BTU/(LB) (R)0.50540.49980.50510.4998

GAMMA (S)1.20391.20671.20411.2067

SON VEL, FT/SEC3883.73702.63872.03702.6

MACH NUMBER0.00001.00000.24591.0000

AE/AT1.00002.48841.0000

CSTAR, FT/SEC544954495449

CF VAC		1.243		1.243		
CF		0.680		0.680		
IVAC,LBF-S/LBM		210.45		210.45		
I, LBF-SEC/LBM		115.08		115.08		

MOLE FRACTIONS

CO	0.195452	CO2	0.164233	H	0.025498	HCO
0.000003						
HO2	0.000100	H2	0.066003	H2O	0.427167	H2O2
0.000006						
O	0.015284	OH	0.067111	O2	0.039141	

MASS FRACTIONS

CO	0.235990	CO2	0.311561	H	0.001108	HCO
0.000004						
HO2	0.000142	H2	0.005736	H2O	0.331720	H2O2
0.000009						
O	0.010541	OH	0.049200	O2	0.053988	

0ADDITIONAL PRODUCTS WHICH WERE CONSIDERED BUT WHOSE MOLE FRACTIONS WERE LESS THAN
.0000005 FOR ALL ASSIGNED CONDITIONS

C	CH	CH4	C2	C2H2	C3	C4
C(GR)	H2O(L)					

NOTE

1 WEIGHT FRACTION OF FUEL IN TOTAL FUELS AND OF OXIDANT IN TOTAL OXIDANTS

CALCULATE ODE AREA RATIO AND PRESSURE SCHEDULES FOR ZONE 1

*** EOF ENCOUNTERED IN READING ODE REACTANTS DATA ***

*****CPU(SEC) = 0.4

LIST OF REFERENCES

1. Curtis, L. A. and Hurlbert, E. A., "Non-Toxic Orbital Maneuvering and Reaction Control System," Joint Propulsion Conference and Exhibit, Los Angeles, California, June 20-24, 1999.
2. Johnson, C. and Baker, A., "ROCCID Analysis for the Aerojet GOX/Ethanol 600 lbf Engine," Purchase Order No. T-7726V, Carson City, Nevada, September 1997.
3. Chen, C. L., Ramakrishnan, S., Ota, D. K., Rajagopal, K., and Wisneski, J., "Computation of Underexpanded Solid Rocket Plume and Its Effects on the Mated Shuttle Configuration," 10th AIAA Applied Aerodynamics Conference, Palo Alto, California, June 22-24, 1992, pp. 117-124.
4. Dash, S. M., "Analysis of Exhaust Plumes and Their Interaction with Missile Airframes," Progress in Astronautics and Aeronautics Volume 104, American Institute of Aeronautics and Astronautics Inc., New York, New York, 1986, pp. 778-851.
5. Buning, P. G., Jespersen, D. C., Pulliam, T. H., Chan, W. H., Slotnick, J. P., Krist, S. E., and Renze, K. J., OVERFLOW USER'S MANUAL Version 1.8b, 25 March 1998.
6. FLUENT 5 Solver Training Notes Days 1 & 2, TRN-1998-006, Lebanon, New Hampshire, December 1998.
7. FLUENT 5 User's Manuals, Volumes 1-5, Fluent Inc., Lebanon, New Hampshire, July 1998.
8. CAD Drawings, Chamber and Igniter, Tag Number 1196095, Aerojet Liquid Rocket Company, April 1983.
9. Cort, R. M., "Aerojet Gox/Ethanol Thruster Test," TD-887-001, Lyndon B. Johnson Space Center, White Sands Test Facility, Las Cruces, New Mexico April 1997.
10. GAMBIT Training Notes, TRN-1998-003, Fluent Inc., Lebanon, New Hampshire, December 1998.
11. Chawner, J. R. and Steinbrenner, J. P., GRIDGEN Release Notes, Version 9.6, MDA Engineering, Inc. Arlington, Texas, October 1994.
12. Suhs, N. E. and Tramel, R. W., PEGSUS 4.0 USER'S MANUAL, Calspan Corporation/AEDC Operations, Air Force Systems Command, Arnold Air Force Base, Tennessee, June 1991.

13. TEP for Windows, A Combustion Analysis Tool, Version 1.0 User's Manual,
Software Engineering Associates Inc., Carson City, Nevada.

INITIAL DISTRIBUTION LIST

1. Defense Technical Information Center 2
8725 John J. Kingman Rd., Suite 0944
Ft. Belvoir, VA 22060-6218

2. Dudley Knox Library 2
Naval Postgraduate School
411 Dyer Rd.
Monterey, CA 93943-5101

3. Director, Training and Education 1
MCCDC, Code C46
1019 Elliot Rd.
Quantico, Virginia 22134-5027

4. Director, Marine Corps Research Center 1
MCCDC, Code C40RC
2040 Broadway Street
Quantico, Virginia 22134-5107

5. Director, Studies and Analysis Division 1
MCCDC, Code C45
300 Russell Road
Quantico, Virginia 22134-5134

6. Prof. Gerald H. Lindsey, Code AA/Li 1
Chairman, Department of Aeronautics and Astronautics
Naval Postgraduate School
Monterey, CA 93943-5000

7. Prof. Garth V. Hobson, Code AA/Hg 3
Department of Aeronautics and Astronautics
Naval Postgraduate School
Monterey, CA 93943-5000

8. Prof. David W. Netzer, Code 09 1
Naval Postgraduate School
Monterey, CA 93943-5000

9. Mr. Warren Brasher, Chief, Energy Systems Division 1
Mail Code EP
NASA, JSC
Houston, TX 77058

10. Mr. John Griffin, Chief, Propulsion and Fluid Systems Branch 1
Mail Code EP-4
NASA, JSC
Houston, TX 77058
11. Mr. Eric Hurlbert, Aerospace Technologist 2
Mail Code EP-4
NASA, JSC
Houston, TX 77058
12. Mr. Adam Williams, Author 2
280 B Rimview Dr.
Colorado Springs, CO 80919